

**UCSF**

**UC San Francisco Electronic Theses and Dissertations**

**Title**

Kv1.1 regulation of adult hippocampal neurogenesis

**Permalink**

<https://escholarship.org/uc/item/05v5r51j>

**Author**

Lin, Yuan-Hung

**Publication Date**

2021

Peer reviewed|Thesis/dissertation

Kv1.1 regulation of adult hippocampal neurogenesis

by  
Yuan-Hung Lin King

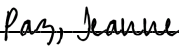
DISSERTATION  
Submitted in partial satisfaction of the requirements for degree of  
DOCTOR OF PHILOSOPHY

in  
Neuroscience

in the  
GRADUATE DIVISION  
of the  
UNIVERSITY OF CALIFORNIA, SAN FRANCISCO

Approved:

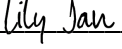
DocuSigned by:

  
129DDCD87B64445...

Paz, Jeanne


Chair

DocuSigned by:

  
DocuSigned by: 94...

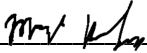
Lily Jan

DocuSigned by:

  
DocuSigned by: 450...

John Rubenstein

DocuSigned by:

  
D52190F39543433...

Mazen Kheirbek

Committee Members

Copyright 2021

By

Yuan-Hung Lin King

This dissertation is dedicated to John Lin King.

## **Acknowledgements**

I am grateful for the support of many mentors, colleagues, friends, and family during my PhD.

First and foremost, I want to thank my thesis advisor, Lily Jan, and Yuh-Nung Jan for their generous support and encouragement. I am grateful that Lily welcomed me into her lab. Over the years, she has shared her boundless enthusiasm for science, given me the freedom to pursue my intellectual interests, and provided me with the resources to succeed. She has taught me to be independent and brave; and molded me into the scientist that I am today. I am incredibly thankful for my experience in the Jan lab, and I hope to one day emulate their mentorship.

Next, I want to acknowledge the current and former members of the Jan lab. My labmates are dedicated scientists and generous mentors. Thank you for making the Jan lab an intellectual home throughout the years. A special thanks to those whose efforts made the work possible: Chao Chen, Shi-Bing Yang, Marena Tynan-La Fontaine, Tong Cheng, Armando Martinez, Rose Lau, Sandra Barbel, Mariati Messinger, and Monika Avdeef.

My thesis owes much of its final form to the guidance of my committee members—Jeanne Paz, Mazen Kheirbek, and John Rubenstein. I am grateful for their valuable professional and scientific advice. My committee chair, Jeanne Paz, kept me on track to graduate through a global pandemic; Mazen Kheirbek provided elegant solutions to thorny scientific problems; and John Rubenstein intuited project hurdles and connected me with experts in the field to overcome them. I am very thankful to have had the opportunity to learn from you over the years and will miss our annual meetings.

I have been fortunate have had the support of the UCSF Neuroscience community. I want to thank Susan Voglmaier, Suzanne Rossi, Vikaas Sohal, Steve Finkbeiner, Li Gan, and Yadong Huang for mentorship during my early graduate school years. Additionally, I am grateful for our program administrators, Pat Veitch and Lucita Nacionales, who guided me through all my PhD milestones.

I also want to thank my high school and undergraduate mentors. My high school teacher, Nanette Andrews instilled in me a love for learning and encouraged me to pursue my potential. When I was interested in learning about life in the laboratory but had no research experience, Seung-Hee Lee and Yang Dan took a chance on me and gave me my first research opportunity. They showed me how great science is done and inspired me to pursue a PhD.

I am fortunate to have made close friendships with students in the Neuroscience program. Lynn Wang and Mario Zobia, thank you for the intellectual and moral support over the years—I am grateful for all the memories we share of the Jan lab. Faten Sayed, Lay Kodama, Jermyn See, Ling Guo, Yelena Kulik, and Chris Zimmerman, thank you for all the adventures. I am grateful to have you all a part of my life, and I hope we share many more big moments together.

Last, I want to thank my family. My parents have always encouraged me to pursue my interests. My siblings have provided many laughs. My PhD would not have been possible without the support of my husband, John Lin King. Thank you for always being there for me. Final thanks go to Flower for dutifully waiting by the front door each day for us to return from the laboratory.

## Contributions

**Chapter 1** of this dissertation were written by Yuan-Hung Lin King.

**Chapter 2** of this dissertation is reproduced in its entirety from:

Chou, S. M.\*, Li, K. X.\*, Huang, M. Y.\*, Chen, C., Lin King, Y. H., Li, G. G., Zhou, W., Teo, C. F., Jan, Y.N., Jan, L.Y., & Yang, S. B. (2021). Kv1.1 channels regulate early postnatal neurogenesis in mouse hippocampus via the TrkB signaling pathway. *Elife*, *10*, e58779.

S.B.Y. conceived and designed the study. S.B.Y and M.Y.H. wrote the paper. S.M.C., K.X.L., M.Y.H., C.C., Y.H.L.K., W.Z., C.F.T., and S.B.Y. performed research and analyzed data. G.G.L., Y.N.J., and L.Y.J., and S.B.Y. provided resources, supervision, and funding. \*Denotes qual contribution.

**Chapter 3** of this dissertation was written by Yuan-Hung Lin King and Lily Jan. The manuscript is in preparation for submission.

Lin King, Y. H., Chen, C., Lin King, J.V., Simms, J., Glasscock, E., Yang, S.B., Jan, Y.N., & Jan, L.Y. (submitted). Kv1. 1 preserves the neural stem cell pool and facilitates neuron maturation during adult hippocampal neurogenesis.

Y.H.L.K., Y.N.J., and L.Y.J. conceived and designed the study. Y.H.L.K. and L.Y.J. wrote the paper. Y.H.L.K., C.C., J.V.L.K., J.S., and S.B.Y. performed research and analyzed data. E.G. contributed new reagents. All authors were involved in editing the manuscript.

## **K<sub>v</sub>1.1 regulation of adult hippocampal neurogenesis**

Yuan-Hung Lin King

### **Abstract**

Bioelectric signaling is evolutionarily conserved and maintained in all living cells through the selective expression of ion channels. In excitable cells like neurons, ion channels play an essential and well characterized role in defining the properties of action potentials. Less is known about their role in non-excitable cells such as neural stem cells and neural progenitor cells. Recent studies in mice have found that the loss of a voltage-gated potassium channel, K<sub>v</sub>1.1, leads to a dramatic increase in hippocampal neurons. The hippocampus is critical for learning and memory, and it harbors one of two well-established neurogenic niches in the adult mouse brain. Here, we investigated the role of K<sub>v</sub>1.1 in early postnatal and adult hippocampal neurogenesis. In Chapter 2, we first examined the role of K<sub>v</sub>1.1 in early postnatal neurogenesis. We found that loss of K<sub>v</sub>1.1 depolarizes the membrane potential of neural progenitor cells and increases the proliferation of neural progenitor cells through the TrkB signaling pathway. Next, we assessed the role of K<sub>v</sub>1.1 in adult hippocampal neurogenesis in Chapter 3. We observed that conditional deletion of K<sub>v</sub>1.1 in adult neural stem cells causes an initial increase in proliferation that eventually depletes the neural stem cell pool. Furthermore, neurons produced from adult neural stem cells lacking K<sub>v</sub>1.1 had impaired maturation and positioning. These mice also displayed hippocampal-dependent learning and memory deficits. Together, these findings support an important role for this voltage-gated ion channel in adult neurogenesis. As aberrant neurogenesis has been implicated in cognitive decline associated with aging and neurological diseases, understanding the role of K<sub>v</sub>1.1 in adult neurogenesis provides a framework for identifying new therapeutic targets to promote healthy neurogenesis and cognition.



## **Table of Contents**

<b>Chapter 1: Introduction</b> .....	1
1.1 Introduction .....	2
1.2 References .....	7
<b>Chapter 2: K<sub>v</sub>1.1 channels regulate early postnatal neurogenesis in mouse hippocampus via the TrkB signaling pathway</b> .....	12
2.1 Introduction .....	13
2.2 Results .....	16
2.3 Discussion.....	24
2.4 Methods .....	30
2.5 Acknowledgments .....	36
2.6 References .....	37
2.7 Main Figures.....	47
2.8 Supplementary Figures.....	59
<b>Chapter 3: K<sub>v</sub>1.1 preserves the neural stem cell pool and facilitates neuron maturation during adult hippocampal neurogenesis</b> .....	65
3.1 Introduction .....	66
3.2 Results .....	69
3.3 Discussion.....	78
3.4 Methods .....	81
3.5 Acknowledgments .....	91
3.6 References .....	92
3.7 Main Figures.....	100

3.8 Supplementary Figures .....	109
---------------------------------	-----

## List of Figures

Figure 2.1: K <sub>v</sub> 1.1 channels control dentate gyrus neuron number in a cell-autonomous manner.....	47
Figure 2.2: Functional expression of K <sub>v</sub> 1.1 channel in SGZ neural progenitor cells expressing Fezf2-GFP at postnatal 2 weeks .....	48
Figure 2.3: Loss of K <sub>v</sub> 1.1 channels depolarizes type 2b neural progenitor cells in SGZ at postnatal 2 weeks .....	49
Figure 2.4: Classification of the Fezf2-GFP progenitor cells in SGZ.....	50
Figure 2.5: Multinomial logistic regression for cell type prediction.....	52
Figure 2.6: TrkB is mostly active in Tbr2 positive neural progenitor cells .....	54
Figure 2.7: K <sub>v</sub> 1.1 channels regulate neural progenitor cell numbers via the TrkB signaling pathway.....	56
Figure 2.8: Summary of the role of K <sub>v</sub> 1.1 channels in regulating early postnatal neurogenesis in SGZ.....	58
Supplementary figure 2.1: K <sub>v</sub> 1.1 channels do not affect embryonic hippocampal neurogenesis .....	59
Supplementary figure 2.2: No detectable difference in interneurons of K <sub>v</sub> 1.1 KO mice at P10 .....	60
Supplementary figure 2.3: The TrkB signaling is active in DCX+ late-stage progenitor cells but not Sox2+ early-stage progenitor cells.....	62
Supplementary figure 2.4: Intraperitoneal injection of GNF-5837 remarkably inhibits the TrkB signaling in SGZ .....	63
Supplementary figure 2.5: Clonal analysis of postnatal born neurons in the SGZ .....	64

Figure 3.1: Neonatal deletion of Kv1.1 increases hippocampal neurogenesis.....	100
Figure 3.2: Deletion of Kv1.1 in adult neural stem cells (NSCs) results in an initial increase of radial glia-like NSCs (RGLs) before eventual depletion of the RGL pool .....	101
Figure 3.3: Loss of Kv1.1 impairs adult hippocampal neurogenesis by altering doublecortin-expressing (DCX+) cell maturation and adult-born granule cell (abGC) positioning .....	103
Figure 3.4: MADM analysis reveals a transient increase in Kv1.1-null progeny cells in the dentate gyrus of 2 to 3-month old mice.....	104
Figure 3.5: Kv1.1 cKO mice display deficits in contextual learning and memory.....	106
Figure 3.6: Model of impaired adult neurogenesis in Kv1.1 cKO mice with deletion of Kv1.1 from adult neural stem cells (NSCs) induced by tamoxifen (TAM) injection .....	108
Supplementary figure 3.1: Generation of Kv1.1 cKO mice and validation of <i>Kcna1</i> gene deletion by qPCR .....	109
Supplementary figure 3.2: Loss of Kv1.1 function in Kv1.1 cKO cells.....	111
Supplementary figure 3.3: Deletion of Kv1.1 in adult neural stem cells (NSCs) results in a trend towards increased early glial-like intermediate progenitor cells (Type 2a) at 4 weeks post-tamoxifen (TAM).....	112
Supplementary figure 3.4: Kv1.1 cKO mice showed no abnormality in elevated plus maze, open field, and hot plate test .....	113

## **Chapter 1**

### **Introduction**

## 1.1 Introduction

In 1952, Hodgkin and Huxley determined that potassium ions regulate the neuronal membrane potential and action potential dynamics [1, 2]. Potassium ions pass through the hydrophobic cell membrane down their electrochemical gradient through dedicated potassium channels, which selectively allow these positively charged ions to cross the otherwise impermeable membrane. Our lab cloned the first voltage-gated potassium channel, Shaker, from *Drosophila* in 1987 [3], and its mammalian homolog, K<sub>v</sub>1.1, in 1988 [4]. Since then, more than 200 potassium channels have been characterized—such channels can be found in virtually all mammalian cell types and in all living organisms [5, 6].

Although potassium channels have diverse channel properties, they share similar characteristics [7]. They are highly selective and efficient—in general, they are hundreds of times more permeable to potassium ions than other cations, such as sodium ions, and can pass  $\sim 10^8$  potassium ions per second, close to the free diffusion limit [8]. A potassium channel is usually composed of four alpha subunits that form the selectivity filter and pore, and four accessory beta subunits that regulate channel gating and trafficking [9]. Potassium channels are divided into four types by their gating mechanism—voltage-gated, calcium activated, inwardly rectifying, and tandem pore domain [10, 11].

Within the voltage-gated potassium channel family, there are 12 subfamilies of alpha subunits (K<sub>v</sub>1-K<sub>v</sub>12)—together they comprise the largest family within the voltage-gated ion channel superfamily [10, 11]. Voltage-gated potassium channels serve a diversity of critical physiological functions, including well-described roles in modulating the membrane potential; action potential

frequency and duration in excitable cells; and regulating dynamics of cell growth, proliferation, and migration in non-excitable cells [12, 13]. The Shaker-related  $K_v1$  subfamily contains eight genes which encode voltage-sensing alpha subunits ( $K_v1.1$ - $K_v1.8$ ) with distinct expression, trafficking, and biophysical properties.  $K_v1$  subunits can form functional homotetramers or heterotetramers with other  $K_v1$ s. Different subunit compositions produce biophysically distinct channels, which presumably support fine-tuning of functional roles *in vivo* [13].  $K_v1$  channels require relatively low levels of depolarization for activation, thus enabling them to regulate action potential threshold and duration [14-16] and contribute to the maintenance of the resting membrane potential [17, 18].

A spontaneous loss-of-function, truncation mutation in  $K_v1.1$ , encoded by the *Kcna1* gene, arose in the Jackson Laboratory in 1983 [19, 20]. The mutation causes a frame shift and introduces a premature stop codon, resulting in the expression of only the N-terminus and the first transmembrane segment of  $K_v1.1$  [21]. Although the truncated protein can co-assemble with other  $K_v1$  subunits, it cannot form functional channels [21]. Because these mice had abnormally large brains, they were named *megencephaly* (*mceph*) mice [19, 20]. The enlargement stems from an increase in both glia and neuron production in the hippocampus and ventral cortex [22, 23]. In addition, *mceph* mice develop seizures around 3 weeks of age [20], approximately when *Kcna1* expression begins to peak [24]. These phenotypes are also recapitulated when  $K_v1.1$  is completely removed in the  $K_v1.1$ -null mice [16, 25].

Although voltage-gated potassium channels are known to regulate cellular proliferation in lymphocytes and cancer cells [26], little is known about the role of  $K_v1.1$  in neurogenesis. Because

neuronal hyperexcitability can trigger both glial and neuronal production [27, 28], our lab set out to determine if loss of  $K_v1.1$  promotes glial and/or neuronal production in a cell autonomous manner. To study the function of  $K_v1.1$  in mice without seizures or other pathologies, we used mosaic analysis with double markers (MADM) of mice heterozygous for the *mceph* allele [29] to create a mosaic mouse with  $K_v1.1$  functionally knocked out of a subpopulation of neurons. In these mice, somatic recombination driven by *Nestin-Cre* yields subsets of neural stem cells with zero (*Kcna1<sup>mceph/mceph</sup>*), one (*Kcna1<sup>mceph/+</sup>*), or two (*Kcna1<sup>+/+</sup>*) functional allele(s) of *Kcna1*. Homozygous *Kcna1<sup>mceph/mceph</sup>* progeny cells are marked by tdTomato; wildtype *Kcna1<sup>+/+</sup>* progeny cells are marked by GFP; and heterozygous *Kcna1<sup>mceph/+</sup>* are either yellow or colorless. We found that loss of  $K_v1.1$  function in neural progenitors increases the number of neurons but not glia in the hippocampus, revealing that  $K_v1.1$  expression in neural stem cells (NSCs) regulates neuronal production [29].

The hippocampus is one of two regions in the adult mouse brain with a well-characterized neurogenic niche. In the subgranular zone, there are different types of well-characterized NSCs and neural progenitor cells (NPCs) in the neurogenesis lineage. Radial glia-like neural stem cells (RGLs / Type 1) divide to either self-renew or differentiate into highly proliferative intermediate progenitor cells with a more glial-like phenotypes (Type 2a). Type 2a cells further differentiate into intermediate progenitor cells with limited proliferative potential and more neuronal-like features (Type 2b). Afterwards, Type 2b cells generate neuroblasts (Type 3) that produce post-mitotic immature neurons [30-32].



In Chapter 2, we investigated the role of  $K_v1.1$  in early postnatal hippocampal neurogenesis in  $K_v1.1$  null mice, before seizure onset. We found that neonatal NSCs and NPCs have distinct membrane potentials as they progress through the stages of neurogenesis, which is regulated by the expression of  $K_v1.1$ . In  $K_v1.1$  null mice, NPCs are more depolarized and proliferative compared to those in  $K_v1.1$  wildtype mice. Because increased BDNF mRNA expression was observed in  $K_v1.1$  null mice [23], we hypothesized that depolarization of NPCs increased their proliferation through TrkB signaling. Indeed, when TrkB signaling was blocked either pharmacologically or through genetic deletion, proliferation was suppressed in the  $K_v1.1$  null mice [33]. Our study showed that  $K_v1.1$  regulates neuron production during neonatal hippocampal development.

However, the dynamics of postnatal hippocampal neurogenesis are age-dependent. During the first postnatal week of hippocampal development, NSCs and NPCs in the subgranular zone undergo extensive proliferation to generate dentate granule cells that survive long-term—only beginning apoptosis 2 months after birth [34, 35]. This process peaks around postnatal day 7 [36-38]. Afterwards, adult neurogenesis continues at a lower level, decreasing until 4 months of age before dropping again at 7 months of age [39]. Neurons born during adulthood go through two critical periods for survival within 4-6 weeks post-mitosis, and indeed such adult-born neurons have been found to be important for memory encoding and retrieval [30-32, 40, 41].

Therefore, we sought to determine whether  $K_v1.1$  acts similarly to restrain proliferation during adult hippocampal neurogenesis in Chapter 3. We created  $K_v1.1$  conditional knockout ( $K_v1.1$  cKO) mice to specifically delete  $K_v1.1$  in adult NSCs. Using this mouse model, we found that  $K_v1.1$

regulates early steps of adult hippocampal neurogenesis by maintaining the balance between RGL activation and quiescence to prevent RGL depletion. In later stages of neurogenesis, loss of  $K_v1.1$  in NSCs produces newborn neurons with impaired maturation and positioning, resulting in decreased adult neurogenesis in  $K_v1.1$  cKO mice. Consistent with these findings, we also observed that  $K_v1.1$  cKO mice have deficits in hippocampal-dependent learning and memory. Together, these results show that  $K_v1.1$  expression in adult NSCs enables healthy adult neurogenesis. Because neurogenesis is dysregulated in aging and disease, determining the role of  $K_v1.1$  in adult neurogenesis may represent an important first step towards identifying new therapeutic targets that can be leveraged to promote healthy neurogenesis and cognition throughout life.

## 1.2 References

1. Hodgkin, A.L. and A.F. Huxley, *The components of membrane conductance in the giant axon of Loligo*. J Physiol, 1952. **116**(4): p. 473-96.
2. Hodgkin, A.L. and A.F. Huxley, *A quantitative description of membrane current and its application to conduction and excitation in nerve*. J Physiol, 1952. **117**(4): p. 500-44.
3. Papazian, D.M., et al., *Cloning of genomic and complementary DNA from Shaker, a putative potassium channel gene from Drosophila*. Science, 1987. **237**(4816): p. 749-53.
4. Tempel, B.L., Y.N. Jan, and L.Y. Jan, *Cloning of a probable potassium channel gene from mouse brain*. Nature, 1988. **332**(6167): p. 837-9.
5. Kuo, M.M., et al., *Prokaryotic K<sup>+</sup> channels: from crystal structures to diversity*. FEMS Microbiol Rev, 2005. **29**(5): p. 961-85.
6. Littleton, J.T. and B. Ganetzky, *Ion channels and synaptic organization: analysis of the Drosophila genome*. Neuron, 2000. **26**(1): p. 35-43.
7. Gutman, G.A., et al., *International Union of Pharmacology. LIII. Nomenclature and molecular relationships of voltage-gated potassium channels*. Pharmacol Rev, 2005. **57**(4): p. 473-508.
8. Hille, B., *Ion channels of excitable membranes*. 3rd ed. 2001, Sunderland, Mass.: Sinauer. xviii, 814
9. Stuhmer, W., et al., *Molecular basis of functional diversity of voltage-gated potassium channels in mammalian brain*. EMBO J, 1989. **8**(11): p. 3235-44.
10. Gonzalez, C., et al., *K<sup>+</sup> channels: function-structural overview*. Compr Physiol, 2012. **2**(3): p. 2087-149.

11. Isacoff, E.Y., L.Y. Jan, and D.L. Minor, Jr., *Conduits of life's spark: a perspective on ion channel research since the birth of neuron*. *Neuron*, 2013. **80**(3): p. 658-74.
12. Jan, L.Y. and Y.N. Jan, *Voltage-gated and inwardly rectifying potassium channels*. *J Physiol*, 1997. **505 ( Pt 2)**: p. 267-82.
13. Jan, L.Y. and Y.N. Jan, *Voltage-gated potassium channels and the diversity of electrical signalling*. *J Physiol*, 2012. **590**(11): p. 2591-9.
14. Brew, H.M., J.L. Hallows, and B.L. Tempel, *Hyperexcitability and reduced low threshold potassium currents in auditory neurons of mice lacking the channel subunit  $K_v1.1$* . *J Physiol*, 2003. **548**(Pt 1): p. 1-20.
15. Robbins, C.A. and B.L. Tempel,  *$K_v1.1$  and  $K_v1.2$ : similar channels, different seizure models*. *Epilepsia*, 2012. **53 Suppl 1**: p. 134-41.
16. Smart, S.L., et al., *Deletion of the  $K_v1.1$  potassium channel causes epilepsy in mice*. *Neuron*, 1998. **20**(4): p. 809-19.
17. Foust, A.J., et al., *Somatic membrane potential and  $K_v1$  channels control spike repolarization in cortical axon collaterals and presynaptic boutons*. *J Neurosci*, 2011. **31**(43): p. 15490-8.
18. Storm, J.F., *Temporal integration by a slowly inactivating  $K^+$  current in hippocampal neurons*. *Nature*, 1988. **336**(6197): p. 379-81.
19. Donahue, L.R., et al., *Megencephaly: a new mouse mutation on chromosome 6 that causes hypertrophy of the brain*. *Mamm Genome*, 1996. **7**(12): p. 871-6.
20. Persson, A.S., et al., *A truncated  $K_v1.1$  protein in the brain of the megencephaly mouse: expression and interaction*. *BMC Neurosci*, 2005. **6**: p. 65.

21. Petersson, S., et al., *Truncation of the Shaker-like voltage-gated potassium channel,  $K_v1.1$ , causes megencephaly*. Eur J Neurosci, 2003. **18**(12): p. 3231-40.
22. Almgren, M., et al., *Lack of potassium channel induces proliferation and survival causing increased neurogenesis and two-fold hippocampus enlargement*. Hippocampus, 2007. **17**(4): p. 292-304.
23. Diez, M., et al., *MRI and in situ hybridization reveal early disturbances in brain size and gene expression in the megencephalic (mceph/mceph) mouse*. Eur J Neurosci, 2003. **18**(12): p. 3218-30.
24. Hallows, J.L. and B.L. Tempel, *Expression of  $K_v1.1$ , a Shaker-like potassium channel, is temporally regulated in embryonic neurons and glia*. J Neurosci, 1998. **18**(15): p. 5682-91.
25. Persson, A.S., et al.,  *$K_v1.1$  null mice have enlarged hippocampus and ventral cortex*. BMC Neurosci, 2007. **8**: p. 10.
26. Pardo, L.A., *Voltage-gated potassium channels in cell proliferation*. Physiology (Bethesda), 2004. **19**: p. 285-92.
27. Almgren, M., M. Schalling, and C. Lavebratt, *Idiopathic megalencephaly-possible cause and treatment opportunities: from patient to lab*. Eur J Paediatr Neurol, 2008. **12**(6): p. 438-45.
28. Holth, J.K., et al., *Tau loss attenuates neuronal network hyperexcitability in mouse and *Drosophila* genetic models of epilepsy*. J Neurosci, 2013. **33**(4): p. 1651-9.
29. Yang, S.B., et al.,  *$K_v1.1$ -dependent control of hippocampal neuron number as revealed by mosaic analysis with double markers*. J Physiol, 2012. **590**(11): p. 2645-58.

30. Bond, A.M., G.L. Ming, and H. Song, *Adult Mammalian Neural Stem Cells and Neurogenesis: Five Decades Later*. Cell Stem Cell, 2015. **17**(4): p. 385-95.
31. Goncalves, J.T., S.T. Schafer, and F.H. Gage, *Adult Neurogenesis in the Hippocampus: From Stem Cells to Behavior*. Cell, 2016. **167**(4): p. 897-914.
32. Ming, G.L. and H. Song, *Adult neurogenesis in the mammalian brain: significant answers and significant questions*. Neuron, 2011. **70**(4): p. 687-702.
33. Chou, S.M., et al., *Kv1.1 channels regulate early postnatal neurogenesis in mouse hippocampus via the TrkB signaling pathway*. Elife, 2021. **10**.
34. Cahill, S.P., et al., *Early survival and delayed death of developmentally-born dentate gyrus neurons*. Hippocampus, 2017. **27**(11): p. 1155-1167.
35. Ciric, T., S.P. Cahill, and J.S. Snyder, *Dentate gyrus neurons that are born at the peak of development, but not before or after, die in adulthood*. Brain Behav, 2019. **9**(10): p. e01435.
36. Li, G. and S.J. Pleasure, *The development of hippocampal cellular assemblies*. Wiley Interdiscip Rev Dev Biol, 2014. **3**(2): p. 165-77.
37. Morales, A.V. and H. Mira, *Adult Neural Stem Cells: Born to Last*. Front Cell Dev Biol, 2019. **7**: p. 96.
38. Noguchi, H., et al., *Suppressor of fused controls perinatal expansion and quiescence of future dentate adult neural stem cells*. Elife, 2019. **8**.
39. Ben Abdallah, N.M., et al., *Early age-related changes in adult hippocampal neurogenesis in C57 mice*. Neurobiol Aging, 2010. **31**(1): p. 151-61.
40. Anacker, C. and R. Hen, *Adult hippocampal neurogenesis and cognitive flexibility - linking memory and mood*. Nat Rev Neurosci, 2017. **18**(6): p. 335-346.

41. Toda, T., et al., *The role of adult hippocampal neurogenesis in brain health and disease.*  
Mol Psychiatry, 2019. **24**(1): p. 67-87.

## **Chapter 2**

### **K<sub>v</sub>1.1 channels regulate early postnatal neurogenesis in mouse hippocampus via the TrkB signaling pathway**



## 2.1 Introduction

In mammals, the majority of neurons in the central nervous system are generated during embryonic development, and postnatal neurogenesis is limited to only a few brain regions, such as the subgranular zone (SGZ) of the dentate gyrus and the subventricular zone (SVZ) of the lateral ventricles [1]. Neural progenitor cells in the SGZ are categorized into different developmental stages based on distinct cellular functions, and cells of each stage can be identified by the expression of specific cell-fate markers. For example, type 1 radial glia-like neural stem cells have the potential for self-renewal and mostly stay quiescent; these cells are positive for Brain Lipid Binding Protein (BLBP), Glial Fibrillary Acidic Protein (GFAP), and nestin. Another widely used neural stem cell marker is Sox2, a transcription factor that is essential for maintaining stem cell pluripotency. Type 1 cells undergo asymmetric cell division to generate highly proliferative type 2a neural progenitor cells, which are double-positive for Sox2 and Tbr2, transcription factors that control cell proliferation and differentiation. Type 2a cells then generate proliferative but lineage-restricted type 2b neural progenitor cells, which express Tbr2 and doublecortin (DCX) [2-4]. Type 2b cells exhibit limited mitotic potential [2], and after two to five rounds of mitosis, these progenitor cells differentiate into immature neurons [5]. In the adult SGZ, the newly generated granule cells contribute to memory formation, likely by facilitating the ability to distinguish similar patterns, a learning process referred to as pattern separation [6]. Importantly, postnatal neurogenesis is tightly regulated by the balance between self-renewal and differentiation [3]. While the regulation of these processes by intrinsic transcription factors has been studied extensively [7], the impacts of membrane potential and ion channels on postnatal neurogenesis are much less clear [8, 9].

Ion channels are expressed in almost all cell types, including highly proliferative stem cells and cancers; however, many ion channel-expressing cell types are considered to be electrically non-excitable [8, 10, 11]. The type 1 stem cells in the SGZ display an immense passive conductance comprised of connexin-based gap junctions [12, 13] as well as  $K_{ir}4.1$ - and  $K_{ir}5.1$ -mediated glial-type inwardly rectifying potassium channels [14]. This passive conductance renders neural stem cells unable to fire action potentials [8, 9]. In addition to the passive conductance, neural stem cells and progenitor cells also exhibit various features of active conductance, such as voltage-gated potassium channels [10, 11], and to a lesser extent, calcium channels [15, 16]. One such voltage-gated potassium channel expressed in the embryonic brain and postnatal neural stem cells is  $K_v1.1$  [11, 17]. This channel is found mainly in mature neurons [18], and it is predominantly localized in axons due to microtubule End-Binding 1 (EB1)-directed targeting [17, 19]. Functionally,  $K_v1.1$  is best-known for its role in tuning action potential firing patterns by regulating the duration of the repolarization phase [20-22]. Mutations of the  $K_v1.1$  channel cause various neurological disorders, such as epilepsy and episodic ataxia, in humans and mouse models [23-26]. Moreover, since  $K_v1.1$  can be activated at a relatively low voltage (near the resting potential), it has been suggested that this potassium channel could modulate membrane electrical properties such as the membrane potential in various cell types, including non-excitable neural progenitor cells [20, 22, 27].

$K_v1.1$  channel, the product of the gene *Kcna1*, is thought to regulate postnatal neurogenesis since megencephaly mice (*mceph*) lacking functional  $K_v1.1$  channels have enhanced adult neurogenesis that leads to enlargement of the hippocampi [28]. However, the mechanism of this action is largely unknown. Many ion channels are widely expressed in the central nervous system, and their

mutations may either directly influence both neural progenitor cells and their progeny neurons (cell-autonomous) or indirectly affect neural progenitor cells by modulating the excitability of mature neurons (non-cell-autonomous) [29, 30]. Whereas seizures resulting from the loss of K<sub>v</sub>1.1 function may impact postnatal neurogenesis [31, 32], our previous study using mosaic analysis with double markers (MADM) [33, 34] on heterozygous *mceph* mice without seizures revealed that K<sub>v</sub>1.1 regulates postnatal neurogenesis via a cell-autonomous mechanism [35]. To avoid the potentially confounding effects of seizures, which start by 3–4 weeks of age in K<sub>v</sub>1.1-null (*Kcna1*<sup>-/-</sup>) mice, we focused on early postnatal neurogenesis in the current study. We first showed that K<sub>v</sub>1.1 affects early postnatal neurogenesis without having a detectable impact on embryonic neurogenesis. Then, we searched for the molecular and physiological mechanisms that mediate the K<sub>v</sub>1.1-dependent postnatal neurogenesis in mouse hippocampus. Our results indicated that K<sub>v</sub>1.1 cell-autonomously modulates the membrane excitability of type 2b neural progenitor cells and TrkB signaling, which accounts for increased proliferating neural progenitor cells in K<sub>v</sub>1.1 KO mice.

## 2.2 Results

### *K<sub>v</sub>1.1 regulates postnatal neuron generation in a cell-autonomous manner*

The K<sub>v</sub>1.1 channel is widely expressed throughout the entire central nervous system [17], and the loss of K<sub>v</sub>1.1 function in mice homozygous for either the *megencephaly* mutation or the K<sub>v</sub>1.1-null mutation (K<sub>v</sub>1.1 KO) causes seizures, starting 3 weeks after birth [25, 36]. Our previous study in 3-month-old *Kcna1*<sup>mceph/+</sup> mice carrying the MADM-6 b cassettes (*Rosa26*<sup>TG/GT</sup>) showed that K<sub>v</sub>1.1 acts cell-autonomously to regulate the number of neuronal progeny [35]. We further carried out the MADM study in *Kcna1*<sup>-/-</sup> mice, which did not show signs of seizures before reaching adulthood (Figure 2.1). We first generated Nestin-cre; *Kcna1*<sup>-/-</sup>; MADM-6 quadruple transgenic mice that carried Nestin-cre, *Kcna1*<sup>-/-</sup>, *Rosa26*<sup>TG</sup>, and *Rosa26*<sup>GT</sup>. Nestin-Cre mediated somatic recombination in a subset of neural progenitor cells that carried the MADM-6 cassettes, and the daughter cells bearing the *Kcna1*<sup>-/-</sup> alleles were labeled with green fluorescent protein (GFP) (green), while the wild-type sibling daughter cells were labeled with tdTomato (red) (Figure 2.1A-D). Comparable numbers of green K<sub>v</sub>1.1 KO neurons and red wild-type neurons were observed in 1-month-old Nestin-cre; *Kcna1*<sup>+/-</sup>; MADM-6 mice; however, a significantly larger number of green K<sub>v</sub>1.1 KO neurons was found in 2- to 3-month-old Nestin-cre; *Kcna1*<sup>+/-</sup>; MADM-6 mice compared to wild-type controls (Figure 2.1E). As expected for granule cells born postnatally, the newly generated green K<sub>v</sub>1.1 KO neurons were located farther from the SGZ in the granule cell layer (Figure 2.1F). Unlike adult-born neurons, which gradually decrease in number over the course of a month owing to apoptosis, developmentally-born neurons generated during late embryogenesis and early postnatal stages typically survive for more than 2 months before the onset of cell death; generation and maturation of these neurons take about 1 month, with those generated early in life located farther from the SGZ [37-40]. Thus, the MADM experiments revealed an

overproduction of developmentally born neurons from  $K_v1.1$  KO neural progenitor cells in early postnatal stages.

To test whether  $K_v1.1$  function is essential for neurogenesis during embryogenesis, we examined embryos with or without  $K_v1.1$  and found no significant difference in the numbers of hippocampal progenitors or neurons at E16.5 (Supplementary figure 2.1). We also analyzed interneurons expressing parvalbumin (PV) or somatostatin (SST) in the dentate gyrus and found no significant difference between mice with or without  $K_v1.1$  at P10 (Supplementary figure 2.2). Taken together, our experiments indicate that  $K_v1.1$  functions in postnatal neural progenitors of the SGZ to regulate the production of neuronal progeny during the first 3 months of life, raising the question regarding the mechanisms underlying this process.

### ***Functional expression of $K_v1.1$ in SGZ neural progenitor cells***

$K_v1.1$  is highly expressed throughout the entire central nervous system [18]. Given that neural progenitor cells only account for a small fraction of total cells in the brain, we decided to utilize *Fezf2*-GFP reporter mice to specifically examine neural stem cells and progenitor cells in the SGZ [41]. The majority of the *Fezf2*-GFP-positive cells in the SGZ co-expressed BLBP and GFAP, two well-established neural stem cell markers [42]. We also found that  $K_v1.1$  mRNA was expressed in the granule cell layer of the dentate gyrus (red dots, Figure 2.2A); a portion of the  $K_v1.1$  mRNA signal was in close proximity to the GFP mRNA (green dots), which indicates *Fezf2*-GFP neural progenitor cells in the SGZ (Figure 2.2A, B). To further corroborate this finding, we performed immunostaining to determine the distribution pattern of the  $K_v1.1$  protein in the mouse dentate gyrus. We found that  $K_v1.1$  protein was highly expressed in mature granule cells and interneurons

as reported previously [18, 43]. A closer look further revealed the presence of  $K_v1.1$  in  $DCX^+$  cells but not in  $Sox2^+$  cells, thereby confirming the expression of  $K_v1.1$  in late-stage neural progenitor cells (Figure 2.2C).

Next, we wanted to determine whether  $K_v1.1$  protein could form functional potassium channels in the  $Fezf2$ -GFP-positive cells. As  $K_v1.1$ -mediated potassium currents can be inactivated by holding at relatively high voltages ( $> -50$  mV) [22] and are sensitive to dendrotoxin-K (DTX-K) [44], a potent blocker of  $K_v1$  family channels, we performed whole-cell patch-clamp recording in wild-type (Figure 2.2D-F) and  $K_v1.1$  KO (Figure 2.2F, G, I)  $Fezf2$ -GFP-positive cells. We could detect DTX-K-sensitive and low-voltage inactivated potassium currents in wild-type but not  $K_v1.1$  KO (Figure 2.2J)  $Fezf2$ -GFP+ cells. These findings reveal that  $K_v1.1$  forms functional channels in  $Fezf2$ -GFP neural progenitor cells.

### ***Loss of $K_v1.1$ depolarizes a subset of the neural progenitor cells in SGZ***

Next, we looked into the impact of removing  $K_v1.1$  from  $Fezf2$ -GFP cells at different developmental stages (Figure 2.3A). This experiment was performed within the first postnatal month to avoid complications from seizures that begin later in life. We sought to evaluate quiescent  $Sox2^+$  type 1 radial glia-like stem cells, highly proliferative  $Sox2^+Tbr2^+$  type 2a neural progenitor cells, and type 2b neural progenitor cells that only express  $Tbr2$ . Based on the expression of cell-type markers, we first calculated the proportions of these three cell types among  $Fezf2$ -GFP cells. We found a high proportion of  $Tbr2^+$ -only type 2b neural progenitor cells in  $K_v1.1$  KO SGZ compared to wild type (Figure 2.3B, C, arrowheads). These results suggested that the presence of  $K_v1.1$  limits the number of late-stage neural progenitor cells.

Voltage-gated potassium channels are known to be involved in regulating action potential waveforms and firing frequencies, but this type of channel plays only minor roles in tuning passive properties such as the resting membrane potential [45]. For example, neurons lacking functional  $K_v1.1$  display normal resting potentials but elevated action potential firing rates [26, 46]. To test whether the loss of  $K_v1.1$  affects the membrane potential of neural progenitor cells, we recorded from *Fezf2*-GFP cells and POMC-GFP immature neurons, as the *Pomc*-GFP transgenic line faithfully labels immature neurons in the dentate gyrus [47]. In addition, a previous study has shown that the radial glia-like cells are coupled by gap junctions that are essential for adult neurogenesis in the SGZ [12]. In order to label the recorded neural progenitor cells in brain slices, we included a gap-junction-permeable tracer neurobiotin in the pipette solution (Figure 2.4, A3-F3, and Figure 2.5A). After whole-cell patch-clamp recording to characterize the membrane properties, the brain slices were fixed with 4% paraformaldehyde (PFA). The cell-type identity of the recorded cell was characterized by examining the expression of cell-fate markers (Figure 2.3A). The membrane potentials of these cells were hyperpolarized and electrically silent; notably, the current injection could cause depolarization of POMC-GFP immature neurons but not firing of action potentials, while such depolarization of mature granule neurons could lead to action potential firing (data not shown). Remarkably, the *Tbr2*<sup>+</sup>/*Fezf2*<sup>+</sup> type 2b neural progenitor cells lacking  $K_v1.1$  displayed more depolarized resting membrane potentials than their wild-type counterparts (Figure 2.4G). Moreover, we found that type 2a progenitor cells were coupled via gap junctions (Figure 2.4B, E), a property that has not been reported previously.

Although we have obtained convincing results showing that the type 2b neural progenitor cells lacking  $K_v1.1$  channels were more depolarized, the invasive nature of the patch-clamp technique caused more than 70% of the recorded cells to be either damaged or lost during the subsequent immunostaining procedure, and therefore, their developmental stages were not determined. We tried to classify those *Fezf2*-GFP-positive cells based on their resting membrane potential, input resistance, and membrane capacitance, the three basic biophysical characteristics obtained from patch-clamp recording (Figure 2.5). First, we used the biophysical characteristics of cells with unequivocal cell-type identification determined by post-hoc immunostaining as a training dataset (Figure 2.4G) to construct separate multinomial logistic regression models for wild-type and  $K_v1.1$  KO cells [48]. The probability of each cell belonging to a given cell type was calculated by fitting biophysical characteristics to the models: resting membrane potentials (Figure 2.5D), input resistance (Figure 2.5E), and membrane capacitance (Figure 2.5F). We found that more than 80% of the *Fezf2*-GFP-positive cells with known cell types could be accurately predicted using this regression model. Interestingly, judging from the gap-junction-permeable neurobiotin labeling, we noticed that cells from the same subtypes clustered closely together (Figure 2.5B, C). Of note, type 1 neural stem cells tended to have a more hyperpolarized resting membrane potential, lower input resistance, and larger membrane capacitance, while type 2b neural progenitor cells tended to have more depolarized resting membrane potentials, higher input resistance, and smaller membrane capacitance. The cell type was then assigned based on the highest probability. Consistent with the results shown in Figure 2.4G, we found that the assigned type 2b neural progenitor cells lacking  $K_v1.1$  channel were also significantly more depolarized than their wild-type counterparts. Nevertheless, both the input resistance (Figure 2.5E) and membrane capacitance (Figure 2.5F) were comparable between wild-type and  $K_v1.1$  KO cells. To validate the progenitor classification



and reveal the cell membrane properties, we plotted  $I$ - $V$  curves for the three subgroups, as classified by the multinomial logistic regression model. Similar to the results of a previous study using progenitor cell recording [49], type 1 neural stem cells characteristically displayed passive, non-inactivating currents with a linear current–voltage relationship (Figure 2.5J, M), similar to the properties of astrocytes. In contrast, type 2b neural progenitor cells expressed small outwardly rectifying currents (Figure 2.5L, M). Of note, in 9 out of 25 type 2b neural progenitor cells, we observed transient inward currents induced by depolarizations more positive than -30 mV, followed by outwardly rectifying currents; these observations are indicative of sodium currents, hence consistent with neuronal differentiation (Figure 2.5P). The delayed outward rectifying currents in type 2b neural progenitor cells were more apparent when characterized by means of leak subtraction (Figure 2.5P, O). Moreover, the electrophysiological features of type 2a neural progenitor cells were suggestive of a transition phase between type 1 neural stem cells and type 2b neural progenitor cells, since type 2a neural progenitor cells displayed outwardly rectifying currents but no detectable sodium currents (Figure 2.5K, M).

### ***K<sub>v</sub>1.1 regulates neural progenitor cell number via the TrkB signaling pathway***

A previous work has shown that suppressing TrkB signaling by removing brain-derived neurotrophic factor (BDNF) from neural progenitor cells drastically reduces the thickness of the dentate gyrus granule cell layer [50], while enhancing TrkB signaling by overexpressing BDNF in neural progenitor cells augments neurogenesis [51]. Notably, increased BDNF expression has been found in the K<sub>v</sub>1.1 KO mouse brains [52]. Carbamazepine, an anti-epileptic drug, could antagonize this increase of BDNF levels and also suppress the excessive neurogenesis in SGZ in adult K<sub>v</sub>1.1 KO mice [53]. We hypothesized that the excessive depolarization of type 2b neural progenitor

cells lacking  $K_v1.1$  (Figure 2.4G and Figure 2.5G) might stimulate neural progenitor cell proliferation by elevating the level of TrkB signaling. Restrained with the antibody incompatibility for double labeling, we stained the neural progenitor cells in SGZ with antibodies against phospho-TrkB (Tyr816), together with either Sox2 or Tbr2. We found most of the phospho-TrkB-positive cells within the SGZ region (Figure 2.6, Supplementary figure 2.3, and Supplementary figure 2.4), and a greater number of phospho-TrkB-positive cells in the dentate gyrus of  $K_v1.1$  KO mice as compared to the wild-type mice (Figure 2.6). Moreover, phospho-TrkB was found primarily in Tbr2<sup>+</sup> or DCX<sup>+</sup> cells (Figure 2.6B and Supplementary figure 2.3) but rarely in Sox2<sup>+</sup> cells (Figure 2.6A and Supplementary figure 2.3), despite the fact that the expression levels of TrkB receptor are higher in type 1 neural progenitor cells [54]. Not only did the loss of  $K_v1.1$  cause an increase of Tbr2<sup>+</sup> cells with phospho-TrkB signals, but also the phospho-TrkB signals in the Tbr2<sup>+</sup> cells were much more intense in the  $K_v1.1$  KO mice, suggesting that the TrkB signaling pathway was activated in the Tbr2-expressing type 2b cells in  $K_v1.1$  KO mice (Figure 2.3).

To test whether antagonizing TrkB activity could reduce the hyperplastic effect of  $K_v1.1$  on adult neurogenesis, we performed daily intraperitoneal injections of GNF-5837 (20 mg/kg), a brain-permeable Trk inhibitor [55], into mice for 3 weeks starting at the first postnatal week. This 3-week GNF-5837 treatment was sufficient to suppress TrkB signaling, as the phospho-TrkB levels were drastically reduced in the hippocampus (Supplementary figure 2.4). Both Fezf2-GFP-positive cells and Ki67-positive cells in  $K_v1.1$  KO and control mice were comparable in number after this GNF-5837 treatment (Figure 2.7B-D). By contrast, age-matched  $K_v1.1$  KO mice receiving vehicle-only injection had significantly more Fezf2-GFP- and Ki67-positive cells in the SGZ than those in control mice (Figure 2.7A-C), in agreement with a previous report [56]. Thus,

pharmacological inhibition of Trk receptors prevented the increase of neural progenitor cells in the SGZ of K<sub>v</sub>1.1 KO mice.

If K<sub>v</sub>1.1 channels limit neural progenitor cell proliferation, K<sub>v</sub>1.1 KO neural progenitor cells should generate larger clones than controls. To estimate the clone size, we generated *Gli1*<sup>creERT2/+</sup>; *Ntrk2*<sup>flox/flox</sup>; *Rosa26*<sup>Tom/+</sup> and *Gli1*<sup>creERT2/+</sup>; *Ntrk2*<sup>flox/+</sup>; *Rosa26*<sup>Tom/+</sup> mice in the background of either wild-type or K<sub>v</sub>1.1 KO. These quadruple transgenic mouse lines carried a tamoxifen-inducible Cre- recombinase *Gli1*<sup>creERT2</sup> that can sparsely delete the floxed-*Ntrk2* gene that encodes the TrkB receptor in the neural stem cells and progenitor cells of the SGZ in the presence of tamoxifen. The Cre- dependent TdTomato reporter (*Rosa26*<sup>Tom</sup>) was used to label tamoxifen-activated CreER recombinase cells and their progeny [57, 58]. We intraperitoneally injected 3-week-old mice with a single dose of tamoxifen (0.5 mg/kg) to delete the floxed-*Ntrk2* in the SGZ, and the clone sizes were estimated at 8 weeks of age. A single clone was defined as encompassing all the cells within a 100-μm radius of the clone center [58]. Indeed, TrkB deletion abolished the hyperplastic phenotype in K<sub>v</sub>1.1 KO mice, as *Kcna1*<sup>-/-</sup>; *Gli1*<sup>creERT2/+</sup>; *Ntrk2*<sup>flox/+</sup>; *Rosa26*<sup>Tom/+</sup> mice had larger clone sizes than *Gli1*<sup>creERT2/+</sup>; *Ntrk2*<sup>flox/+</sup>; *Rosa26*<sup>Tom/+</sup>, *Kcna1*<sup>-/-</sup>; *Gli1*<sup>creERT2/+</sup>; *Ntrk2*<sup>flox/flox</sup>; *Rosa26*<sup>Tom/+</sup>, and *Gli1*<sup>creERT2/+</sup>; *Ntrk2*<sup>flox/flox</sup>; *Rosa26*<sup>Tom/+</sup> mice (Figure 2.7E and Supplementary figure 2.5). The cumulative clone-size plots further confirmed a rightward skewness distribution rather than just an outlier bias (red trace) in *Kcna1*<sup>-/-</sup>; *Gli1*<sup>creERT2/+</sup>; *Ntrk2*<sup>flox/+</sup>; *Rosa26*<sup>Tom/+</sup> mice, and this shift was not observed for the neural progenitor cells lacking TrkB receptors (green trace) (Figure 2.7F).

## 2.3 Discussion

In this study, we have shown that  $K_v1.1$ , a voltage-gated potassium channel, functions as a brake to fine-tune the rate of neurogenesis in mouse dentate gyrus within the first 2 months of postnatal life. Removing the  $K_v1.1$  channel depolarized the late-stage neural progenitor cells that exhibit high input resistance and small capacitance (Figure 2.5), presumably the transit-amplifying type 2b neural progenitor cells (Figure 2.4D). Depolarization of type 2b neural progenitor cells causes cell-autonomous over-activation of the TrkB signaling pathway that promotes neural progenitor cell proliferation. Consequently, mice lacking functional  $K_v1.1$  develop a megencephalic phenotype at early postnatal stages, as the neural progenitor cells without  $K_v1.1$  over-proliferate due to elevated TrkB signaling (Figure 2.8).

In the central nervous system, mature neurons are capable of generating action potentials, while neural progenitor cells and immature neurons are considered electrically non-excitabile and do not fire action potentials [8, 59]. In this study, our electrophysiological characterization of postnatal neural progenitors raised the possibility that alterations in membrane potential could impact postnatal neurogenesis. Although neural progenitor cells are not electrically excitable, these cells do express a variety of ion channels [11, 60]. The radial glia-like type 1 neural stem cells express high levels of glial inwardly rectifying potassium channels, mostly  $K_{ir}4.1$  and  $K_{ir}5.1$  [14]. In addition to the inwardly rectifying potassium channels, type 1 neural stem cells in the SGZ are electrically coupled via gap junctions formed by connexins (Figure 2.4) [12, 13] Both inwardly rectifying potassium channels and gap junctions contribute to the extremely low input resistance in type 1 cells (Figure 2.5E, H) and keep these neural stem cells hyperpolarized (Figure 2.4D and 2.5D, G). Once a type 1 cell commits to the neural progenitor cell fate, it will leave the extensive

network of type 1 radial glia-like neural stem cells that are electrically coupled via gap junctions, as evidenced by the reduced capacitance and increased input resistance. Eventually, type 2b neural progenitor cells lose all gap junction connections and exist as single cells. Our multinomial logistic regression models faithfully depicted this process; when cells transitioned from the hyperpolarized network of quiescent type 1 neural stem toward individual highly proliferative type 2b neural progenitor cells, the input resistance was gradually increased, and the membrane capacitance was decreased due to the loss of gap junction coupling (Figure 2.5E, F, H, I). Moreover, our regression model provides a simple method for studying neural progenitor cell physiology. We showed that the identity of the neural progenitor cells within the SGZ could be accurately predicted based on the membrane potential, input resistance, and membrane capacitance obtained from patch-clamp recording, and there was no further need for post-hoc immunostaining of cell-type markers, a time-consuming procedure with a low success rate.

Among all voltage-gated potassium channels, the  $K_v1$  family is crucial for regulating the resting membrane potential, as  $K_v1$  channels can be activated at subthreshold membrane potentials [44, 61]. Although  $K_v1.1$  is expressed in most cells in the dentate gyrus, especially the inhibitory interneurons (yellow arrows, Figure 2.2C) [62], we only observed significant depolarization of type 2b neural progenitor cells lacking  $K_v1.1$  (Figure 2.4G and 2.5D, G). One plausible explanation for this specificity of effect is that the type 1 stem cells and type 2a neural progenitor cells remain hyperpolarized by the immense inwardly rectifying potassium currents and are further stabilized by the extensive electrical coupling through gap junctions. As stipulated by the Goldman-Hodgkin-Katz equation [63], conditions of low input resistance and large capacitance (Figure 2.5E, F, H, I) will diminish the effect of voltage-gated channels, such as  $K_v1.1$ , on the membrane potential to

negligible levels. By contrast, a small potassium conductance could be sufficient to keep cells with higher input resistance and smaller capacitance at relatively hyperpolarized membrane potentials.

Despite decades of extensive studies on postnatal neurogenesis, how ion channels and membrane potentials affect neurogenesis remains an intriguing open question. Ion channels have been shown to regulate postnatal and adult neurogenesis via both environmental (non-cell-autonomous) and intrinsic (cell-autonomous) mechanisms. Several studies have found that neural circuits may regulate the neural stem cell fate via non-cell-autonomous synaptic mechanisms. For example, increased gamma aminobutyric acid (GABA) tone of hippocampal parvalbumin-expressing interneurons facilitates the transition of radial glia-like cells into a quiescent state via  $\gamma$ 2-containing GABA<sub>A</sub> receptors expressed in SGZ neural stem cells [64]. Furthermore, moderate activation of indirect glutamatergic mossy cells increases the radial glia-like stem cell quiescence [65]. On the other hand, several voltage-gated ion channels regulate neurogenesis in a cell-autonomous manner. Deleting *Paralytic*, the only voltage-gated sodium channel in *Drosophila*, shrinks the brain lobes due to reduced proliferation and enhanced apoptosis in type I and type II neuroblasts [29]. Moreover, in addition to regulating progenitor cell proliferation, hyperpolarization of progenitor cells in the cortex by inwardly rectifying potassium channels shifts neurogenesis from direct corticogenesis to indirect corticogenesis via suppression of WNT (Wingless-related integration site) activity [66]. In our study, the affected type 2b neural progenitor cells had already lost gap junctions and displayed high input resistance, so the minuscule K<sub>v</sub>1.1 window current may be sufficient to keep wild-type but not K<sub>v</sub>1.1 KO type 2b neural progenitor cells hyperpolarized (Figure 2.4G and 2.5) [67]. This finding further raises the possibility that the plasticity of neurogenesis can be affected by bioelectric membrane properties [68].

One intriguing question concerns how membrane depolarization might activate the TrkB receptor in a cell-autonomous manner. The canonical ligands that activate the TrkB receptor are BDNF, released via the regulated secretory pathway, and neurotrophin 4/5 (NT4/5), released via the constitutive secretory pathway [69]. BDNF is a plausible candidate for the endogenous neurotrophin that mediates the  $K_v1.1$ -dependent postnatal neurogenesis in mouse hippocampus, because BDNF is the only neurotrophin that has been detected in the SGZ in the mouse brain, and genetic deletion of NT4/5 did not impair adult neurogenesis [54]. BDNF plays a multifaceted role in the central nervous system, including promoting synaptogenesis, axonal guidance, dendrite outgrowth, and postnatal neurogenesis [70-72]. Depolarizing the neural progenitor cells may elevate the intracellular calcium level through the voltage-gated calcium channels, which could trigger BDNF release via activating the SNARE complex [16, 73, 74]. Furthermore, the unique biochemical properties of BDNF may allow such a diffusible signaling molecule to act cell-autonomously in regulating neurogenesis in mouse hippocampus. BDNF is a sticky peptide with multiple positively charged residues, and therefore, BDNF has a limited range of diffusion upon release [75]. In brain slices, BDNF only acts within 4.5 mm of its release site, which is less than the diameter of a single neural progenitor cell [76]. Hence, depolarization of the neural progenitor cells could release BDNF to activate TrkB signaling in a cell-autonomous manner due to its short effective range. Interestingly, GABA, another diffusible factor, has also been shown to cell-autonomously regulate neurogenesis in adult hippocampus. GABA activates the inhibitory  $GABA_A$  receptors on the same neural progenitor cells by involving the GABA transporter VGAT. Removal of this inhibitory GABA signaling promotes neural progenitor cell proliferation by shortening the cell cycle via activation of S-phase checkpoint kinases and the histone variant

H2AX [77]. Moreover, deleting a subset of GABA<sub>A</sub> receptors in neural progenitor cells not only stimulates neurogenesis, but also alters the positioning of newborn neurons in adult hippocampus, reminiscent of our finding that K<sub>v</sub>1.1 KO neurons are positioned farther away from the SGZ (Figure 2.1F) [78]. Consistent with our results, over-activation of BDNF modulates the positioning in the SGZ of granule cells generated during early postnatal stages [39, 79]. Nevertheless, we cannot exclude the possible involvement of other signaling pathways, such as GSK3b and DISC1, since disrupting these signaling pathways causes failures of guidance for newborn neuron migration and positioning [80, 81].

Given that previous studies have shown that TrkB receptors can be activated by mechanisms other than the neurotrophins, the elevated TrkB signaling we observed in K<sub>v</sub>1.1 KO mice could be BDNF-independent. For example, membrane depolarization itself could activate TrkB via elevating the intracellular cAMP levels, which has been demonstrated in cultured neurons previously [82]. Under certain circumstances, TrkB receptors can also be auto-activated in the absence of neurotrophins by increasing the receptor abundance [83]. The immature form of TrkB receptor that lacks N-glycosylation on the extracellular domain is constitutively active, even if it is located intracellularly; the membrane potential could indirectly regulate TrkB activity by tuning the cellular glycosylation process [83, 84]. Moreover, TrkB receptors can also be transactivated via crosstalk with certain G-protein-coupled receptors, such as EGF [85] and adenosine A2a receptors [86]. Lastly, TrkB signaling can be elevated by increasing *Ntrk2* gene expression [87]. It will be of interest to pursue experiments to investigate whether these mechanisms are involved in K<sub>v</sub>1.1- dependent postnatal neurogenesis in mouse hippocampus.



One important limitation of our study is the age of animals we used. To avoid the confounding effects of seizures that begin in 3- to 4-week-old  $K_v1.1$  KO mice, we focused our study on early postnatal neurogenesis. A recent work using virally labeled neural progenitor cells in the SGZ has revealed a massive burst of postnatal neurogenesis within the first week, as evidenced by viral labeling of neural progenitor cells at P6; these neurons persist for about 2 months before undergoing apoptosis, a time course distinct from adult-born neurons produced later in life [88]. Our study of young mice describes the involvement of  $K_v1.1$  in the generation of neurons by neural progenitor cells beginning in the first postnatal week. How the loss of  $K_v1.1$  function affects neurogenesis later in life will require further study.

In summary, our study has uncovered a unique role of  $K_v1.1$  in regulating neurogenesis within the postnatal dentate gyrus during the first 2 months of life. Alterations in adult neurogenesis in the dentate gyrus have been reported for patients with psychiatric and neurological diseases [2, 89], and recent studies have suggested that neural progenitor cells might be potential targets for treating neurodegenerative disorders such as Alzheimer's disease and Parkinson's disease [90]. Thus, our findings regarding  $K_v1.1$  modulation of early postnatal neurogenesis may help lay the groundwork for future identification of novel therapeutic targets for neurodegenerative and psychiatric diseases [91].

## 2.4 Methods

### *Animals*

This study was carried out in strict accordance with the recommendations found in the Guide for the Care and Use of Laboratory Animals of the National Institutes of Health. The experimental protocols were approved by the Institutional Animal Care and Use Committee of Academia Sinica (protocol #: 15-01-813) and the University of California, San Francisco. Mice (3–5 per cage) were housed in the animal facility and fed with a regular chow diet on a standard 12 hr light/12 hr dark cycle. At least three animals were used for every experimental group. The *Kcna1*<sup>-</sup> mice were obtained from Dr. Bruce Tempel's lab at the University of Washington, USA. *Rosa26*<sup>GT</sup> (*Gt(ROSA)26*<sup>Sortm6</sup>(ACTB-EGFP\*, -tdTomato)) and *Rosa26*<sup>TG</sup> (*Gt(ROSA)26*<sup>Sortm7</sup>(ACTB-EGFP\*)), two transgenic mouse lines for producing MADM-6 mice, were obtained from Dr. Liqun Luo's lab at Stanford University, USA. The *Ntrk2*<sup>fllox</sup> mice were obtained from Dr. Louis Reichardt's lab at the University of California, San Francisco, USA. POMC-GFP (*Tg(Pomc-EGFP)1*) mice were obtained from Dr. Jeffery Friedman's lab at Rockefeller University, USA. *Fezf2*-GFP (*Tg(Fezf2-EGFP)CO61Gsat*) mice were obtained from Dr. Su Guo's lab at the University of California, San Francisco, USA. *Nestin-cre* (*Tg(Nes-cre)1Kln*), *Gli1*<sup>creERT2</sup> (*Gli1*<sup>tm3(cre/ERT2)</sup>), and *Rosa26*<sup>Tom</sup> (*Gt(ROSA)26*<sup>Sortm14</sup>(CAG-tdTomato)) mice were obtained from Jackson Laboratory (Bar Harbor, Maine, USA). All mice were maintained on an ICR (Institute of Cancer Research) background. GNF-5837 (Tocris, UK) was dissolved in dimethyl sulfoxide (DMSO) (Sigma, USA), and then diluted in a solvent composed of 65% PEG400 (Sigma, USA) and 35% Cremophor EL (Sigma, USA) for intraperitoneal injection.

## *Electrophysiology*

Brain slices (250  $\mu$ m thickness) containing the hippocampus were prepared as described previously [92]. Mice were first anesthetized with isoflurane and then decapitated. The brain was swiftly removed and placed in cutting solution: 110 mM choline chloride, 25 mM NaHCO<sub>3</sub>, 11 mM glucose, 2.5 mM KCl, 1.25 mM NaH<sub>2</sub>PO<sub>4</sub>, 11.6 mM sodium ascorbate, 3.1 mM sodium pyruvate, 7 mM MgCl<sub>2</sub>, and 0.5 mM CaCl<sub>2</sub>, equilibrated with 95% O<sub>2</sub>/5% CO<sub>2</sub>. Brain slices were obtained from tissue immersed in the cutting solution using a compresstome (Precisionary Instruments, USA). Slices were then incubated in artificial cerebrospinal fluid (aCSF): 126 mM NaCl, 21.4 mM NaHCO<sub>3</sub>, 10 mM glucose, 2.5 mM KCl, 1.25 mM NaH<sub>2</sub>PO<sub>4</sub>, 1.2 mM MgCl<sub>2</sub>, and 2 mM CaCl<sub>2</sub>, equilibrated with 95% O<sub>2</sub>/5% CO<sub>2</sub>. An Axon700B amplifier (Molecular Devices Corp, USA) was used to measure membrane currents and membrane capacitance in the standard whole-cell patch-clamp configuration. Data were acquired at 5 kHz with Clampex10 software (Molecular Devices Corp, USA). The intracellular solution contained 135 mM potassium gluconate, 15 mM KCl, 10 mM HEPES, 5 mM Mg<sub>2</sub>ATP, 1 mM Na<sub>3</sub>GTP, 10 mM sodium phosphocreatine, and 0.05 mM EGTA; pH was adjusted to 7.2 with KOH. Dendrotoxin-k (Alomone Labs, Israel) was used to specifically block the K<sub>v</sub>1.1 channel. Pipettes were pulled from 1.5 mm borosilicate glass capillaries (Sutter Inc, USA) and had a resistance of 3–5 MW when filled with the intracellular solution; data were excluded from further analyses if the series resistance was higher than 20 MW and the holding current at -70 mV was lower than -100 pA. All experiments were performed at room temperature.

## ***Immunostaining***

Mice were fed ad libitum and were anesthetized with intraperitoneal Zoletil/Xylazine injection before transcardial perfusion with saline followed by 4% PFA. Brains were removed and post-fixed overnight in 4% PFA. Brains were then cryoprotected overnight in saline containing 30% sucrose at 4°C until they sank. For antigen retrieval, the brain sections (16 mm) were boiled in sodium citrate buffer (10 mM sodium citrate, 0.05% Tween 20, pH 6.0) between 95 and 100°C for 20 min. After the buffer was cooled to room temperature, the samples were further processed. The brain sections were washed in a blocking medium containing 0.1% Triton X-100 and 5% donkey serum (Jackson ImmunoResearch Laboratories), and incubated overnight (4°C) with primary antibodies against GFP (chicken, 1:400; Aves, USA), Sox2 (mouse IgG2b, 1:400; Millipore, USA), Ctip2 (rabbit, 1:500; Abcam, USA), Tbr2 (rabbit, 1:400; Abcam, USA.), Tbr2 (chicken, 1:400; Millipore, USA), Doublecortin (rabbit, 1:400; Cell Signaling, USA), Kv1.1 (1:200; Antibodies Inc, USA), phospho-TrkB (rabbit, 1:200; Millipore, USA), or Ki67 (rabbit, 1:500; Invitrogen, USA), followed by Alexa dye-tagged secondary antibodies (donkey 1:100; Invitrogen, USA). For immunostaining of samples after electrophysiology recording, the brain slices were fixed in 4% PFA at 4°C for 2 hr. The internal solution contained Neurobiotin (0.3%, MW: 367 Da; Vector Laboratories, USA) and Lucifer yellow-conjugated dextrans (0.2%, MW: 10 kDa; Invitrogen, USA) to respectively label gap junction-coupled cells and recorded cells. The slices were washed three times at room temperature for 40 min in 0.3% Triton X-100 and 3% Bovine Serum Albumin (BSA) (Sigma Aldrich, USA) for blocking and permeabilization, followed by incubation overnight at 4°C with Neutravidin (0.25%; Thermo Fisher Scientific, USA) and primary antibodies against GFP (chicken, 1:400; Aves, USA), Sox2 (mouse IgG2b, 1:400; Millipore, USA) or Tbr2 (rabbit, 1:400; Abcam, USA). Secondary antibodies conjugated with goat anti-rabbit IgG

Alexa 405, goat anti-chicken IgG Alexa 488, and goat anti-mouse IgG2b Alexa 633 were purchased from Invitrogen. The slides were mounted using Fluoromount G mounting medium containing 4',6-diamidino-2-phenylindole (DAPI) (Southern Biotech, USA), and images were acquired using a confocal microscope (Zeiss, Germany).

### ***In situ hybridization***

The mouse brains were frozen and sectioned, as previously described [93]. Sections were fixed with chilled 4% PFA for 15 min and then washed with 0.1 M phosphate buffered saline (PBS) twice. Sections were then dehydrated with 50% ethanol, 70% ethanol, and 100% ethanol sequentially. Slides were treated with protease and then incubated with a customized probe for 2 hr. Signal was detected using Probe-Mm-GFP and Probe-Mm-Kcna and further amplified by RNAscope Fluorescent Multiplex Kit (Advanced Cell Diagnostics, USA). Images were acquired using a confocal microscope (Zeiss, Germany).

### ***Clonal analysis***

The clonal analysis was performed as described previously [58]. Briefly, for sparsely labeling the progenitor cells, 3-week-old mice carrying *Gli1<sup>creERT2</sup>*; *Rosa26<sup>Tom</sup>* with wild-type or *Kcna1<sup>-/-</sup>* and *Ntrk2<sup>flox/flox</sup>* or *Ntrk2<sup>flox/+</sup>* were injected with a single dose of 0.5 mg/kg of tamoxifen (Sigma, USA) dissolved in corn oil (Sigma, USA). At 8 weeks of age, mice were killed by an intraperitoneal injection of 150 mg/kg Zoletil + 20 mg/kg xylazine. Both hippocampi were dissected out and fixed overnight in a PBS solution containing 4% PFA. The hippocampi were rendered transparent in scale 0 for 2 days at 37°C, and then transferred to scale 4 for 1 day at 4°C (Hama *et al.*, 2015). The whole-mount hippocampus was imaged in 3D using a Zeiss LSM700 confocal microscope system

(Zeiss, Germany). Imaris9.7 (Oxford Instruments, Switzerland) was used to identify TdTomato-positive neural progenitor cells. The clonal clusters were defined as the TdTomato-positive cells within 100- $\mu$ m radius of the clone center, as illustrated in Supplementary figure 2.4 [58].

### ***Multinomial logistic regression classification of cell types***

To classify cells and make associations between cell type and resting membrane potentials, input resistance and membrane capacitance, we applied the multinomial logistic regression model as follows:

$$\frac{P(C=c|X=x)}{P(C=0|X=x)} = \exp(\beta_{c,0} + x_1\beta_{c,1} + x_2\beta_{c,2} + x_3\beta_{c,3}), \quad c=1,2,$$

where  $C = 0, 1, 2$  represents type 1, 2a, and 2b cells, respectively, and  $X = (X_1, X_2, X_3)$  represents the centralized and standardized ( $\log C_m, \log R_m, V_m$ ). By using a standard maximum likelihood estimation, the estimated coefficients are

$$(\beta_{1,0}, \beta_{1,1}, \beta_{1,2}, \beta_{1,3}, \beta_{2,0}, \beta_{2,1}, \beta_{2,2}, \beta_{2,3}) = (-0.343, -1.067, -1.317, 1.681, -3.074, -2.746, 0.782, 1.359)$$

for wildtype cells and

$$(\beta_{1,0}, \beta_{1,1}, \beta_{1,2}, \beta_{1,3}, \beta_{2,0}, \beta_{2,1}, \beta_{2,2}, \beta_{2,3}) = (0.567, -1.373, -0.051, 0.302, -5.353, -6.935, -1.626, 5.549)$$

for  $K_v1.1$  KO cells.

Each cell was then assigned to the class with the highest probability  $P(C=c|X=x)$ ,  $c=0,1,2$ . Based on the estimated coefficients, it appeared that smaller values of  $C_m$  and larger values of  $V_m$  were associated with a higher probability of being type 2b neural progenitor cells than being type 1 neural stem cells.

### ***Statistical analyses***

For immunostaining experiments, cell counts were performed on two to three images per mouse, and *n*-values indicate numbers of different mice, except for the assessment of clonal analysis, where *n*-values correspond to numbers of different clonal pools from four to six mice per genotype. For electrophysiological experiments, *n*-values correspond to numbers of different cells from each individual brain slice. Statistical analyses were performed with Prism software (Graphpad, USA) or R Project for Statistical Computing (The R Foundation, USA). Two-way ANOVA with Sidak's multiple comparisons post-hoc test, one-way ANOVA with Tukey's test, Mann-Whitney *U*-test, or Student's *t*-test for pair-wise comparisons were used as appropriate.  $p < 0.05$  was considered statistically significant.

## **2.5 Acknowledgments**

We thank Drs. Su Guo (University of California, San Francisco), Bruce Tempel (University of Washington), Liqun Luo (Stanford University), and Hui Zong (University of Oregon) for providing transgenic mice. We thank the outstanding technical supports provided by the Neuroimaging core facility of the Neuroscience Program, Microscopy facility and Electrophysiology facility of the Institute of Biomedical Sciences, Academia Sinica. This work was supported by the Institute of Biomedical Sciences at Academia Sinica and the Ministry of Science and Technology (106-2320-B-001-013 and 107-2320-B-001-026-MY3 to SBY) and by the National Institute of Health (R01MH065334 to LYJ). YNJ and LYJ are Howard Hughes Medical Institute investigators.



## 2.6 References

1. Kriegstein, A. and A. Alvarez-Buylla, *The glial nature of embryonic and adult neural stem cells*. *Annu Rev Neurosci*, 2009. **32**: p. 149-84.
2. Goncalves, J.T., S.T. Schafer, and F.H. Gage, *Adult Neurogenesis in the Hippocampus: From Stem Cells to Behavior*. *Cell*, 2016. **167**(4): p. 897-914.
3. Ming, G.L. and H. Song, *Adult neurogenesis in the mammalian brain: significant answers and significant questions*. *Neuron*, 2011. **70**(4): p. 687-702.
4. Spampanato, J., et al., *Properties of doublecortin expressing neurons in the adult mouse dentate gyrus*. *PLoS One*, 2012. **7**(9): p. e41029.
5. Gao, P., et al., *Deterministic progenitor behavior and unitary production of neurons in the neocortex*. *Cell*, 2014. **159**(4): p. 775-88.
6. Sahay, A., et al., *Increasing adult hippocampal neurogenesis is sufficient to improve pattern separation*. *Nature*, 2011. **472**(7344): p. 466-70.
7. Aimone, J.B., et al., *Regulation and function of adult neurogenesis: from genes to cognition*. *Physiol Rev*, 2014. **94**(4): p. 991-1026.
8. Fukuda, S., et al., *Two distinct subpopulations of nestin-positive cells in adult mouse dentate gyrus*. *J Neurosci*, 2003. **23**(28): p. 9357-66.
9. Swayne, L.A. and L. Wicki-Stordeur, *Ion channels in postnatal neurogenesis: potential targets for brain repair*. *Channels (Austin)*, 2012. **6**(2): p. 69-74.
10. Bates, E., *Ion channels in development and cancer*. *Annu Rev Cell Dev Biol*, 2015. **31**: p. 231-47.
11. Shin, J., et al., *Single-Cell RNA-Seq with Waterfall Reveals Molecular Cascades underlying Adult Neurogenesis*. *Cell Stem Cell*, 2015. **17**(3): p. 360-72.

12. Kunze, A., et al., *Connexin expression by radial glia-like cells is required for neurogenesis in the adult dentate gyrus*. Proc Natl Acad Sci U S A, 2009. **106**(27): p. 11336-41.
13. Rozental, R., et al., *Changes in the properties of gap junctions during neuronal differentiation of hippocampal progenitor cells*. J Neurosci, 1998. **18**(5): p. 1753-62.
14. Yasuda, T., P.F. Bartlett, and D.J. Adams, *K<sub>ir</sub> and K<sub>v</sub> channels regulate electrical properties and proliferation of adult neural precursor cells*. Mol Cell Neurosci, 2008. **37**(2): p. 284-97.
15. D'Ascenzo, M., et al., *Role of L-type Ca<sup>2+</sup> channels in neural stem/progenitor cell differentiation*. Eur J Neurosci, 2006. **23**(4): p. 935-44.
16. Xu, J., et al., *T-type calcium channel enhancer SAK3 produces anti-depressant-like effects by promoting adult hippocampal neurogenesis in olfactory bulbectomized mice*. J Pharmacol Sci, 2018. **137**(4): p. 333-341.
17. Hallows, J.L. and B.L. Tempel, *Expression of K<sub>v</sub>1.1, a Shaker-like potassium channel, is temporally regulated in embryonic neurons and glia*. J Neurosci, 1998. **18**(15): p. 5682-91.
18. Wang, H., et al., *Localization of K<sub>v</sub>1.1 and K<sub>v</sub>1.2, two K channel proteins, to synaptic terminals, somata, and dendrites in the mouse brain*. J Neurosci, 1994. **14**(8): p. 4588-99.
19. Gu, C., et al., *The microtubule plus-end tracking protein EBI is required for K<sub>v</sub>1 voltage-gated K<sup>+</sup> channel axonal targeting*. Neuron, 2006. **52**(5): p. 803-16.
20. Foust, A.J., et al., *Somatic membrane potential and K<sub>v</sub>1 channels control spike repolarization in cortical axon collaterals and presynaptic boutons*. J Neurosci, 2011. **31**(43): p. 15490-8.

21. Jan, L.Y. and Y.N. Jan, *Voltage-gated potassium channels and the diversity of electrical signalling*. J Physiol, 2012. **590**(11): p. 2591-9.
22. Storm, J.F., *Temporal integration by a slowly inactivating K<sup>+</sup> current in hippocampal neurons*. Nature, 1988. **336**(6197): p. 379-81.
23. Beraud, E., et al., *Block of neural K<sub>v</sub>1.1 potassium channels for neuroinflammatory disease therapy*. Ann Neurol, 2006. **60**(5): p. 586-96.
24. Heeroma, J.H., et al., *Episodic ataxia type 1 mutations differentially affect neuronal excitability and transmitter release*. Dis Model Mech, 2009. **2**(11-12): p. 612-9.
25. Petersson, S., et al., *Truncation of the Shaker-like voltage-gated potassium channel, K<sub>v</sub>1.1, causes megencephaly*. Eur J Neurosci, 2003. **18**(12): p. 3231-40.
26. Robbins, C.A. and B.L. Tempel, *K<sub>v</sub>1.1 and K<sub>v</sub>1.2: similar channels, different seizure models*. Epilepsia, 2012. **53 Suppl 1**: p. 134-41.
27. Sundelacruz, S., M. Levin, and D.L. Kaplan, *Depolarization alters phenotype, maintains plasticity of predifferentiated mesenchymal stem cells*. Tissue Eng Part A, 2013. **19**(17-18): p. 1889-908.
28. Persson, A.S., et al., *K<sub>v</sub>1.1 null mice have enlarged hippocampus and ventral cortex*. BMC Neurosci, 2007. **8**: p. 10.
29. Piggott, B.J., et al., *Paralytic, the Drosophila voltage-gated sodium channel, regulates proliferation of neural progenitors*. Genes Dev, 2019. **33**(23-24): p. 1739-1750.
30. Espinosa, J.S., et al., *Uncoupling dendrite growth and patterning: single-cell knockout analysis of NMDA receptor 2B*. Neuron, 2009. **62**(2): p. 205-17.

31. Almgren, M., M. Schalling, and C. Lavebratt, *Idiopathic megalencephaly-possible cause and treatment opportunities: from patient to lab*. Eur J Paediatr Neurol, 2008. **12**(6): p. 438-45.
32. Holth, J.K., et al., *Tau loss attenuates neuronal network hyperexcitability in mouse and Drosophila genetic models of epilepsy*. J Neurosci, 2013. **33**(4): p. 1651-9.
33. Muzumdar, M.D., L. Luo, and H. Zong, *Modeling sporadic loss of heterozygosity in mice by using mosaic analysis with double markers (MADM)*. Proc Natl Acad Sci U S A, 2007. **104**(11): p. 4495-500.
34. Zong, H., et al., *Mosaic analysis with double markers in mice*. Cell, 2005. **121**(3): p. 479-92.
35. Yang, S.B., et al., *Kv1.1-dependent control of hippocampal neuron number as revealed by mosaic analysis with double markers*. J Physiol, 2012. **590**(11): p. 2645-58.
36. Donahue, L.R., et al., *Megencephaly: a new mouse mutation on chromosome 6 that causes hypertrophy of the brain*. Mamm Genome, 1996. **7**(12): p. 871-6.
37. Cahill, S.P., et al., *Early survival and delayed death of developmentally-born dentate gyrus neurons*. Hippocampus, 2017. **27**(11): p. 1155-1167.
38. Dayer, A.G., et al., *Short-term and long-term survival of new neurons in the rat dentate gyrus*. J Comp Neurol, 2003. **460**(4): p. 563-72.
39. Kerloch, T., et al., *Dentate Granule Neurons Generated During Perinatal Life Display Distinct Morphological Features Compared With Later-Born Neurons in the Mouse Hippocampus*. Cereb Cortex, 2019. **29**(8): p. 3527-3539.
40. Toni, N. and A.F. Schinder, *Maturation and Functional Integration of New Granule Cells into the Adult Hippocampus*. Cold Spring Harb Perspect Biol, 2015. **8**(1): p. a018903.

41. Gong, S., et al., *A gene expression atlas of the central nervous system based on bacterial artificial chromosomes*. Nature, 2003. **425**(6961): p. 917-25.
42. Berberoglu, M.A., et al., *Heterogeneously expressed fezf2 patterns gradient Notch activity in balancing the quiescence, proliferation, and differentiation of adult neural stem cells*. J Neurosci, 2014. **34**(42): p. 13911-23.
43. Grosse, G., et al., *Expression of K<sub>v</sub>1 potassium channels in mouse hippocampal primary cultures: development and activity-dependent regulation*. J Neurosci, 2000. **20**(5): p. 1869-82.
44. Grissmer, S., et al., *Pharmacological characterization of five cloned voltage-gated K<sup>+</sup> channels, types K<sub>v</sub>1.1, 1.2, 1.3, 1.5, and 3.1, stably expressed in mammalian cell lines*. Mol Pharmacol, 1994. **45**(6): p. 1227-34.
45. Corbin-Leftwich, A., et al., *A Xenopus oocyte model system to study action potentials*. J Gen Physiol, 2018. **150**(11): p. 1583-1593.
46. Smart, S.L., et al., *Deletion of the K<sub>v</sub>1.1 potassium channel causes epilepsy in mice*. Neuron, 1998. **20**(4): p. 809-19.
47. Overstreet, L.S., et al., *A transgenic marker for newly born granule cells in dentate gyrus*. J Neurosci, 2004. **24**(13): p. 3251-9.
48. Fahrmeir, L. and G. Tutz, *Introduction*, in *Multivariate Statistical Modelling Based on Generalized Linear Models*, L. Fahrmeir and G. Tutz, Editors. 1994, Springer New York: New York, NY. p. 1-13.
49. Steiner, B., et al., *Type-2 cells as link between glial and neuronal lineage in adult hippocampal neurogenesis*. Glia, 2006. **54**(8): p. 805-14.

50. Li, Y., et al., *TrkB regulates hippocampal neurogenesis and governs sensitivity to antidepressive treatment*. *Neuron*, 2008. **59**(3): p. 399-412.
51. Quesseveur, G., et al., *BDNF overexpression in mouse hippocampal astrocytes promotes local neurogenesis and elicits anxiolytic-like activities*. *Transl Psychiatry*, 2013. **3**: p. e253.
52. Diez, M., et al., *MRI and in situ hybridization reveal early disturbances in brain size and gene expression in the megencephalic (mceph/mceph) mouse*. *Eur J Neurosci*, 2003. **18**(12): p. 3218-30.
53. Lavebratt, C., et al., *Carbamazepine protects against megencephaly and abnormal expression of BDNF and Nogo signaling components in the mceph/mceph mouse*. *Neurobiol Dis*, 2006. **24**(2): p. 374-83.
54. Vilar, M. and H. Mira, *Regulation of Neurogenesis by Neurotrophins during Adulthood: Expected and Unexpected Roles*. *Front Neurosci*, 2016. **10**: p. 26.
55. Albaugh, P., et al., *Discovery of GNF-5837, a Selective TRK Inhibitor with Efficacy in Rodent Cancer Tumor Models*. *ACS Medicinal Chemistry Letters*, 2012. **3**(2): p. 140-145.
56. Almgren, M., et al., *Lack of potassium channel induces proliferation and survival causing increased neurogenesis and two-fold hippocampus enlargement*. *Hippocampus*, 2007. **17**(4): p. 292-304.
57. Li, G., et al., *The ventral hippocampus is the embryonic origin for adult neural stem cells in the dentate gyrus*. *Neuron*, 2013. **78**(4): p. 658-72.
58. Singh, S.P., et al., *Clonal Analysis of Newborn Hippocampal Dentate Granule Cell Proliferation and Development in Temporal Lobe Epilepsy*. *eNeuro*, 2015. **2**(6).
59. Bean, B.P., *The action potential in mammalian central neurons*. *Nat Rev Neurosci*, 2007. **8**(6): p. 451-65.

60. Yamashita, M., *Ion channel activities in neural stem cells of the neuroepithelium*. Stem Cells Int, 2012. **2012**: p. 247670.
61. Dodson, P.D., M.C. Barker, and I.D. Forsythe, *Two heteromeric Kv1 potassium channels differentially regulate action potential firing*. J Neurosci, 2002. **22**(16): p. 6953-61.
62. Li, M., et al., *A TRPC1-mediated increase in store-operated Ca<sup>2+</sup> entry is required for the proliferation of adult hippocampal neural progenitor cells*. Cell Calcium, 2012. **51**(6): p. 486-96.
63. Hille, B., *Ion channels of excitable membranes*. 3rd ed. 2001, Sunderland, Mass.: Sinauer. xviii, 814 p.
64. Song, J., et al., *Neuronal circuitry mechanism regulating adult quiescent neural stem-cell fate decision*. Nature, 2012. **489**(7414): p. 150-4.
65. Yeh, C.Y., et al., *Mossy Cells Control Adult Neural Stem Cell Quiescence and Maintenance through a Dynamic Balance between Direct and Indirect Pathways*. Neuron, 2018. **99**(3): p. 493-510 e4.
66. Vitali, I., et al., *Progenitor Hyperpolarization Regulates the Sequential Generation of Neuronal Subtypes in the Developing Neocortex*. Cell, 2018. **174**(5): p. 1264-1276 e15.
67. Maylie, B., et al., *Episodic ataxia type 1 mutations in the human Kv1.1 potassium channel alter hKvβ1-induced N-type inactivation*. J Neurosci, 2002. **22**(12): p. 4786-93.
68. Sundelacruz, S., M. Levin, and D.L. Kaplan, *Role of membrane potential in the regulation of cell proliferation and differentiation*. Stem Cell Rev Rep, 2009. **5**(3): p. 231-46.
69. Bothwell, M., *NGF, BDNF, NT3, and NT4*. Handb Exp Pharmacol, 2014. **220**: p. 3-15.
70. Jan, Y.N. and L.Y. Jan, *Branching out: mechanisms of dendritic arborization*. Nat Rev Neurosci, 2010. **11**(5): p. 316-28.

71. Jeanneteau, F., et al., *The MAP kinase phosphatase MKP-1 regulates BDNF-induced axon branching*. Nat Neurosci, 2010. **13**(11): p. 1373-9.
72. Liu, P.Z. and R. Nusslock, *Exercise-Mediated Neurogenesis in the Hippocampus via BDNF*. Front Neurosci, 2018. **12**: p. 52.
73. Shimojo, M., et al., *SNAREs Controlling Vesicular Release of BDNF and Development of Callosal Axons*. Cell Rep, 2015. **11**(7): p. 1054-66.
74. Wong, Y.H., et al., *Activity-dependent BDNF release via endocytic pathways is regulated by synaptotagmin-6 and complexin*. Proc Natl Acad Sci U S A, 2015. **112**(32): p. E4475-84.
75. Sasi, M., et al., *Neurobiology of local and intercellular BDNF signaling*. Pflugers Arch, 2017. **469**(5-6): p. 593-610.
76. Mandl, S., et al., *Investigation on plasma immersion ion implantation treated medical implants*. Biomol Eng, 2002. **19**(2-6): p. 129-32.
77. Andang, M., et al., *Histone H2AX-dependent GABA<sub>A</sub> receptor regulation of stem cell proliferation*. Nature, 2008. **451**(7177): p. 460-4.
78. Duveau, V., et al., *Spatiotemporal specificity of GABA<sub>A</sub> receptor-mediated regulation of adult hippocampal neurogenesis*. Eur J Neurosci, 2011. **34**(3): p. 362-73.
79. Scharfman, H., et al., *Increased neurogenesis and the ectopic granule cells after intrahippocampal BDNF infusion in adult rats*. Exp Neurol, 2005. **192**(2): p. 348-56.
80. Duan, X., et al., *Disrupted-In-Schizophrenia 1 regulates integration of newly generated neurons in the adult brain*. Cell, 2007. **130**(6): p. 1146-58.



81. Ng, T., et al., *Neuropilin 2 signaling is involved in cell positioning of adult-born neurons through glycogen synthase kinase-3 $\beta$  (GSK3 $\beta$ )*. Journal of Biological Chemistry, 2016. **291**(48): p. 25088-25095.
82. Meyer-Franke, A., et al., *Depolarization and cAMP elevation rapidly recruit TrkB to the plasma membrane of CNS neurons*. Neuron, 1998. **21**(4): p. 681-93.
83. Gupta, R., et al., *Constitutively active TrkB kinase signalling reduces actin filopodia dynamics and cell migration*. bioRxiv, 2020.
84. Watson, F.L., et al., *TrkA glycosylation regulates receptor localization and activity*. J Neurobiol, 1999. **39**(2): p. 323-36.
85. Puehringer, D., et al., *EGF transactivation of Trk receptors regulates the migration of newborn cortical neurons*. Nat Neurosci, 2013. **16**(4): p. 407-15.
86. Lee, F.S. and M.V. Chao, *Activation of Trk neurotrophin receptors in the absence of neurotrophins*. Proc Natl Acad Sci U S A, 2001. **98**(6): p. 3555-60.
87. Yamashita, R., et al., *Induction of cellular senescence as a late effect and BDNF-TrkB signaling-mediated ameliorating effect on disruption of hippocampal neurogenesis after developmental exposure to lead acetate in rats*. Toxicology, 2021. **456**: p. 152782.
88. Ciric, T., S.P. Cahill, and J.S. Snyder, *Dentate gyrus neurons that are born at the peak of development, but not before or after, die in adulthood*. Brain Behav, 2019. **9**(10): p. e01435.
89. Sahay, A. and R. Hen, *Adult hippocampal neurogenesis in depression*. Nat Neurosci, 2007. **10**(9): p. 1110-5.

90. Christie, K. and A. Turnley, *Regulation of endogenous neural stem/progenitor cells for neural repair-factors that promote neurogenesis and gliogenesis in the normal and damaged brain*. *Frontiers in cellular neuroscience*, 2013. **6**: p. 70.
91. Christian, K.M., H. Song, and G.L. Ming, *Functions and dysfunctions of adult hippocampal neurogenesis*. *Annu Rev Neurosci*, 2014. **37**: p. 243-62.
92. Yang, S.B., et al., *Rapamycin ameliorates age-dependent obesity associated with increased mTOR signaling in hypothalamic POMC neurons*. *Neuron*, 2012. **75**(3): p. 425-36.
93. Li, K.X., et al., *TMEM16B regulates anxiety-related behavior and GABAergic neuronal signaling in the central lateral amygdala*. *Elife*, 2019. **8**.

## 2.7 Main Figures

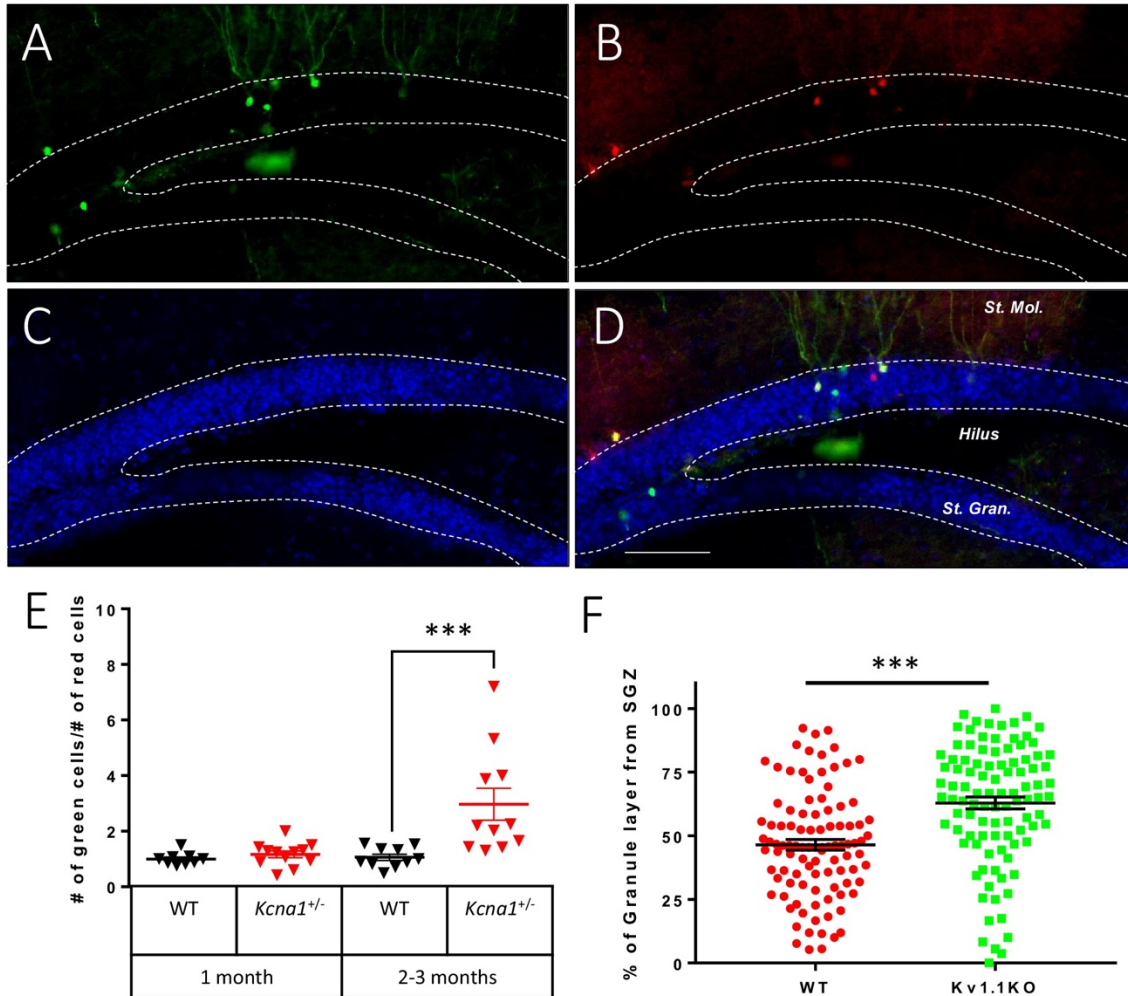


**Figure 2.1: K<sub>v</sub>1.1 channels control dentate gyrus neuron number in a cell-autonomous manner.** Mosaic analysis with double markers (MADM) of the dentate gyrus in wild-type or *Kcna1*<sup>+/-</sup> mice. K<sub>v</sub>1.1 KO and wild-type neurons can be respectively identified as green (GFP) (A) and red (TdTomato) (B) neurons. (C) DAPI counterstain. (D) Overlay of signals in (A) and (B), scale bar = 100 μm. (E) Statistical analysis of the red wild-type and green K<sub>v</sub>1.1 KO neurons in the dentate gyrus. The numbers of red wild-type and green K<sub>v</sub>1.1 KO neurons were comparable in the dentate gyrus of 1-month-old mice; however, compared to the numbers of red wild-type neurons, the numbers of green K<sub>v</sub>1.1 KO neurons were much higher in the dentate gyrus of 2- to 3-month-old mice (two-way ANOVA followed by Sidak's multiple comparisons test,  $p = 0.0008$ , for 2- to 3-month-old mice).  $n = 9-12$  for each group. (F) Compared to the red wild-type neurons, green K<sub>v</sub>1.1 KO neurons were more often positioned farther away from the SGZ in 2- to 3-month-old mice, indicating that the green K<sub>v</sub>1.1 KO neurons were born in the postnatal period. ( $p = 0.0002$ , Mann-Whitney *U*-test).  $n = 100$  for each group.

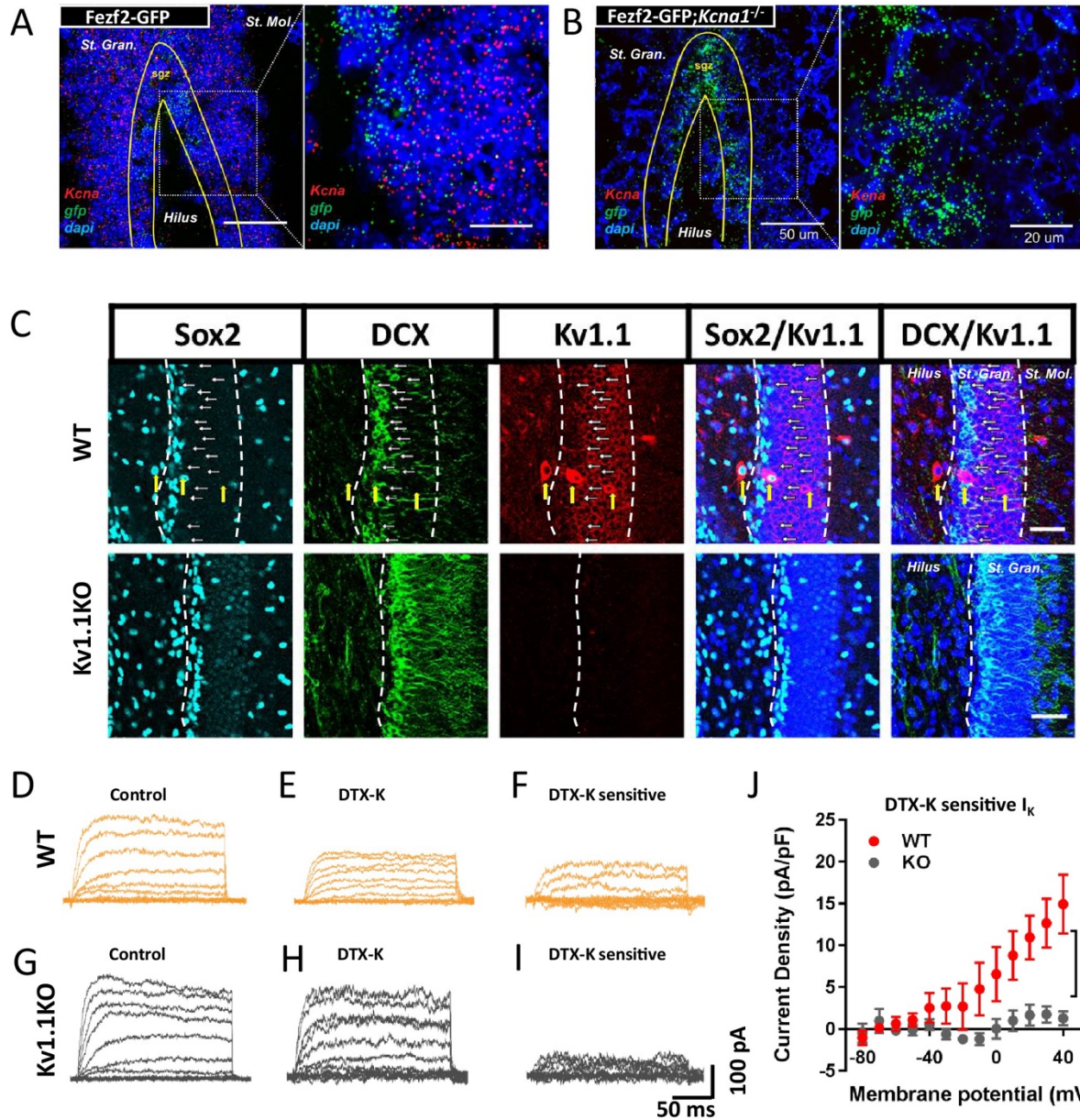


**Figure 2.2: Functional expression of  $K_v1.1$  channel in SGZ neural progenitor cells expressing Fezf2-GFP at postnatal 2 weeks.** (A) In situ hybridization results showed that *Kcna1* mRNA is expressed in Fezf2-GFP-positive neural progenitor cells. Inset is displayed at higher magnification. (B) *Kcna1* mRNA was not detected in the  $K_v1.1$  KO mouse, which served as a negative control. (C)  $K_v1.1$  protein was expressed in the doublecortin (DCX)-expressing late-stage neural progenitor cells (arrows) but not Sox2-positive early-stage neural progenitor cells.  $K_v1.1$  protein was highly expressed in the inhibitory interneurons (yellow arrows). (D-J) Pharmacological isolation of  $K_v1$  currents in Fezf2-GFP-positive cells.  $K_v1.1$  currents were elicited by trains of voltage steps from -80 mV to +40 mV in 10 mV increments from the holding potential of -80 mV in the absence (D and G) or presence of the  $K_v1$ -specific blocker dendrotoxin-k (DTX-K; 100 nM) (E and H). The DTX-K sensitive currents were considered  $K_v1$ -mediated potassium current (F, I and J), which were much reduced in the  $K_v1.1$  KO mice.  $n = 4$  cells from each phenotype. Scale bar = 20  $\mu$ m in (C). Data are presented as mean  $\pm$  SEM.

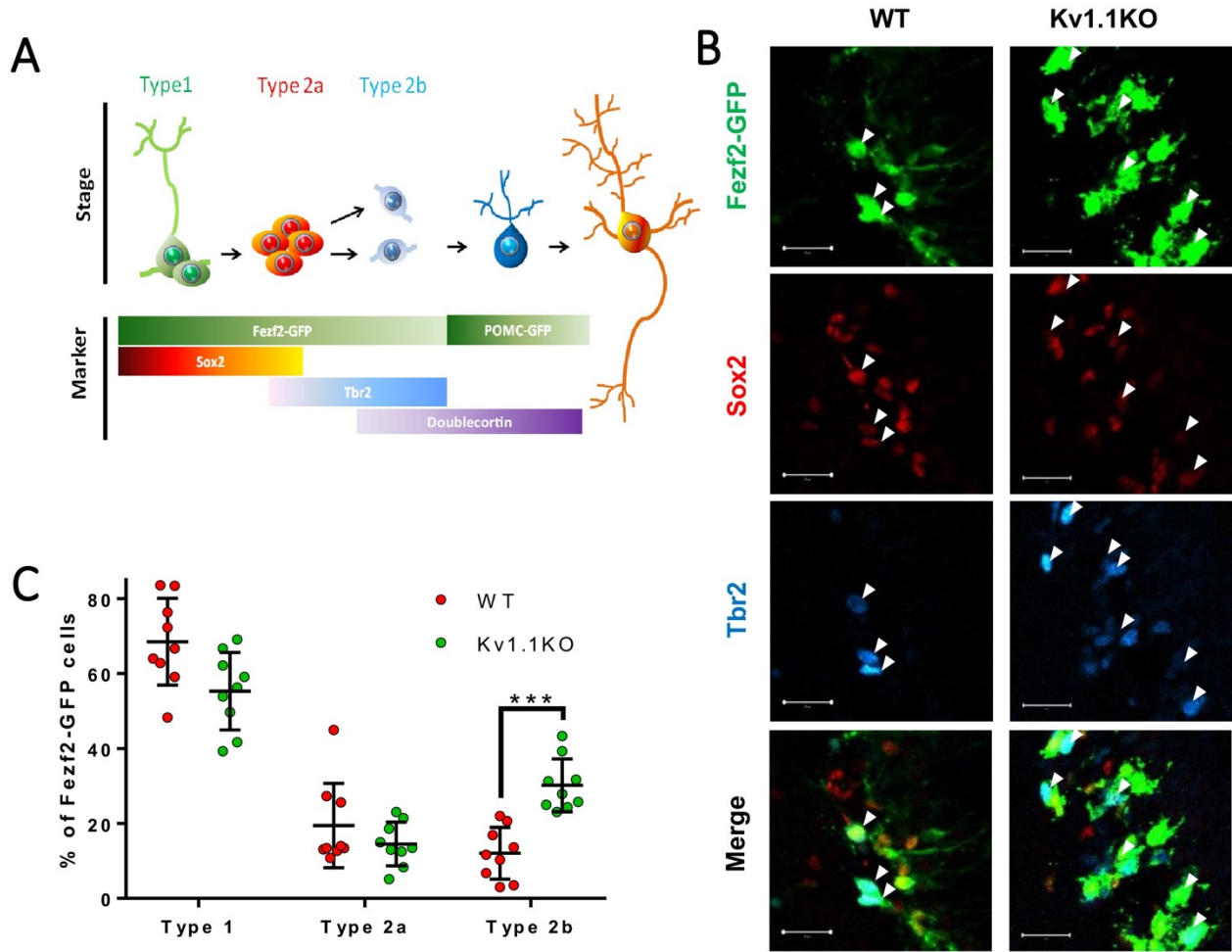


**Figure 2.3: Loss of  $K_v1.1$  channels depolarizes type 2b neural progenitor cells in SGZ at postnatal 2 weeks.** (A) Based on the expression of the cell-fate markers, the neural progenitor cells in sub-granular zone (SGZ) can be categorized into several developmental stages (see Figure 2.4 for detailed images). (B) Among all the Fezf2-GFP-positive cells in the SGZ, radial glia-like type 1 neural progenitor cells expressed predominantly Sox2, type 2a neural progenitor cells expressed both Sox2 and Tbr2 (white arrows), and type 2b progenitor cells expressed Tbr2. Post-mitotic immature neurons express doublecortin (DCX) and can also be identified as POMC-GFP-positive cells. (C) Among these cell types, type 2b cells were significantly increased in adult  $K_v1.1$  KO dentate gyrus compared to wild type (WT), according to the numbers of Tbr2-positive Fezf2-GFP-positive cells ( $n = 9$  for each group; two-way ANOVA followed by Sidak's multiple comparisons test,  $p = 0.0009$ , for type 2b cells). Scale bar = 20  $\mu\text{m}$ .

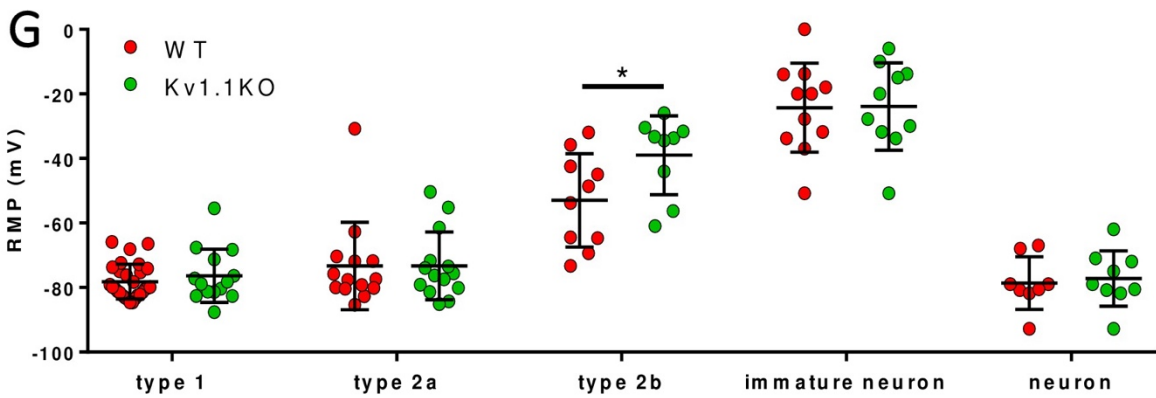
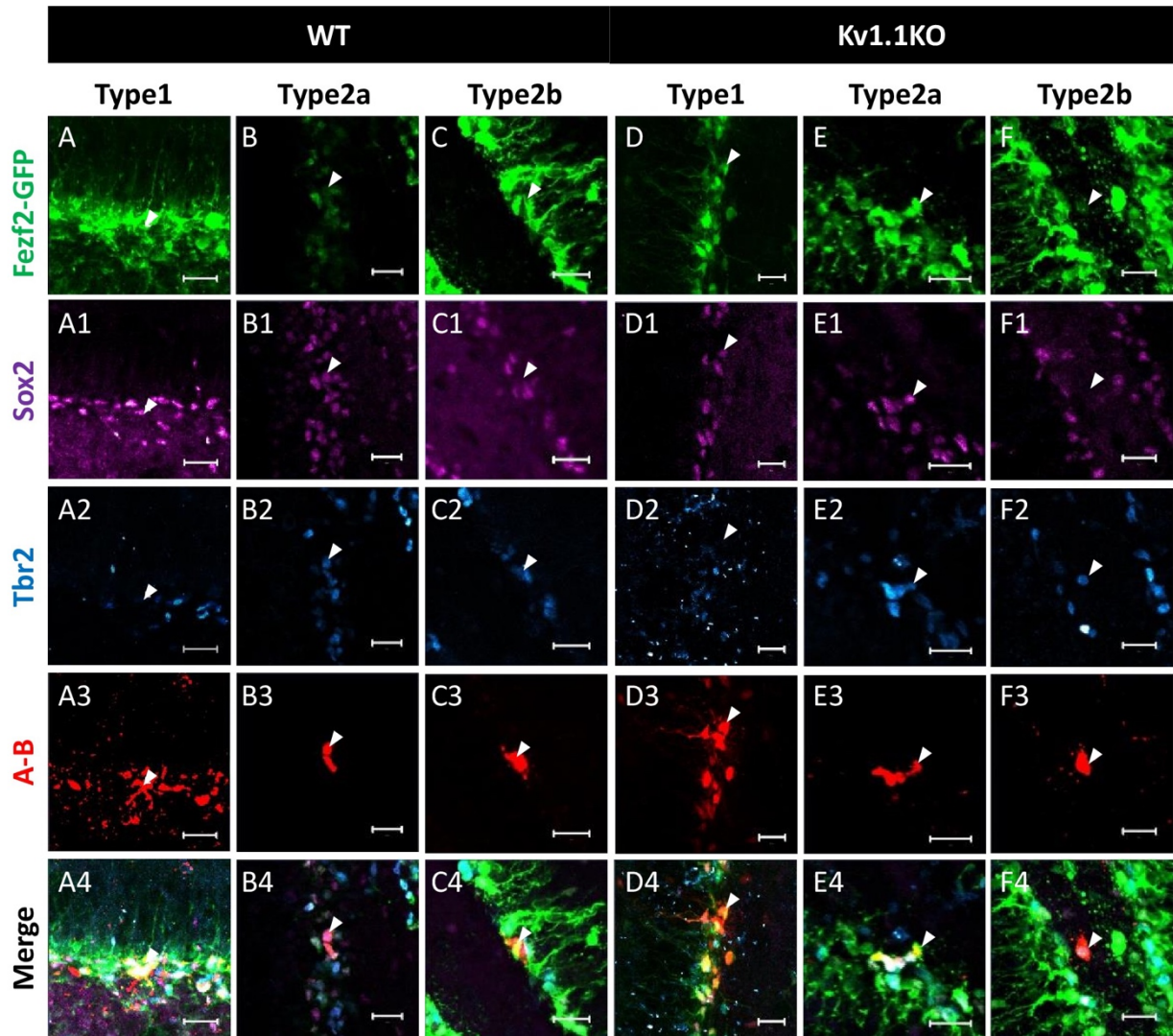


**Figure 2.4: Classification of the Fezf2-GFP progenitor cells in SGZ.** Based on the expression of the cell-fate markers, neural progenitor cells in the subgranular zone (SGZ) can be categorized into several developmental stages. Among all the Fezf2-GFP-positive cells (A-F), Sox2-positive type 1 cells (A1-F1) are radial glia-like cells (A-A4; C-C4) and can give rise to Sox2+/Tbr2+ type 2a transit-amplifying progenitor cells (B-B4; D-D4). Type 2a cells further differentiate into type 2b neuroblasts that are positive for Tbr2 only (C-C4; F-F4). Type 1 (A3 and D3) and type 2a (B3 and E3) cells formed extensive syncytial connections with other cells from the same developmental stage, as indicated by the gap-junction permeable avidin-neurobiotin (A-B) staining. Scale bar = 20  $\mu$ m. (G) Type1 and type 2a Fezf2-GFP-positive neural progenitor cells were hyperpolarized; by contrast, type 2b cells lacking  $K_v1.1$  channels were significantly more depolarized than the wild-type (WT) cells (n = 14, 14, 9, 10, 9 (WT) and 28, 14, 10, 11, 8 ( $K_v1.1$  KO) for type1 cells (Fezf2-GFP+/Sox2+), type 2a cells (Fezf2-GFP+/Sox2+/Tbr2+), type 2b cells (Fezf2-GFP+/Tbr2+), immature neurons (POMC-GFP+), and label-free mature neurons; (two-way ANOVA followed by Sidak's multiple comparisons test, p = 0.02, for type 2b cells).

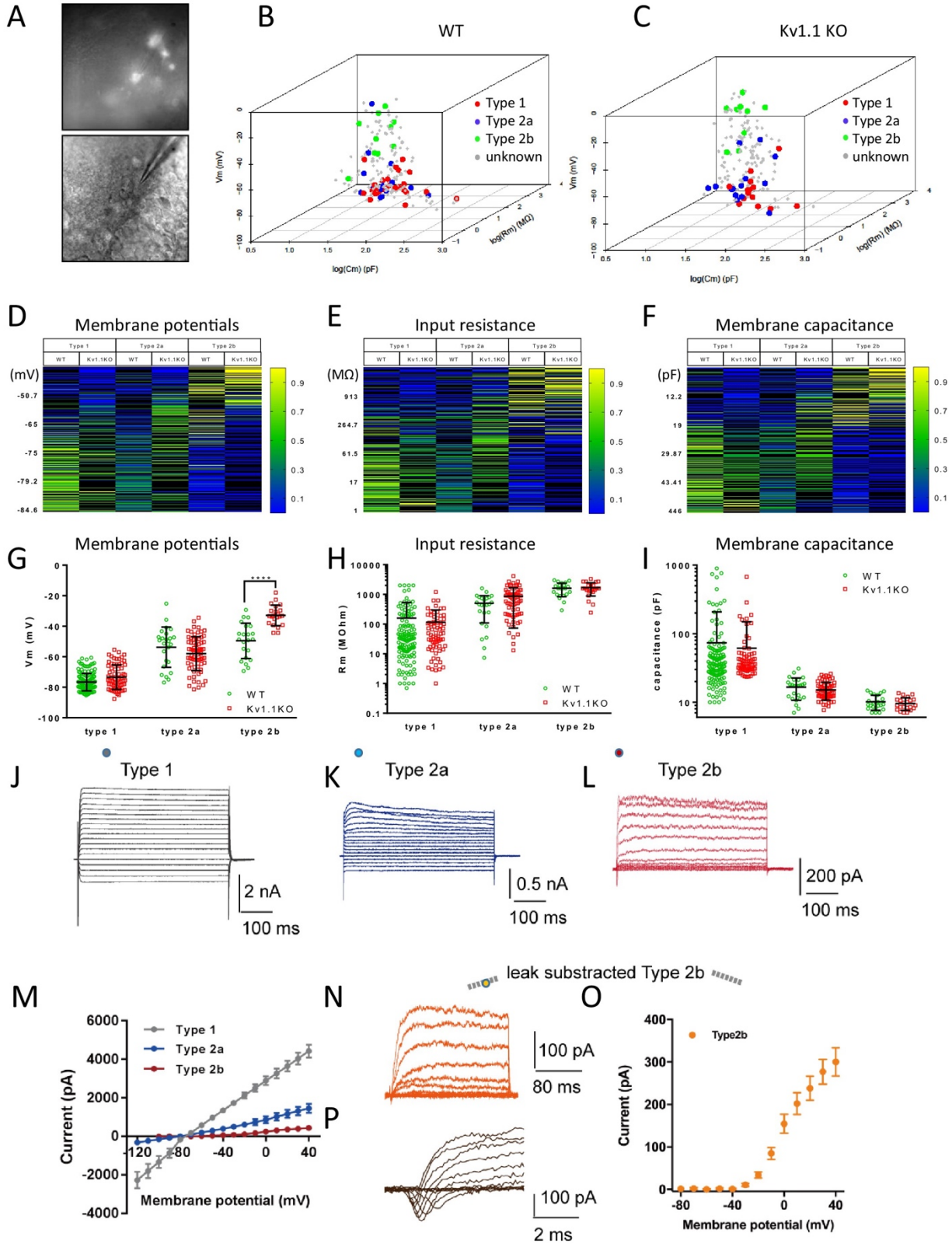




**Figure 2.5: Multinomial logistic regression for cell type prediction.** (A) Acute brain slice recording from the DG of a *Fezf2*-GFP mouse. (B and C) A multinomial logistic regression model was constructed using the biophysical characteristics of cells that were identified previously (same cohort of cells from Figure 2.3 D) as the training dataset. Two individual regression models were generated for wild-type (B) and *K<sub>v</sub>1.1* KO (C) cells. The cell types of unknown cells were later classified according to the resting membrane potential, input resistance, and membrane capacitance. Heatmaps show the estimated probabilities for each cell type against membrane potential (D), input resistance (E), and membrane capacitance (D). The cell types were determined based on maximum likelihood. (G) Resting membrane potentials of wild-type and *K<sub>v</sub>1.1* KO progenitor cells. The predicted type 2b cells lacking *K<sub>v</sub>1.1* channels were significantly more depolarized (two-way ANOVA, followed by Sidak's multiple comparisons test,  $p < 0.0001$  for type 2b cells). Comparable input resistances (H) and membrane capacitances (I) were observed between wild-type and *K<sub>v</sub>1.1* KO cells.  $n = 144, 25$  and  $22$  for type 1, 2a and 2b cells, respectively, in the wild-type group;  $n = 71, 70$  and  $22$  for type 1, 2a and 2b cells, respectively, in the *K<sub>v</sub>1.1* KO group. (J–L) Voltage responses from type 1 (J), type 2a (K), type 2b (L) to series voltage from  $-120$  mV to  $+40$  mV or  $-80$  mV to  $+40$  mV, with a holding potential at  $-80$  mV. (M) Current-voltage curves in J–L (the circles indicate the positions of measurements; type 1 (7 cells), type 2a (7 cells), type 2b (10 cells)). (N, O) Voltage response from  $-80$  mV to  $+40$  mV, with a holding potential of  $-80$  mV and leak subtraction, shown for type 2b (N); current-voltage curve of type 2b ( $n = 17$  cells) with leak subtraction (O). (P) A representative transient inward current (sodium current) was observed in 9 out of 25 type 2b cells. Data are presented as mean  $\pm$  SD in (G), (H), (I); mean  $\pm$  SEM in (M), (O).

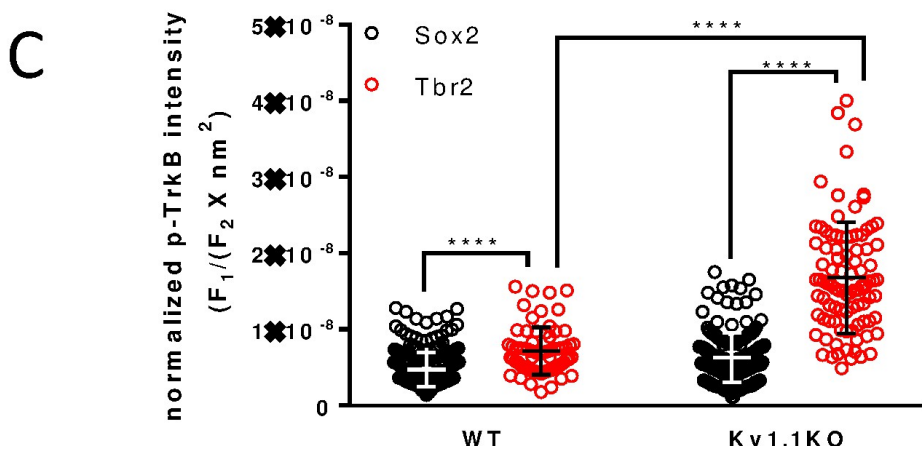
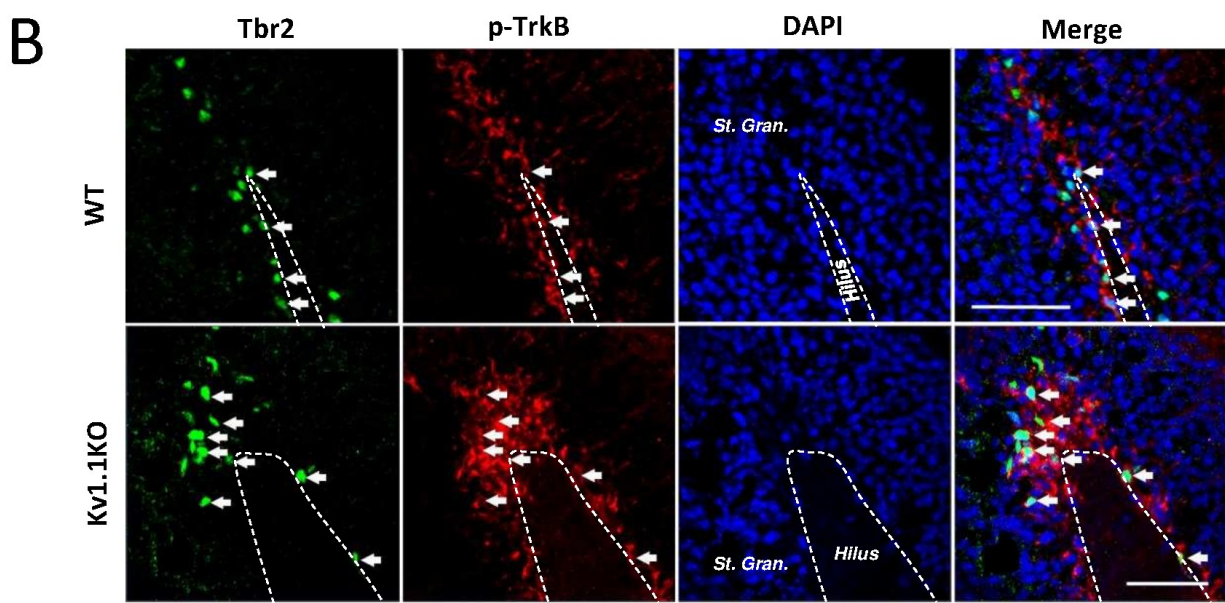
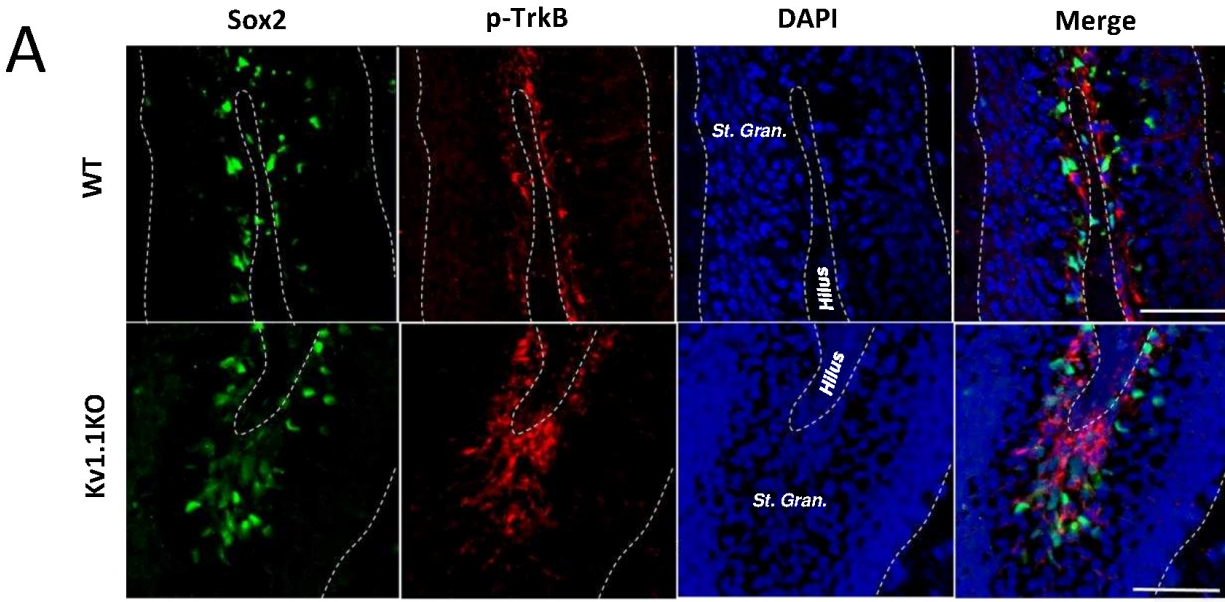


**Figure 2.6: TrkB is mostly active in Tbr2 positive neural progenitor cells.** Phospho-TrkB (Tyr816) signal represents a surrogate measure for the TrkB activity. Phospho-TrkB positive cells rarely colocalized with the Sox2 positive, presumably type 1 and type 2b neural progenitor cells (A); by contrast, phospho-TrkB positive cells colocalized with the majority of Tbr2 positive, presumably type 2b cells (B) More Tbr2<sup>+</sup>/phospho-TrkB<sup>+</sup> neural progenitor cells can be found in the subgranular zone (SGZ) of the K<sub>v</sub>1.1 KO mice. Scale bar = 100 μm (A) and 50 μm (B). (C) Quantification analysis of the phospho-TrkB levels in Sox2<sup>+</sup> or Tbr2<sup>+</sup> cells. The phospho-TrkB fluorescent intensity (F<sub>1</sub>) of each Sox2<sup>+</sup> or Tbr2<sup>+</sup> cells was measured and normalized to the Sox2<sup>+</sup> or Tbr2<sup>+</sup> fluorescent intensity and the total measured cell area (F<sub>2</sub> X nm<sup>2</sup>). n = 246, 243, 69 and 92 for Sox2<sup>+</sup>/WT, Sox2<sup>+</sup>/K<sub>v</sub>1.1 KO, Tbr2<sup>+</sup>/WT, Tbr2<sup>+</sup>/K<sub>v</sub>1.1 KO cells, respectively. \*\*\*\* indicates p<0.0001.)

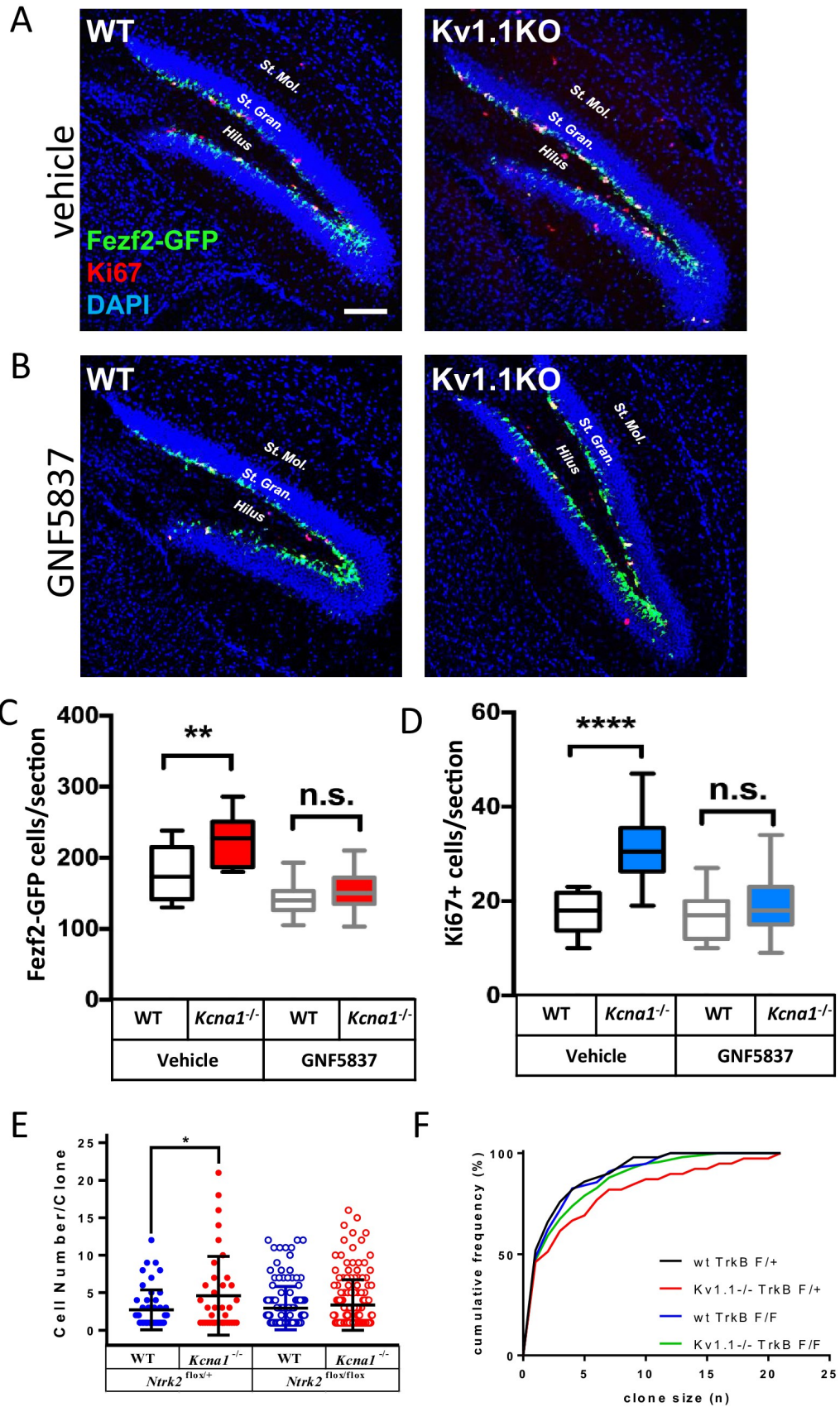


**Figure 2.7: Kv1.1 channels regulate neural progenitor cell numbers via the TrkB signaling pathway.** (A, C and D) Kv1.1 KO mice have more Fezf2-GFP- (C) and Ki67-positive cells (D) than wild-type mice, with vehicle treatment.  $p = 0.0014$ , one-way ANOVA followed by Tukey's test in (C);  $p < 0.0001$ , one-way ANOVA followed by Tukey's test in (D). (B, C and D) Suppression of Kv1.1-dependent neurogenesis by GNF-5837, a potent Trk inhibitor. Mice receiving daily GNF5837 (20mg/kg) administration had comparable numbers of Fezf2-GFP (C) and Ki67-positive cells (D) between wild-type and Kv1.1 KO mice;  $n = 6-8$  mice from each genotype with vehicle-only or GNF5837 treatment. (E) Clonal analysis of adult neurogenesis. Tamoxifen (0.5 mg) was administered at postnatal 3 weeks to sparsely delete *Ntrk2* (a gene that encodes the TrkB receptor) in a subset of neural progenitor cells. In cells lacking only one allele of TrkB, Kv1.1 KO had larger clone sizes than wild-type cells; by contrast, the Kv1.1-dependent proliferation advantage was abrogated in clones lacking both TrkB alleles.  $p = 0.0389$ , comparing wild-type and Kv1.1 KO on the *Ntrk2*<sup>flox/+</sup> background; two-way ANOVA followed by Sidak's multiple comparisons test;  $n = 39-157$  for each group. Scale bar = 100  $\mu\text{m}$ . Data are presented as mean  $\pm$  SEM. \* $p < 0.05$ , \*\* $p < 0.01$ ; \*\*\* $p < 0.001$ ; \*\*\*\* $p < 0.0001$ ; n.s., no significant difference. (F) Kolmogorov-Smirnov plots show a rightward shift of clone sizes in *Kcna1*<sup>-/-</sup>; *Gli1*<sup>creERT2/+</sup>; *Ntrk2*<sup>flox/+</sup>; *Rosa26*<sup>Tom/+</sup> mice (red trace) comparing to wild-type *Gli1*<sup>creERT2/+</sup>; *Ntrk2*<sup>flox/+</sup>; *Rosa26*<sup>Tom/+</sup> mice (black trace) ( $p=0.0029$ , *t*-test), but this effect was absent in mice lacking TrkB receptor ( $p>0.05$  between wild-type *Gli1*<sup>creERT2/+</sup>; *Ntrk2*<sup>flox/+</sup>; *Rosa26*<sup>Tom/+</sup> (black trace) and *Gli1*<sup>creERT2/+</sup>; *Ntrk2*<sup>flox/flox</sup>; *Rosa26*<sup>Tom/+</sup> (blue trace); *Kcna1*<sup>-/-</sup>; *Gli1*<sup>creERT2/+</sup>; *Ntrk2*<sup>flox/flox</sup>; *Rosa26*<sup>Tom/+</sup> (green trace).

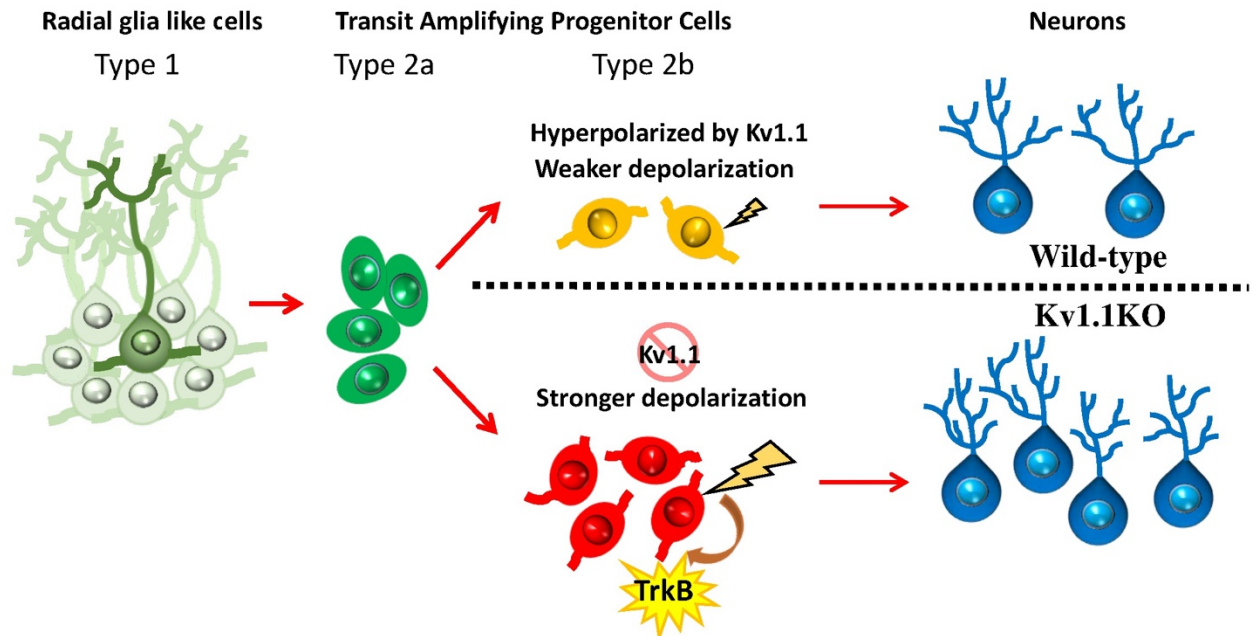
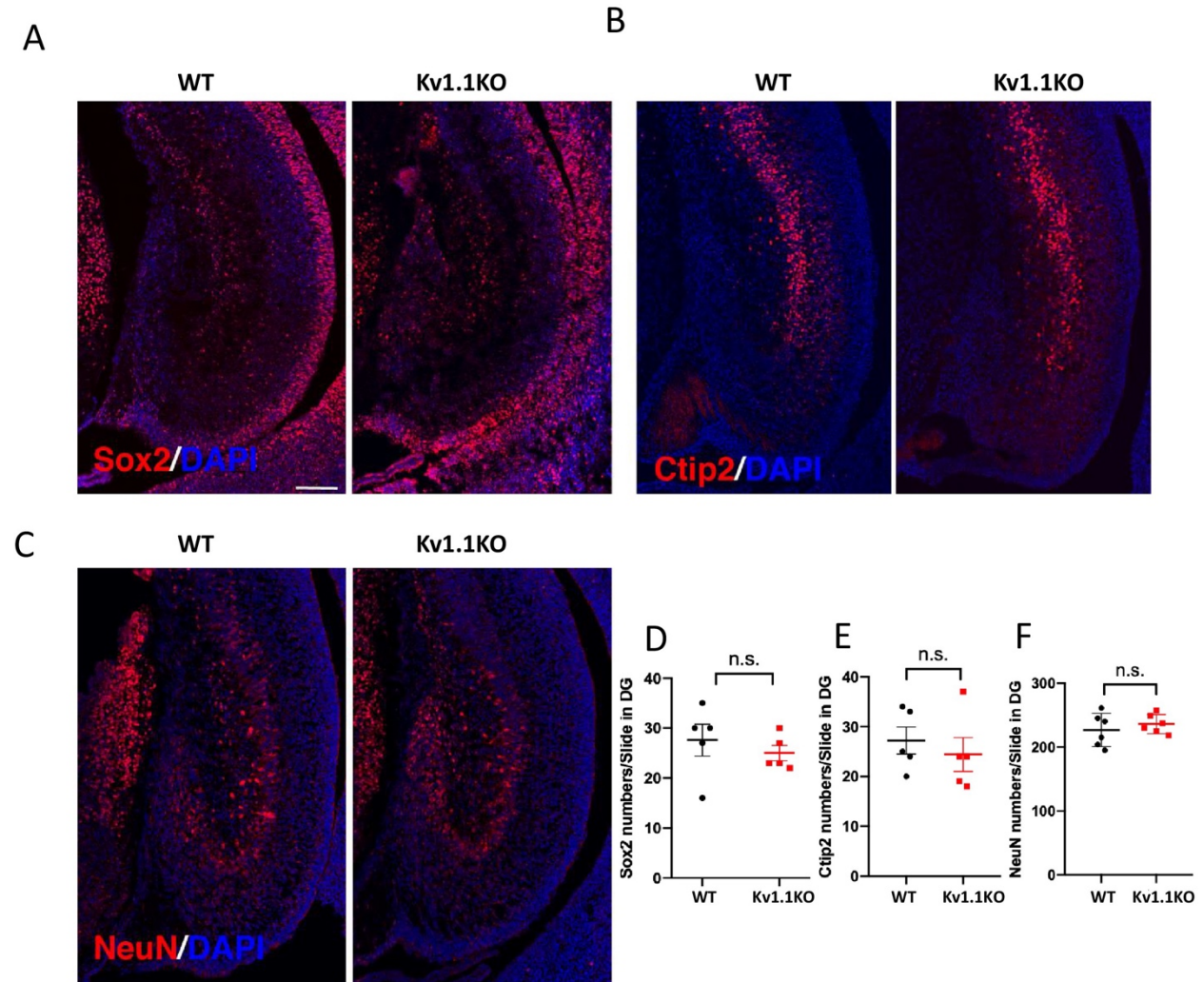


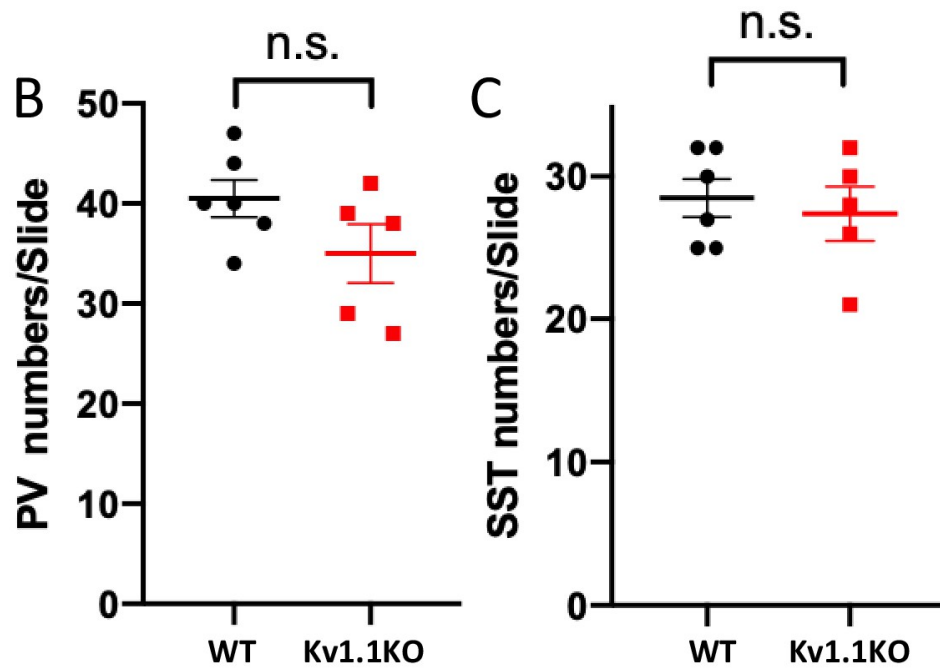
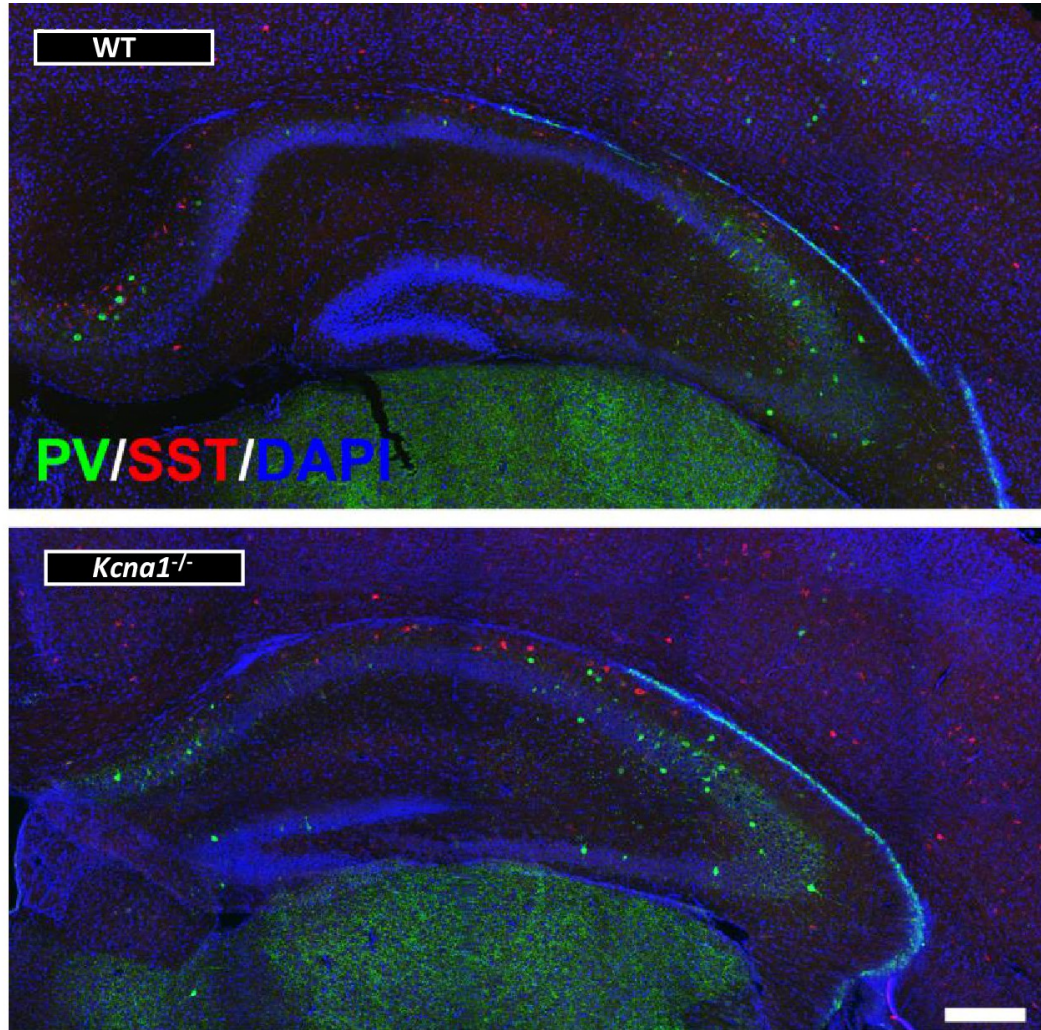
**Figure 2.8: Summary of the role of  $K_v1.1$  channels in regulating early postnatal neurogenesis in SGZ.** The membrane potentials of type 1 radial glia-like neural stem cells and type 2a transit-amplifying progenitor cells indicate relative hyperpolarization. In type 2b neural progenitors, cells lacking the  $K_v1.1$  channel become more depolarized than wild types, further stimulating the proliferation of type 2b cells via activating the TrkB signaling pathway. The mature granule cells become hyperpolarized again.

## 2.8 Supplementary Figures



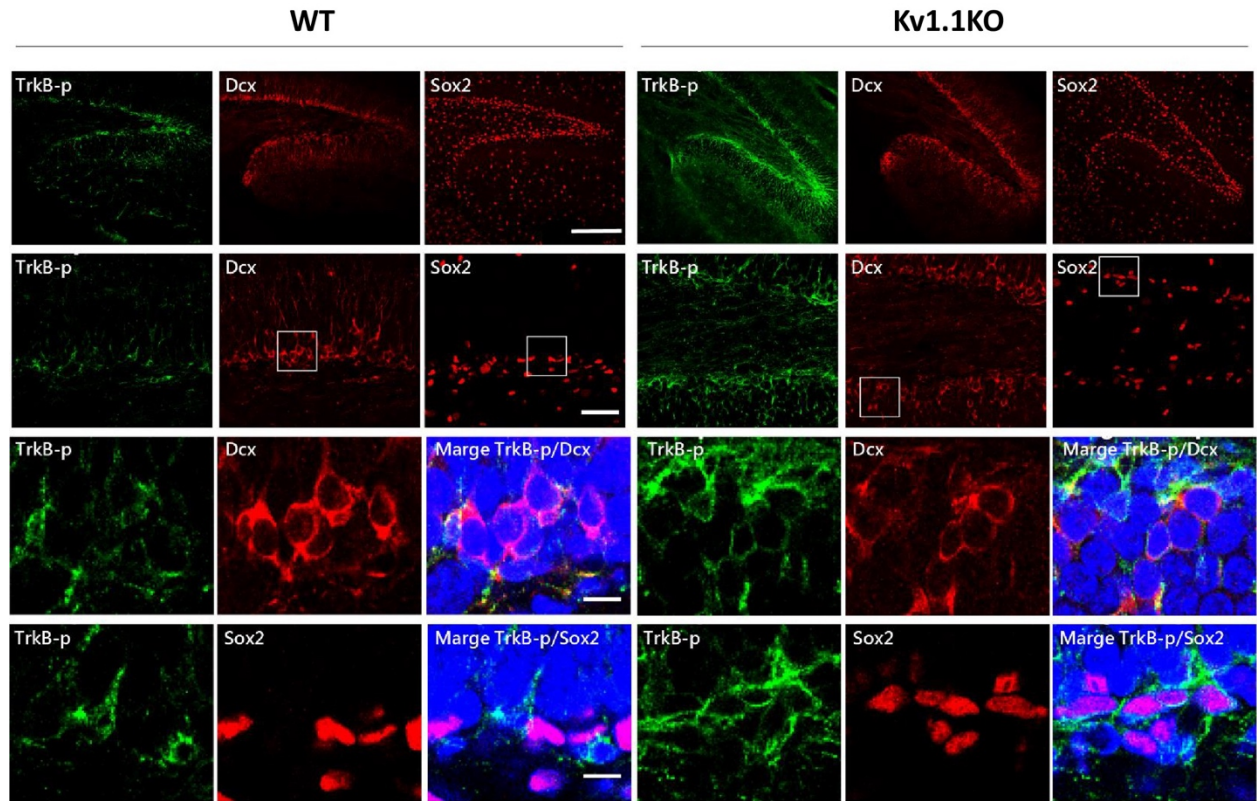
**Supplementary figure 2.1: Kv1.1 channels do not affect embryonic hippocampal neurogenesis.** Immunostaining indicated that there was no difference in dentate gyrus (DG) between wild-type and Kv1.1 KO mice, in terms of Sox2+ progenitors (A, D) ( $p = 0.4807$ ,  $t$ -test), Ctip2+ postmitotic marker (B, E) ( $p = 0.5365$ ,  $t$ -test) or NeuN+ neurons (C, F) ( $p = 0.4606$ ,  $t$ -test) at E16.5.  $n = 5-6$  for each genotype. Scale bar = 100  $\mu\text{m}$ . Data are presented as mean  $\pm$  SEM. n.s., no significant difference.

A

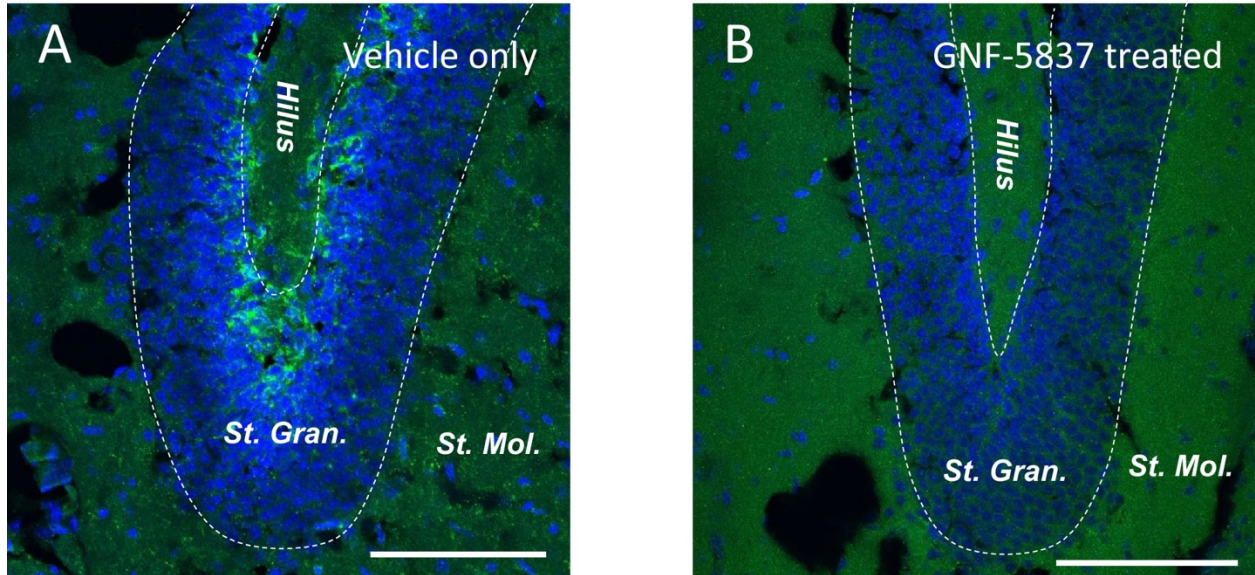




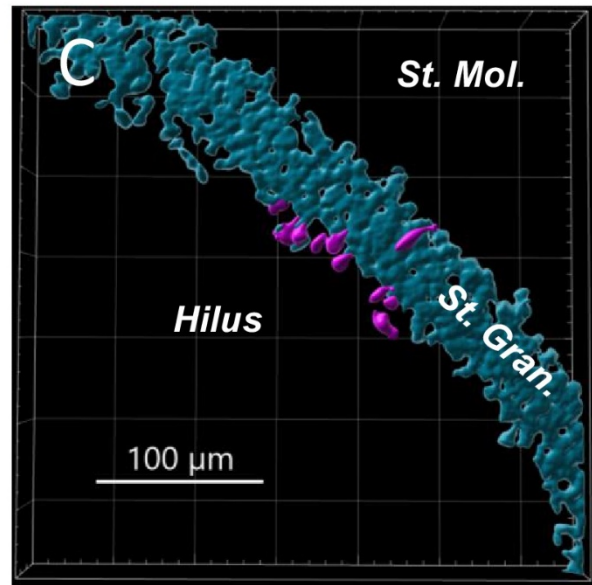
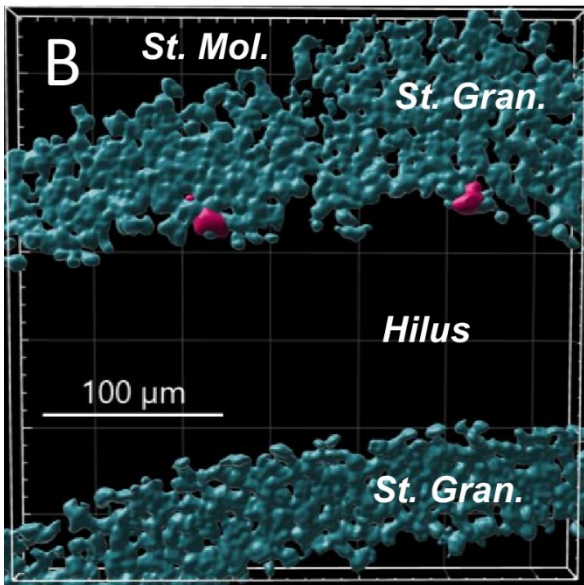
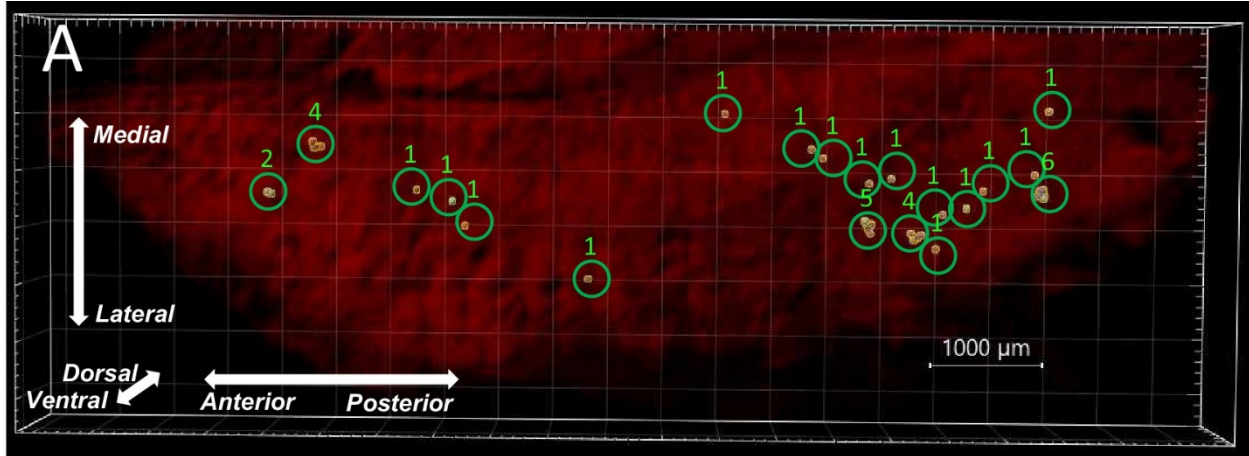
**Supplementary figure 2.2: No detectable difference in interneurons of Kv1.1 KO mice at P10.**  
(A) Immunostaining and quantification show no significant difference in hippocampus between wild-type and Kv1.1 KO mice, in terms of PV+ interneurons (B) ( $p = 0.1363$ ,  $t$ -test,) or SST+ interneurons (C) ( $p = 0.6372$ ,  $t$ -test).  $n = 5-6$  for each genotype. Scale bar = 250  $\mu\text{m}$ . Data are presented as mean  $\pm$  SEM. n.s., no significant difference.



**Supplementary figure 2.3: The TrkB signaling is active in DCX+ late-stage progenitor cells but not Sox2+ early-stage progenitor cells.** Phospho-TrkB positive cells rarely colocalized with the Sox2 positive, presumably type 1 and type 2b neural progenitor cells but mostly colocalized with the DCX+ late-stage progenitor cells. Scale bar =50  $\mu$ m.



**Supplementary figure 2.4: Intraperitoneal injection of GNF-5837 remarkably inhibits the TrkB signaling in SGZ.** Immunostaining of the dentate gyrus from mice treated with daily intraperitoneal vehicle-only (A) or GNF-5837 (20mg/kg) (B) injection for 3 weeks. phospho-TrkB signal (green) can be detected in the SGZ region in control (A) but not GNF-5837 (B). Scale bar =100  $\mu$ m.



**Supplementary figure 2.5: Clonal analysis of postnatal born neurons in the SGZ.** Single low-dose tamoxifen (0.5 mg/kg) was injected into a 3 week old *Gli1*<sup>creERT2/+</sup>; *Rosa26*<sup>Tom/+</sup> mouse and later sacrificed at 8 weeks old. The clonal clusters were defined as the TdTomato<sup>+</sup> cells contained within a 100-µm radius of the clone center. (A) An overview of a whole-mount 3D hippocampus (red) from a *Gli1*<sup>creERT2/+</sup>; *Ntrk2*<sup>flox/flox</sup>; *Rosa26*<sup>Tom/+</sup> mouse. The neural progenitor cells were identified automatically by the software, and the clone sizes were labeled as the number above the green circles. (B) Higher magnification of two single-cell clones that were separated by more than 150 µm. (C) A group of cells that are clustered within the radius of 45 µm are considered as a single clone with 10 cells. Both (B) and (C) were obtained from the hippocampus of a *Kcna1*<sup>-/-</sup>; *Gli1*<sup>creERT2/+</sup>; *Ntrk2*<sup>flox/+</sup>; *Rosa26*<sup>Tom/+</sup> mouse.

## **Chapter 3**

**K<sub>v</sub>1.1 preserves the neural stem cell pool and facilitates neuron maturation during adult hippocampal neurogenesis**

### 3.1 Introduction

The subgranular zone of the hippocampus is one of two well-characterized neurogenic niches in the adult mouse brain. Integration of adult-born granule cells (abGCs) into the dentate gyrus is important for learning and memory, and impaired adult neurogenesis has been implicated in neurodegenerative and neuropsychiatric diseases [1, 3-7]. Adult hippocampal neurogenesis is divided into several developmental stages. Initially, quiescent neural stem cells (NSCs) with radial glia-like morphology—known as radial glia-like NSCs (RGLs / Type 1 cells)—activate and proliferate, either self-renewing or differentiating into intermediate neural progenitor cells (NPCs) with a glial-like phenotype (Type 2a). As these cells differentiate, they lose their stem cell properties and display more neuronal-like features (Type 2b). Then, they develop into neuroblasts (Type 3) within a few days. Over the course of the next 2-4 weeks, Type 3 cells become immature abGCs that extend an apical dendrite into the dentate granule cell layer and grow secondary and tertiary dendrites. Simultaneously, they migrate from the subgranular zone into the dentate granule cell layer. Finally, abGCs mature into highly excitable neurons and integrate into the dentate gyrus circuitry [1, 3-9].

While adult hippocampal neurogenesis is regulated by various environmental and endogenous factors, recent studies have also begun to explore the role of bioelectric signaling in this process. In non-excitable cells such as NSCs and NPCs, changes in the membrane potential can orchestrate proliferation, differentiation, migration, and survival during development [10]. The membrane potential is controlled by ion channels, and ion channel dysfunction often result in neurodevelopmental disorders [11, 12]. Interestingly, ion channels not only modulate NSC and NPC membrane potential and cell dynamics during prenatal development [11, 13-15] but also

during postnatal neurogenesis [2, 16-21]. Adult RGLs express gap junctions and inward rectifying potassium channels to maintain their membrane potential [17, 20, 22]. RGL division is also regulated by GABAergic and glutamatergic signaling, where these neurotransmitters activate their corresponding ligand-gated ion channels to alter the membrane potential [16, 18, 21]. Additionally, local circuit activity is critical for young abGCs, which receive, in order: depolarizing GABAergic inputs, excitatory glutamatergic inputs, and finally inhibitory GABAergic inputs to advance through stages of maturation and survival [23-26].

In this study, we examined the role of the voltage-gated potassium channel  $K_v1.1$  in adult neurogenesis.  $K_v1.1$  is encoded by the *Kcna1* gene in mice, and its expression begins to increase at ~2 weeks after birth and stabilizes in adulthood [27].  $K_v1.1$  is well known for its role in regulating neuronal excitability and seizure activity [28, 29]. Mice without functional  $K_v1.1$ — $K_v1.1$  null mutant mice and *megencephaly* (*mceph*) mice—not only develop seizures but also have increased number of neurons in the dentate gyrus [2, 30-35]. Using mosaic analysis with double markers (MADM) [36-38] on heterozygous *mceph* mice, we showed that  $K_v1.1$  regulates neurogenesis in a cell-autonomous manner [35]. We also found that loss of  $K_v1.1$  function in  $K_v1.1$  null mice depolarizes neonatal NPCs and increases proliferation through enhanced TrkB signaling in neonatal hippocampal neurogenesis [2], which is more similar to embryonic neurogenesis than adult neurogenesis [39-41]. Because  $K_v1.1$  null mice exhibit seizures beginning a few weeks after birth [30, 32-34] and seizure activity can affect neurogenesis [42, 43], it has not been feasible to assess the function of  $K_v1.1$  in adult neurogenesis.

To address this issue and clarify the role of  $K_v1.1$  in adult neurogenesis, we created inducible  $K_v1.1$  conditional knockout ( $K_v1.1$  cKO) mice, which allowed us to specifically delete  $K_v1.1$  from adult NSCs via tamoxifen (TAM) injection without the confounding effect of seizure. Using this mouse model, we first deleted  $K_v1.1$  in neonatal NSCs to validate our previous results with increased temporal resolution. Indeed, we recapitulated our previous observations showing that loss of  $K_v1.1$  in neonatal NSCs increases proliferation and neuron production. Interestingly, the role of  $K_v1.1$  in adult NSCs is more complex. We discovered that  $K_v1.1$  prevents over-proliferation and depletion of RGLs and enables proper abGC maturation and positioning during adult neurogenesis. We further corroborated our findings of an age-dependent role of  $K_v1.1$  using mosaic analysis with double markers (MADM) of heterozygous  $K_v1.1$  ( $Kcna1^{+/-}$ ) mice [36-38]. Finally, we determined that decreased adult neurogenesis in  $K_v1.1$  cKO mice causes deficits in contextual fear conditioning and discrimination. These results demonstrate that  $K_v1.1$  expression in adult NSCs is integral for preserving hippocampal neurogenesis and hippocampal-dependent learning and memory.



## 3.2 Results

### *Time-controlled deletion of $K_v1.1$ from neural stem cells*

To investigate the function of  $K_v1.1$  in NSCs at various postnatal stages, we generated  $K_v1.1$  cKO mice. We bred mice expressing a TAM-inducible Cre recombinase (Cre) in NSCs (*Nestin-Cre<sup>ERT2</sup>*) [44-46] with *Kcna1* floxed mice (*Kcna1<sup>fl/fl</sup>*) [47] and a Cre-reporter (PC::*G5-tdT*) [48] to achieve temporal and cell type-specific control of  $K_v1.1$  deletion. Upon TAM injection, Cre begins expression in NSCs, resulting in the deletion of *Kcna1* and expression of tdTomato and GCaMP5G in the NSCs and their progeny. As the Cre-expressing NSCs are a small subset of all cell types in the dentate gyrus, we expressed tdTomato and GCaMP5G in these cells to identify them for lineage tracing. We amplified GCaMP5G signal with an anti-GFP antibody, because the anti-GFP antibody was compatible with our histology techniques using multiple cell markers. In this way, we successfully read-out Cre expression in NSCs. To control for the possible effects of TAM, Cre, and reporter expression on NSC dynamics, we bred mice with *Kcna1* wildtype (*Kcna1<sup>+/+</sup>*) with *Nestin-Cre<sup>ERT2</sup>* and PC::*G5-tdT* mice ( $K_v1.1$  WT) for our control cohort (Supplementary figure 3.1A).

To validate  $K_v1.1$  knock-out after TAM-injection, we injected 8-week-old  $K_v1.1$  cKO and  $K_v1.1$  WT mice with TAM for 3 consecutive days and used fluorescence-activated cell sorting to isolate Cre-expressing tdTomato+ cells from the dentate gyrus at 2 weeks post-TAM (Supplementary figure 3.1B–E). We found that *Kcna1* mRNA expression was decreased by ~90% in tdTomato+ cells in the dentate gyrus of  $K_v1.1$  cKO mice compared to those of  $K_v1.1$  WT mice ( $P = 0.0001$ ) (Supplementary figure 3.1F). We also recorded the resting membrane potential of acutely dissociated dentate gyrus cells expressing tdTomato at 2 weeks post-TAM to determine whether

K<sub>v</sub>1.1 has been functionally deleted (Supplementary figure 3.2A). To assess the effect of acute K<sub>v</sub>1.1 inhibition on resting membrane potential, we applied the selective K<sub>v</sub>1.1 blocker, Dendrotoxin-K (DTx-K) to tdTomato<sup>+</sup> K<sub>v</sub>1.1 WT cells and observed a depolarized resting membrane potential ( $-70.01 \pm 2.563$  mV) ( $P = 0.0002$ ) (Supplementary figure 3.2B, C). Consistent with our findings using DTx-K for acute K<sub>v</sub>1.1 inhibition, we found that resting membrane potential of tdTomato<sup>+</sup> K<sub>v</sub>1.1 cKO cells were similarly depolarized ( $-67.94 \pm 0.9525$  mV) compared to K<sub>v</sub>1.1 WT cells ( $-86.73 \pm 0.5791$  mV) ( $P = 0.0002$ ). Together, these results show that K<sub>v</sub>1.1 is functionally knocked out of the Cre-expressing tdTomato<sup>+</sup> NSC lineage of K<sub>v</sub>1.1 cKO mice by 2 weeks post-TAM, which results in depolarized cells.

***Conditional knockout of K<sub>v</sub>1.1 in neonatal neural stem cells increases early postnatal hippocampal neurogenesis***

Both K<sub>v</sub>1.1 null mice and *mceph* mutant mice display increased neonatal neurogenesis before seizure onset around one month after birth [2, 30-35]. As K<sub>v</sub>1.1 cKO mice allowed us to examine the role of K<sub>v</sub>1.1 in early postnatal neurogenesis with more precise temporal resolution, we focused on the role of K<sub>v</sub>1.1 during peak hippocampal neurogenesis at postnatal day 7 (P7), just before the second postnatal week when hippocampal neurogenesis begins transitioning from a more embryonic phenotype to adult phenotype [40, 41].

We injected TAM at postnatal day 0 (P0) to knock out K<sub>v</sub>1.1 and conducted lineage tracing by injecting Bromodeoxyuridine (BrdU), which is incorporated into the DNA of actively dividing cells [49-52], at P7. We then quantified the number of progeny cells in the dentate gyrus of K<sub>v</sub>1.1 cKO mice and K<sub>v</sub>1.1 WT mice at postnatal day 14 (P14) (Figure 3.1A). To determine which cell

types were altered in the Cre-expressing GFP<sup>+</sup> NSC lineage, we co-stained the sections with established NSC and NPC marker, Sox2, and the neuronal marker, NeuN. We found that NSC and NPC progenies from cells dividing at P7 (GFP<sup>+</sup>, BrdU<sup>+</sup>, Sox2<sup>+</sup>) in K<sub>v</sub>1.1 cKO subgranular zone were increased by ~60% ( $P = 0.0360$ ) (Figure 3.1B-C). Within the dentate granule cell layer, neurons produced from cells dividing at P7 (GFP<sup>+</sup>, BrdU<sup>+</sup>, NeuN<sup>+</sup>) were increased by ~55% ( $P = 0.0007$ ) (Figure 3.1D-E). The enhanced neonatal neurogenesis that we observed in K<sub>v</sub>1.1 cKO mice is similar to our previous findings in K<sub>v</sub>1.1 null mice [2], providing further evidence that K<sub>v</sub>1.1 acts as a brake on early postnatal neurogenesis before the subgranular zone develops its adult phenotype.

***Deletion of K<sub>v</sub>1.1 in adult neural stem cells leads to a transient activation followed by a depletion of radial glial-like cells***

Next, we investigated the role of K<sub>v</sub>1.1 in adult hippocampal neurogenesis. To specifically ablate K<sub>v</sub>1.1 in the adult NSC lineage, we injected 8-week-old adult mice with TAM for 3 consecutive days. Unlike the K<sub>v</sub>1.1 null and *mceph* mutant mice, adult K<sub>v</sub>1.1 cKO mice injected with TAM did not display seizure phenotypes, which enabled us to examine the role of K<sub>v</sub>1.1 in adult neurogenesis without the confounding effects of seizures. We first examined mice 4 weeks after TAM injection to assess the early effects of K<sub>v</sub>1.1 deletion on adult NSC dynamics. We started by investigating the role of K<sub>v</sub>1.1 in Cre-expressing GFP<sup>+</sup> quiescent RGLs, which are labeled by Sox2 and the glial marker, GFAP. As they become activated, RGLs begin expressing the mitotic marker, MCM2 (Figure 3.2A) [53]. At 4 weeks post-TAM, the quiescent (GFP<sup>+</sup>, GFAP<sup>+</sup>, Sox2<sup>+</sup>, MCM2<sup>-</sup>) and activated (GFP<sup>+</sup>, GFAP<sup>+</sup>, Sox2<sup>+</sup>, MCM2<sup>+</sup>) RGLs were increased by ~100% ( $P = 0.0481$ ) and ~80% ( $P = 0.0461$ ), respectively, in K<sub>v</sub>1.1 cKO mice as compared to K<sub>v</sub>1.1 WT mice

(Figure 3.2B-E). This suggests that loss of  $K_v1.1$  initially promotes both RGL division and self-renewal. RGLs can also divide and differentiate into Type 2a cells, losing their GFAP expression (Supplementary figure 3.3A). We quantified the amount of Type 2a cells (GFP+, GFAP-, Sox2+, MCM2+) and found a trend towards statistical significance that Type 2a cells in  $K_v1.1$  cKO mice are increased by ~70% at 4 weeks post-TAM ( $P = 0.0680$ ) (Supplementary figure 3.3B, D). It is possible that the enhanced RGL proliferation pushed RGLs to both self-renewal and differentiation and/or both RGLs and Type 2a cells have increased proliferation in  $K_v1.1$  cKO mice. Interestingly, the increase in RGLs and Type 2a cells does not lead to additional Type 2b and proliferating Type 3 cells (GFP+, GFAP-, Sox2-, MCM2+) ( $P = 0.8418$ ) (Supplementary figure 3.3C-D).  $K_v1.1$  expression seems to discourage RGLs from dividing to self-renew and differentiate.

To determine the long-term effects of  $K_v1.1$  deletion, we investigated changes in the NSC lineage at 8 weeks after TAM-injection. Surprisingly, both quiescent (GFP+, GFAP+, Sox2+, MCM2-) and activated (GFP+, GFAP+, Sox2+, MCM2+) RGLs were reduced by ~40% ( $P = 0.0391$ ) and ~65% ( $P = 0.0158$ ), respectively, in  $K_v1.1$  cKO mice as compared to  $K_v1.1$  WT mice (Figure 3.2F-I), suggesting that the initial increase in RGL proliferation eventually exhausted their ability to self-renew and depleted the RGL pool. We also examined the role of  $K_v1.1$  in Type 2a and proliferating Type 2b/3 cells and found that the amount of both Type 2a (GFP+, GFAP-, Sox2+, MCM2+) ( $P = 0.1391$ ) and Type 2b/3 cells (GFP+, GFAP-, Sox2-, MCM2+) ( $P = 0.2686$ ) were similar between  $K_v1.1$  cKO mice and  $K_v1.1$  WT mice at 8 weeks post-TAM (Supplementary figure 3.3E-G). These results indicate that  $K_v1.1$  acts as a break on over-proliferation to prevent early depletion of the neurogenic stem cell pool.

### ***Loss of Kv1.1 impairs adult-born granule cell maturation and positioning***

To investigate the role of Kv1.1 in later stages of hippocampal abGC production, we stained for doublecortin (DCX) at 8 weeks post-TAM. DCX begins to express in a subset of Type 2b cells and ceases to express as they become NeuN<sup>+</sup> mature neurons [54-56]. Interestingly, there was a ~55% decrease in GFP<sup>+</sup>, DCX<sup>+</sup> cells (Figure 3.3A, D) in Kv1.1 cKO mice although the amount of proliferating Type 2b/3 cells was not altered (Supplementary figure 3.3F). This raises the question whether the observed decrease in GFP<sup>+</sup>, DCX<sup>+</sup> cells was due to the altered development of young abGCs. We relied on the distinct morphology of DCX<sup>+</sup> cells at different stages of maturation to identify more developed DCX<sup>+</sup> abGCs as those with tertiary dendrites [54-56]. Interestingly, in the Kv1.1 cKO lineage, there was a ~75% decrease in the number of GFP<sup>+</sup>, DCX<sup>+</sup> cells with tertiary dendrites ( $P = 0.0117$ ) as well as a ~45% decrease in the proportion of more developed GFP<sup>+</sup>, DCX<sup>+</sup> cells with tertiary dendrites amongst all GFP<sup>+</sup>, DCX<sup>+</sup> cells ( $P = 0.0165$ ) (Figure 3.3B–D). Taken together, these results indicate that loss of Kv1.1 hinders young abGC maturation.

Those Kv1.1 cKO neurons that successfully matured were also more likely to be inappropriately positioned. As young abGCs mature, they migrate from the subgranular zone into the dentate granule cell layer such that a majority are positioned within the inner two-thirds of the dentate granule cell layer (Figure 3.3E) [23, 57]. Interestingly, the percentage of mature GFP<sup>+</sup> abGCs (GFP<sup>+</sup>, NeuN<sup>+</sup>) found in the outer third of the dentate granule cell layer at 8 weeks post-TAM in Kv1.1 cKO mice was ~215% higher than that of Kv1.1 WT mice ( $P = 0.0330$ ) (Figure 3.3F, H), indicating that loss of Kv1.1 impairs abGC positioning. These findings point towards a critical role of Kv1.1 in facilitating successful abGC development, as aberrant migration and positioning of

abGCs has been found in mouse models of traumatic brain injury and schizophrenia [58, 59]. These findings may also explain why we observed a ~50% reduction in mature GFP+ abGCs (GFP+, NeuN+) in Kv1.1 cKO mice by 8 weeks post-TAM ( $P = 0.0204$ ) (Figure 3.3G-H). As young abGCs from NSCs lacking Kv1.1 cannot properly mature and position themselves, they are likely unable to successfully integrate into the dentate gyrus circuitry. Taken together, our observations indicate that Kv1.1 is integral for abGCs to develop proper morphology and positioning, which would allow them to incorporate synaptic inputs, integrate into the hippocampal circuitry and fulfil their critical functions in learning and memory.

### **MADM analyses reveal a transient increase of neural stem cell lineage lacking Kv1.1**

In our previous studies, we performed mosaic analysis with double markers (MADM) [36-38] with heterozygous Kv1.1 (*Kcna1*<sup>+/-</sup>) mice, in which sparse somatic recombination driven by constitutively active Nestin-Cre generates a subpopulation of NSCs that lack Kv1.1 (Nestin-Cre; *Kcna1*<sup>+/-</sup>; MADM-6) (Figure 3.4A) [2]. Homozygous Kv1.1-null NSC lineages are marked with GFP and homozygous Kv1.1-wildtype NSC lineages are marked with tdTomato. Using this model, we observed a three-fold increase in progeny neurons from Kv1.1-null NSCs in the dentate granule cell layer of 2 to 3-month-old Nestin-Cre; *Kcna1*<sup>+/-</sup>; MADM-6 mice ( $P < 0.0001$ ) (Figure 3.4B-C; data from 1-month-old and 2 to 3-month-old cohorts originally published in Figure 1 of Chou *et al.*, 2021). This is consistent with our findings from Kv1.1-null and cKO mice that loss of Kv1.1 in neonatal NSCs promotes neonatal RGL proliferation and neuronal production (Figure 3.1) [2]. In 2 to 3-month-old Nestin-Cre; *Kcna1*<sup>+/-</sup>; MADM-6 mice, presumably a large population of neonatal-born neurons remains, as neonatal-born neurons just begin apoptosis ~2 months after birth [60-62]. However, once the mice have aged 6 to 13 months, neonatal-born Kv1.1-null

progeny neurons would have begun apoptosis and therefore appear as a smaller portion of the GFP+ population. Indeed, we found no increase in Kv1.1-null progeny neurons in the dentate granule cell layer of 6 to 13-month-old mice (Figure 3.4B-C). As the loss of Kv1.1 negatively impacts adult neurogenesis (Figure 3.3), adult-born Kv1.1-null progeny neurons are unable to adequately replenish the GFP+ population. Thus, the transient increase of Kv1.1-null progeny neurons in the MADM mice with heterozygous Kv1.1 supports the hypothesis that Kv1.1 plays an age-dependent role in adult neurogenesis.

### **Eliminating Kv1.1 from adult neural stem cells results in learning and memory deficits**

Since decreased adult neurogenesis is detrimental to hippocampal-dependent learning and memory [1, 3-7] and the deletion of Kv1.1 in adult NSCs reduces adult hippocampal neurogenesis, we hypothesized that Kv1.1 cKO mice have learning deficits. Adult neurogenesis is important for two aspects of hippocampal-dependent learning and memory—contextual fear conditioning, where the mice learn to associate an environment with fear [63-66], and pattern separation, where they learn to discriminate between two similar contexts [44, 46, 67, 68]. We decided to conduct behavioral tests of Kv1.1 cKO mice starting at ~4 months of age, because adult neurogenesis is less variable for 4-month-old mice compared to 2-month-old mice [69]. We injected ~4-month-old Kv1.1 cKO mice with TAM for 5 consecutive days to induce Cre expression and Kv1.1 deletion in more cells (Figure 3.5A). In control behavioral experiments, we did not find statistically significant differences between Kv1.1 cKO and Kv1.1 WT mice in open field (total distance traveled ( $P = 0.2652$ ), percent time on open arm ( $P = 0.1079$ ), percent time on closed arm ( $P = 0.3838$ ), open arm entries ( $P = 0.1826$ ), and closed arm entries ( $P = 0.4879$ )), elevated plus maze (total movement ( $P = 0.8644$ ), total movement over time between genotype ( $P = 0.8606$ ), ambulatory movement

( $P = 0.8704$ ), fine movement ( $P = 0.8435$ ), center/total movement ( $P = 0.3979$ ), and rearing ( $P = 0.7873$ ), and hotplate test ( $P = 0.3763$ ). These results indicate that the mobility, anxiety, and pain perception of  $K_v1.1$ cKO mice are similar to those of  $K_v1.1$  WT mice (Supplementary figure 3.5A-J).

To test for the effects of  $K_v1.1$  cKO on hippocampal-dependent learning and memory, we used the contextual fear conditioning and discrimination test. During the first part of the test, mice underwent three days of contextual fear conditioning where they learned to associate the fear context with a foot shock (Figure 3.5B). We found that  $K_v1.1$  cKO mice displayed a deficit in their ability to acquire the fear memory, which manifested as a ~25% and ~20% reduction in freezing time prior to foot shock as compared to  $K_v1.1$  WT on Day 2 and Day 3 (Day 1 ( $P = 0.3719$ ), Day 2 ( $P = 0.0339$ ), Day 3 ( $P = 0.0035$ )) (Figure 3.5C). This observation is consistent with previous studies reporting diminished adult neurogenesis resulting in deficient contextual fear conditioning [63-66].

Second, we assessed their ability to recall the fear context and to generalize their learned fear to a similar novel neutral context by measuring their freezing in both contexts without shock applied (Figure 3.5D). For this portion of the test, we examined each genotype for their ability to generalize by performing similarly in the two contexts. On Day 4, both  $K_v1.1$  WT ( $P < 0.0001$ ) and  $K_v1.1$  cKO ( $P = 0.0003$ ) froze more in the fear context than the neutral context (Figure 3.5E). As the mice were not shocked in either context on Day 4, they experienced an extinction of the freezing response in the fear context and generalized their freezing responses to the neutral context, resulting in a similar percent freezing in both contexts within genotype on Day 5 ( $K_v1.1$  WT ( $P =$



0.2849),  $K_v1.1$  cKO ( $P = 0.4097$ ) (Figure 3.5F). Once their ability to generalize was established, we continued to the third step of our experiment to assess their ability to discriminate between the two contexts.

Third, we examined their performance on the pattern separation task. On Days 6-19, the mice were placed in the two contexts daily and the shock was again administered in the fear context. Percent freezing was measured and averaged for a two-day block to lower variability (Figure 3.5G). As the mice began to discriminate between the fear context and the neutral context, they began freezing more in the fear context than the neutral context. We observed a mild impairment in discrimination of  $K_v1.1$  cKO mice compared to  $K_v1.1$  WT mice. Whereas  $K_v1.1$  WT mice froze significantly less in the neutral context compared to the fear context by Block 3 ( $K_v1.1$  WT Block 1 ( $P = 0.2049$ ), Block 2 ( $P = 0.2112$ ), Block 3 ( $P = 0.0283$ ), Block 4 ( $P = 0.0036$ ), Block 5 ( $P = 0.0028$ ), Block 6 ( $P < 0.0001$ ), and Block 7 ( $P < 0.0001$ )) (Figure 3.5H),  $K_v1.1$  cKO mice did not consistently freeze significantly less in the neutral context compared to the fear context until Block 6 ( $K_v1.1$  cKO Block 1 ( $P = 0.6384$ ), Block 2 ( $P = 0.5937$ ), Block 3 ( $P = 0.0696$ ), Block 4 ( $P = 0.0232$ ), Block 5 ( $P = 0.0614$ ), Block 6 ( $P = 0.0106$ ), and Block 7 ( $P = 0.0055$ )) (Figure 3.5I). This mild behavioral phenotype is consistent with the slight ~20% decrease in neurogenesis in the  $K_v1.1$  cKO behavioral cohort as compared to  $K_v1.1$  WT behavioral cohort ( $P = 0.0431$ ) (Figure 3.5J). Past studies using x-ray irradiation to reduce adult neurogenesis by more than 90% have revealed a similar impairment in contextual fear discrimination [46, 67]. These observations indicate that deletion of  $K_v1.1$  impaired adult neurogenesis, resulting in deficits in contextual fear conditioning and mild impairments in contextual discrimination.

### 3.3 Discussion

Adult hippocampal neurogenesis is critical for learning and memory and altered adult neurogenesis has been implicated in aging and neurological disorders [1, 3-7]. Although voltage-gated ion channels have been shown to modulate NSC and NPC membrane potential and cell dynamics during vertebrate and invertebrate neurodevelopment [10, 12-15], the role of bioelectric signaling in adult hippocampal neurogenesis has only been recently explored. In our previous study, we found that genetic ablation of  $K_v1.1$  depolarizes neonatal NPCs and increases proliferation through enhanced TrkB signaling in neonatal hippocampal development [2]. As  $K_v1.1$  null mice develop seizures that could impact adult neurogenesis [30, 32-34, 42, 43] and confound possible impact of  $K_v1.1$  deletion on adult neurogenesis, we developed a strategy for inducible conditional knockout of  $K_v1.1$  from NSCs of adult mice (Supplementary figure 3.1A). These  $K_v1.1$  cKO mice allowed us to examine the role of  $K_v1.1$  at different stages of adult neurogenesis and better elucidate the role of  $K_v1.1$  during neonatal and adult development.

During early steps of adult hippocampal neurogenesis,  $K_v1.1$  is important for preventing RGL over-proliferation to preserve the RGL pool (Figure 3.6A), which is maintained by a delicate balance between RGL quiescence and activation [70]. Initially, RGLs without  $K_v1.1$  rapidly divide to (1) self-renew, generating more quiescent RGLs (Figure 3.2B), and (2) differentiate, producing more Type 2a cells (Supplementary figure 3.3B). However, RGLs have varying self-renewal capacity. Over time, the increased proliferation may become unsustainable and might exhaust the RGLs with limited proliferative potential as they undergo terminal differentiation and are eliminated from the progenitor pool [71, 72]. Interestingly, the switch between RGL quiescence and activation can be regulated by network activity of glutamatergic mossy cells and long-range

GABAergic neurons. Ablation of both cell types can produce a similar initial activation followed by depletion of RGLs [16, 18, 21]. In addition to regulation via synaptic inputs, RGLs may rely on  $K_v1.1$  channel activity to prevent their subsequent activation and depletion (Supplementary figure 3.2 and Figure 3.2). Perhaps, as we previously observed in neonatal neurogenesis [2], depolarization of NSCs and NPCs also increases TrkB signaling and promotes proliferation in adult neurogenesis.

Our studies further reveal that loss of  $K_v1.1$  in the NSC lineage impedes abGC development in later stages of adult neurogenesis. In  $K_v1.1$  cKO mice, there was a reduction of DCX-expressing cells as well as impairment of abGC maturation and positioning (Figure 3.3A-F). Notably, aberrant positioning of abGCs is displayed by mouse models of traumatic brain injury and schizophrenia [58, 59] which suggests that proper positioning of abGCs is important for normal brain function. Failing to properly mature and position themselves, young abGCs produced from NSCs lacking  $K_v1.1$  likely struggle to integrate into the dentate gyrus circuit, resulting in decreased survival of new abGCs and reduction of mature abGCs (NeuN+) in  $K_v1.1$  cKO mice (Figure 3.3G-H). Failures in adult neurogenesis often leads to impairments in hippocampal-dependent learning and memory [44, 46, 63-68]. Indeed,  $K_v1.1$  cKO mice have diminished fear learning and mild deficit in pattern separation (Figure 3.5). Together, these results underscore the critical function of  $K_v1.1$  in maintaining abGC maturation and positioning for proper integration into the dentate gyrus circuit and preserving hippocampal-dependent learning and memory (Figure 3.6B).

Our understanding of the role of  $K_v1.1$  in adult neurogenesis also helps to clarify the role of  $K_v1.1$  in neonatal neurogenesis. Given that we observed an initial increase in RGL proliferation when

K<sub>v</sub>1.1 is removed from adult K<sub>v</sub>1.1 cKO mice, the increase in neonatal neurogenesis observed in both K<sub>v</sub>1.1 null mice [2] and K<sub>v</sub>1.1 cKO mice (Figure 3.1) is likely to have arisen from neonatal RGL over-proliferation. Unlike adult NSCs and NPCs, neonatal NSCs and NPCs have extensive proliferative potential [40, 41] and produce neurons with delayed cell death [60-62]. These properties of neonatal neurogenesis allow the neuronal progenies to last for a longer period, which would account for the initial increase in K<sub>v</sub>1.1-null progeny of 2 to 3-month-old Nestin-Cre; *Kcna1*<sup>+/-</sup>; MADM-6 mice (Figure 3.4) before neuron death starting at 2 months post-mitosis. As the MADM mice age, neonatal-born K<sub>v</sub>1.1-null neurons begin cell death and the RGLs lacking K<sub>v</sub>1.1 become depleted as in the case of adult K<sub>v</sub>1.1 cKO mice. Together, these factors contribute to the transient increase of K<sub>v</sub>1.1-null progeny neurons in 2 to 3-month-old but not 6 to 13-month-old Nestin-Cre; *Kcna1*<sup>+/-</sup>; MADM-6 mice (Figure 3.4). These results support our model that K<sub>v</sub>1.1 functions to maintain hippocampal neurogenesis at multiple developmental timepoints.

In summary, we demonstrate that K<sub>v</sub>1.1 is important for adult hippocampal neurogenesis and hippocampal-dependent learning and memory. K<sub>v</sub>1.1 likely regulates the neurogenic niche by preventing the over-proliferation and depletion of RGLs. As young abGCs develop, loss of K<sub>v</sub>1.1 impedes their dendritic maturation and positioning, likely hampering their integration into the circuit. These developmental failures in K<sub>v</sub>1.1 cKO mice contribute to decreased abGCs and deficits in context encoding and discrimination (Figure 3.6). These findings provide the basis for future studies of the impact of K<sub>v</sub>1.1 regulation on adult neurogenesis under normal and pathophysiological conditions.

### 3.4 Methods

#### *Animals.*

All experiments were approved by the Institutional Animal Care and Use Committees of the University of California, San Francisco and Academia Sinica. Two to five mice per cage were maintained in a temperature-controlled environment on a 12 hr light/dark cycle with *ad libitum* access to food and water.

*Kcna1<sup>fl/fl</sup>* mice [47] were obtained from Dr. Edward Glasscock's lab at Southern Methodist University. *Nestin-Cre<sup>ERT2</sup>* mice [44-46] were obtained from Dr. Mazen Kheirbek's lab at University of California, San Francisco. PC::G5-tdT mice [48] were obtained from the Jackson Laboratory. We utilized the PC::G5-tdT reporter line because its Cre-reporter alleles are located on a different chromosome (Chr 11) from *Kcna1* (Chr 6). These 3 lines were bred together to create Kv1.1 cKO mice (*Kcna1<sup>fl/fl</sup>; Nestin-Cre<sup>ERT2+</sup>; PC::G5-tdT<sup>+/-</sup>*) and maintained on a C57BL/6 background.

To create the Nestin-Cre; *Kcna1<sup>+/-</sup>*; MADM-6 mice, the lines bred together were: *Kcna1<sup>-/-</sup>* mice [34], obtained from Dr. Bruce Tempel's lab at the University of Washington; Nestin-Cre (Tg(Nes-cre)1Kln) [73], obtained from Jackson Laboratory; and MADM-6 mice with Rosa26<sup>GT</sup> (Gt(ROSA)26<sup>Sortm6</sup>(ACTB-EGFP\*, -tdTomato)) and Rosa26<sup>TG</sup> (Gt(ROSA)26<sup>Sortm7</sup>(ACTB-EGFP\*)) [74], obtained from Dr. Liqun Luo's lab at Stanford University. All these mice were maintained on an ICR background. MADM experiments were performed as previously described [2].

### ***Drug Administration***

For neonatal tamoxifen (TAM) (MilliporeSigma) administration, TAM was dissolved in 100% corn oil (MilliporeSigma) at 10 mg TAM/mL. At postnatal day 0, pups were injected once subcutaneously with 30  $\mu$ L of 10 mg TAM/mL. For adult tamoxifen administration, TAM was dissolved in a solution of 10% ethanol (200 proof, VWR) in corn oil at 20 mg TAM/mL. Adult 8-week-old mice were intraperitoneally injected with 100 mg TAM/kg body weight once per day for 3 consecutive days. For behavior experiments, a cohort of ~4-month-old mice were intraperitoneally injected with 100 mg TAM/kg body weight once per day for 5 consecutive days. Behavioral experiments were then carried out 5 weeks after the last TAM injection. Bromodeoxyuridine (BrdU) (MilliporeSigma) was dissolved in sterile normal (0.9%) saline at 5 mg BrdU/mL. One dose of 50 mg BrdU/kg body weight was injected subcutaneously at postnatal day 7. Lineage tracing experiments were then carried out at postnatal day 14.

### ***Single-cell suspension***

Adult 8-week-old mice were injected with TAM for 3 consecutive days. At 2 weeks post-TAM, mice were euthanized and their brains were transferred into ice-cold 1x HBSS (Hanks' Balanced Salt solution). Under a dissecting microscope, dentate gyri were isolated and pooled from 4 mice of the same genotype. The Neural Tissue Dissociation (P) Kit (Miltenyi Biotec) was used to dissociate tissue into single cells. After a final HBSS wash, the cell pellet was resuspended in 800  $\mu$ L of Hibernate A Low Fluorescence medium (BrainBits).

### ***Cell sorting and qPCR.***

The single-cell suspension was incubated with LIVE/DEAD™ stain 633nm (1:2000, Invitrogen) for 30 min at 4°C to identify dead cells. Cells were then filtered using a 40 µm strainer and sorted on the FACS Aria™ III Cell Sorter (BD Bioscience). Based on forward and side scatter, cells were gated to exclude debris and doublets. The cell population was selected based on the intensity of tdTomato fluorescence and LIVE/DEAD™ stain 633nm.

Pooled tdTomato+ live cell mRNA was extracted using RNAqueous-Micro Total RNA Isolation Kit (Invitrogen). The qPCR reactions were run using PowerUp™ SYBR™ Green master mix (Applied Biosystems) along with 100 nM primers (IDT). Relative mRNA levels were determined using the  $2^{-\Delta\Delta C_T}$  method [75]. *K<sub>v</sub>1.1* WT and *K<sub>v</sub>1.1* cKO mice *Kcna1* mRNA levels were normalized by the mRNA levels of the house keeping gene *glyceraldehyde-3-phosphate dehydrogenase (GAPDH)*. The primer sequences used to amplify the target genes were: GAPDH-F:5'- TCACCACCATGGAGAAGGC; GAPDH-R:5'- GCTAAGCAGTTGGTGGTGCA; KCNA1-F:5'- AGATCGTGGGCTCCTTGTGT; KCNA1-R:5'- ACGGGCAGGGCAATTGT.

### ***Electrophysiology***

Dissociated cells were plated onto coverslips coated with 0.01% poly-L-Lysine (poly-L, MW 70-150,000, MilliporeSigma) and mouse laminin (10 µg/ml). Then, they were allowed to adhere for at least 30 min at room temperature. To record from *K<sub>v</sub>1.1* WT and *K<sub>v</sub>1.1* cKO cells, capillary glass pipettes were created from filamented borosilicate glass (O.D × I.D, 1.10 × 0.86 mm, Sutter Instruments) and fire-polished to 6-10 MΩ resistance. These pipettes were backfilled with solution containing (in mM) 120 K-Gluconate, 15 KCl, 1.4 MgCl<sub>2</sub>, 0.1 EDTA, 10 HEPES, 4 Mg-ATP, 0.3

Na<sub>3</sub>-GTP, 7 Phosphocreatine, at pH 7.4 with KOH and 290-300 mOsm/kg. As indicated, this solution was supplemented with 10 nM Dendrotoxin K (Alomone Labs), which is a selective inhibitor of K<sub>v</sub>1.1 at this concentration [76]. Then, the cell-coated coverslips were transferred into an artificial cerebrospinal fluid recording buffer that contained (in mM) 127 NaCl, 1.8 KCl, 10 HEPES, 1.3 MgCl<sub>2</sub>, 2.4 CaCl<sub>2</sub>, 15 Glucose, at pH 7.4 with HCl and 300-310 mOsm/kg. Cells that had undergone Cre-mediated recombination expressed tdTomato and were identified by red epifluorescence. Cell-attached patch-clamp electrophysiological recordings were then carried out at room temperature under laminar flow of artificial cerebrospinal fluid using a pressure-driven micro-perfusion system (SmartSquirt, Automate Scientific). An Axopatch 200B amplifier (Axon Instruments) was employed to collect the data, which was digitized via a Digidata 1550B (Axon Instruments). Voltage stimulus protocols were applied, and their evoked currents were measured on-line with pClamp10 (Molecular Devices), sampling data at 20 kHz and filtering it at 2 kHz. To measure cells' resting membrane potential, K<sup>+</sup> currents were evoked by applying a 50 msec. Voltage ramp from -100 to 100 mV. Current-voltage (I-V) relationships were analyzed off-line in pClamp and Prism (GraphPad). Because we set the pipette [K<sup>+</sup>] approximately equal to the intracellular [K<sup>+</sup>], the equilibrium potential for K<sup>+</sup> across the patch was approximately zero. Therefore, K<sup>+</sup> currents reversed direction when the pipette potential was equal to the membrane potential, allowing us to measure resting membrane potential [77, 78].

### ***Immunostaining***

Mice were anesthetized with isoflurane (Henry Schein Animal Health) before transcardial perfusion with cold PBS followed by cold 4% paraformaldehyde in PBS (4% PFA) (Electron Microscopy Services). Brains were removed, post-fixed overnight in 4% PFA for ~24 hrs at 4°C,



washed in PBS, and immersed in 30% sucrose in PBS for a minimum of 48 hrs at 4°C for cryoprotection. Then, the brains were frozen in OCT (Fisher Scientific). Free-floating 30 µm sections were collected into PBS using a cryostat (Leica CM3050 S, Leica Microsystems). Afterwards, the sections were transferred into cryoprotectant (30% ethylene glycol, 30% glycerol, 40% PBS) and stored at -20°C. Sagittal sections were collected from the lineage tracing cohort while coronal sections were collected from the behavior cohort. For immunohistochemistry, sections were removed from the cryoprotectant, washed 3 x 10 min in PBS, treated with 15 min of .5% triton in PBS, and transferred into blocking buffer (5% NDS, 1% BSA, 0.05% triton in PBS) for 1 hr at room temperature. Then, they were incubated in primary antibodies overnight at 4°C. The next day, they were washed 3 x 10 min with 0.05% triton in PBS and incubated in secondary antibodies for 1 hr at room temperature. After 3 x 10 min PBS washes, they were mounted using Fluoromount G mounting media with DAPI (Southern Biotech) on Superfrost Plus microscope slides (Fisher Scientific).

If additional treatments were required, they were performed before the blocking step described above. For MCM2 staining, which requires antigen retrieval, sections were placed in sodium citrate buffer (10 mM sodium citrate, 0.05% tween 20, pH 6.0) for 3 hrs at 70°C in a convection drying oven (Yamato), then allowed to cool for 15 min on ice. For BrdU visualization, DNA denaturation with 2N HCl was required. Sections were placed in 2N HCl for 30 min at 37°C. After 3 x 10 min PBS washes, sections were moved into blocking buffer.

Primary antibodies were diluted in blocking buffer as listed: chicken GFP antibody (GFP-1020, Aves Labs) at 1:1000, mouse MCM2 antibody (610701, BD Biosciences) at 1:500, rabbit Sox2

antibody (ab97959, Abcam) at 1:500, goat GFAP antibody (ab53554, Abcam) at 1:1000, rabbit NeuN antibody (12943, Cell Signaling Technology) at 1:1000, guinea pig DCX antibody (AB2253, MilliporeSigma) at 1:1000, and mouse BrdU antibody (B35128, ThermoFisher) at 1:500.

Secondary antibodies were diluted in blocking buffer at 1:1000 as listed: donkey anti-mouse Alexa Fluor 488 (A21202, ThermoFisher Scientific), donkey anti-chicken Cy3 (703-165-155, Jackson ImmunoResearch Laboratories, Inc.), donkey anti-rabbit Alexa Fluor-594 (711-585-152, Jackson ImmunoResearch Laboratories, Inc.), donkey anti-rabbit Alexa Fluor-647 (A31573, ThermoFisher Scientific), donkey anti-goat Alexa Fluor Plus 647 (A32849, ThermoFisher Scientific), and donkey anti-guinea pig Alex Flour-647 (706-605-148, Jackson ImmunoResearch Laboratories, Inc.).

### ***Microscopy and sampling***

One of every 10 sections in a series spanning the entire dentate gyrus was imaged on a confocal microscope (Leica Sp8) using a 40x or 63x HC PL Apo oil CS2 objective. For lineage analysis, a z-stack of five 3- $\mu$ m z-steps were collected per dentate gyrus section. The dorsal dentate gyrus was quantified, given that Cre-expression was variable in the ventral dentate gyrus [79].

The upper third of the dentate granule cell layer was defined as being within two dentate granule cell layers from the molecular layer. For behavioral analysis, the medial sections of both hemispheres were quantified. Images were processed and analyzed using Fiji (ImageJ, NIH). Experimenters were blinded to the genotype of the mice during analysis.

### ***Behavioral tests***

For all behavioral testing, the experimenters were blinded to the genotype of the mice. We did not observe overt differences in health between the two genotypes. Mice used for these experiments were healthy without injuries that would interfere with behavioral testing. Behavioral data were obtained with the help of the Gladstone Institutes' Behavioral Core.

For behavior experiments, a cohort of adult ~4-month-old (age range 13-17 weeks) mice were injected with TAM for 5 consecutive days. Five weeks after the last TAM injection, behavioral testing began with the elevated plus maze, followed by the open field. Contextual conditioning and discrimination testing began at ~6.5 weeks post-TAM. Afterwards, at ~10.5 weeks post-TAM, the hot plate test was conducted. Finally, mice were perfused at ~17.5 weeks post-TAM.

### ***Elevated plus maze***

The elevated plus maze (EPM) (Hamilton-Kinder, Poway, CA) consisted of two open arms (without walls, 15" long x 2" wide), two closed arms (with walls 6.5" tall), and an intersection of the arms (2" x 2" wide). Mice were habituated in the testing room under dim light for 1 hr before being placed into the intersection of the two arms in the EPM and allowed to explore freely for 10 min. Total distance traveled and time on the open and closed arms were recorded by the system using infrared photobeam breaks. The maze was cleaned with 70% ethanol between animals.

### ***Open field***

Mice were habituated in the testing room under normal light for 1 hr before being placed into the center of the arena and allowed to explore freely for 15 min. The Flex-Field/Open Field Photobeam

Activity System (San Diego Instruments, San Diego, CA) was used for this experiment. It consisted of a clear acrylic chamber (41 x 41 x 30 cm) inside sound and light attenuating shells to eliminate external stimuli. Within the chamber, there were two 16 x 16 photobeam arrays that automatically detect horizontal and vertical movements. Total movements, ambulatory movement (disruption of 3 or more consecutive photobeams), fine movement (repeated disruption of the same 2 photobeams), center/total movement, and rearing were collected by the system for analysis. The arena was cleaned with 70% ethanol between animals.

### ***Contextual fear conditioning and discrimination***

The pattern separation task was adapted from [67] and [80]. A conditioning chamber (Med Associates Inc) was used for the experiment. The fear context consisted of background noise from a 60 dB fan and scent of 70% Windex sprayed into the bedding pan. The neutral context consisted of a black A-frame insert, no background noise, and 10% Simple Green scent. For contextual conditioning experiments, mice were placed in the fear context for a 4 min session for 3 consecutive days. There were no stimuli for the first 3 min baseline period followed by a single mild foot shock (0.45 mA) lasting 2 sec. Animals were exposed to 1 shock per session per day followed by a 1 min interval before being returned to their home cage. Conditioning was assessed by measuring "freezing" behavior. "Freezing" was defined as a defensive posture characterized by lack of all movement except that required for respiration. Contextual memory recall and generalization tests were conducted over the next 2 days (Days 4 and 5) in the absence of any foot shocks. On Day 4, the mice were placed in the fear training context in the morning for a 4 min session. In the afternoon, animals were introduced to the neutral no-shock context for a 4 min session to provide a measure of context generalization. On Day 5 of testing, the mice were placed

in the neutral context in the morning and the fear context in the afternoon. A 4-hr delay separated the two sessions in which the mice were returned to the colony room. For measurements of pattern separation between the two contexts, mice were again given two 4 min sessions each day over the course of the next 14 consecutive days except that during this phase of the testing, a single foot shock was again delivered to the mice in the fear context after an initial 3 min baseline period. No foot shocks were delivered while the mice were in the neutral context. Discrimination learning between the 2 contexts was determined by comparing the percent freezing behavior exhibited in the first 3 min of each 4 min testing session in each context.

### ***Hot plate***

Mice were habituated in the testing room under normal light for 1 hr before being placed on top of the hot plate in a clear, open-ended cylindrical enclosure. The temperature was set to 52°C. The latency to respond (for example a hindpaw lick, hindpaw flick, or jump) was measured. The mouse was immediately removed from the hot plate after responding. The maximum latency to respond allowed was 30 sec to prevent injury.

### ***Statistical Analyses***

All data were summarized as mean  $\pm$  SEM. Comparisons between two genotypes were analyzed by a two-tailed Student's t-test. If the data did not meet the Student's t-test's assumptions of normality and variance, the data were analyzed using the two-tailed t-test with Welch's correction or the non-parametric Mann-Whitney U-test, as indicated in the figure legends. Multiple group comparisons were assessed using one-way ANOVA with Holm-Sidak correction for multiple comparisons, two-way ANOVA followed by Sidak's multiple comparisons test, two-way repeated

measures ANOVA with the Geisser-Greenhouse correction, or mixed-effects analysis with the Geisser-Greenhouse correction followed by Sidak's multiple comparisons test, as indicated in the figure legends. The null hypothesis was rejected at  $P > 0.05$ . Data were analyzed using Prism 9 (GraphPad).

### **3.5 Acknowledgments**

We thank Jeanne Paz, Mazen Kheirbek, John Rubenstein, Mario Zubia, Adeline Yong, and all members of the Jan lab for helpful discussions. We also recognize Marena Tynan-La Fontaine for technical support with mouse experiments, Hirofumi Noguchi for expert technical advice, and members of the Gladstone Behavioral Core, Michael Gill and Iris Lo, for assistance in behavioral experiments. We are grateful to Mazen Kheirbek, Liqun Luo, and David Julius for providing reagents and resources. This work was supported by NSF Graduate Research Fellowships (2034836 to Y.H.L.K; 1650113 to J.V.L.K.), National Institute of Health (R01MH065334 to L.Y.J.; NS100954 and NS099188 to E. G.), the Ministry of Science and Technology, Taiwan (106-2320-B-001-013, 107-2320-B-001-026-MY3 and 110-2314-B-001-007 to S.B.Y.), and a UCSF Chuan-Lyu Discovery Fellowship (J.V.L.K.). Y.N.J. and L.Y.J. are Howard Hughes Medical Institute Investigators.

### 3.6 References

1. Goncalves, J.T., S.T. Schafer, and F.H. Gage, *Adult Neurogenesis in the Hippocampus: From Stem Cells to Behavior*. Cell, 2016. **167**(4): p. 897-914.
2. Chou, S.M., et al., *K<sub>v</sub>1.1 channels regulate early postnatal neurogenesis in mouse hippocampus via the TrkB signaling pathway*. Elife, 2021. **10**.
3. Aimone, J.B., et al., *Regulation and function of adult neurogenesis: from genes to cognition*. Physiol Rev, 2014. **94**(4): p. 991-1026.
4. Anacker, C. and R. Hen, *Adult hippocampal neurogenesis and cognitive flexibility - linking memory and mood*. Nat Rev Neurosci, 2017. **18**(6): p. 335-346.
5. Ming, G.L. and H. Song, *Adult neurogenesis in the mammalian brain: significant answers and significant questions*. Neuron, 2011. **70**(4): p. 687-702.
6. Sahay, A. and R. Hen, *Adult hippocampal neurogenesis in depression*. Nat Neurosci, 2007. **10**(9): p. 1110-5.
7. Toda, T., et al., *The role of adult hippocampal neurogenesis in brain health and disease*. Mol Psychiatry, 2019. **24**(1): p. 67-87.
8. Bond, A.M., G.L. Ming, and H. Song, *Adult Mammalian Neural Stem Cells and Neurogenesis: Five Decades Later*. Cell Stem Cell, 2015. **17**(4): p. 385-95.
9. Kriegstein, A. and A. Alvarez-Buylla, *The glial nature of embryonic and adult neural stem cells*. Annu Rev Neurosci, 2009. **32**: p. 149-84.
10. McLaughlin, K.A. and M. Levin, *Bioelectric signaling in regeneration: Mechanisms of ionic controls of growth and form*. Dev Biol, 2018. **433**(2): p. 177-189.
11. Bates, E., *Ion channels in development and cancer*. Annu Rev Cell Dev Biol, 2015. **31**: p. 231-47.



12. Smith, R.S. and C.A. Walsh, *Ion Channel Functions in Early Brain Development*. Trends Neurosci, 2020. **43**(2): p. 103-114.
13. Piggott, B.J., et al., *Paralytic, the Drosophila voltage-gated sodium channel, regulates proliferation of neural progenitors*. Genes Dev, 2019. **33**(23-24): p. 1739-1750.
14. Smith, R.S., et al., *Sodium Channel SCN3A (Na<sub>v</sub>1.3) Regulation of Human Cerebral Cortical Folding and Oral Motor Development*. Neuron, 2018. **99**(5): p. 905-913 e7.
15. Vitali, I., et al., *Progenitor Hyperpolarization Regulates the Sequential Generation of Neuronal Subtypes in the Developing Neocortex*. Cell, 2018. **174**(5): p. 1264-1276 e15.
16. Bao, H., et al., *Long-Range GABAergic Inputs Regulate Neural Stem Cell Quiescence and Control Adult Hippocampal Neurogenesis*. Cell Stem Cell, 2017. **21**(5): p. 604-617 e5.
17. Rozental, R., et al., *Changes in the properties of gap junctions during neuronal differentiation of hippocampal progenitor cells*. J Neurosci, 1998. **18**(5): p. 1753-62.
18. Song, J., et al., *Neuronal circuitry mechanism regulating adult quiescent neural stem-cell fate decision*. Nature, 2012. **489**(7414): p. 150-4.
19. Tozuka, Y., et al., *GABAergic excitation promotes neuronal differentiation in adult hippocampal progenitor cells*. Neuron, 2005. **47**(6): p. 803-15.
20. Yasuda, T., P.F. Bartlett, and D.J. Adams, *K<sub>ir</sub> and K<sub>v</sub> channels regulate electrical properties and proliferation of adult neural precursor cells*. Mol Cell Neurosci, 2008. **37**(2): p. 284-97.
21. Yeh, C.Y., et al., *Mossy Cells Control Adult Neural Stem Cell Quiescence and Maintenance through a Dynamic Balance between Direct and Indirect Pathways*. Neuron, 2018. **99**(3): p. 493-510 e4.

22. Kunze, A., et al., *Connexin expression by radial glia-like cells is required for neurogenesis in the adult dentate gyrus*. Proc Natl Acad Sci U S A, 2009. **106**(27): p. 11336-41.
23. Esposito, M.S., et al., *Neuronal differentiation in the adult hippocampus recapitulates embryonic development*. J Neurosci, 2005. **25**(44): p. 10074-86.
24. Ge, S., et al., *GABA regulates synaptic integration of newly generated neurons in the adult brain*. Nature, 2006. **439**(7076): p. 589-93.
25. Overstreet-Wadiche, L.S., A.L. Bensen, and G.L. Westbrook, *Delayed development of adult-generated granule cells in dentate gyrus*. J Neurosci, 2006. **26**(8): p. 2326-34.
26. Tashiro, A., et al., *NMDA-receptor-mediated, cell-specific integration of new neurons in adult dentate gyrus*. Nature, 2006. **442**(7105): p. 929-33.
27. Hallows, J.L. and B.L. Tempel, *Expression of Kv1.1, a Shaker-like potassium channel, is temporally regulated in embryonic neurons and glia*. J Neurosci, 1998. **18**(15): p. 5682-91.
28. Jan, L.Y. and Y.N. Jan, *Voltage-gated and inwardly rectifying potassium channels*. J Physiol, 1997. **505 ( Pt 2)**: p. 267-82.
29. Jan, L.Y. and Y.N. Jan, *Voltage-gated potassium channels and the diversity of electrical signalling*. J Physiol, 2012. **590**(11): p. 2591-9.
30. Almgren, M., et al., *Lack of potassium channel induces proliferation and survival causing increased neurogenesis and two-fold hippocampus enlargement*. Hippocampus, 2007. **17**(4): p. 292-304.
31. Donahue, L.R., et al., *Megencephaly: a new mouse mutation on chromosome 6 that causes hypertrophy of the brain*. Mamm Genome, 1996. **7**(12): p. 871-6.

32. Persson, A.S., et al., *K<sub>v</sub>1.1 null mice have enlarged hippocampus and ventral cortex*. BMC Neurosci, 2007. **8**: p. 10.
33. Petersson, S., et al., *Truncation of the Shaker-like voltage-gated potassium channel, K<sub>v</sub>1.1, causes megencephaly*. Eur J Neurosci, 2003. **18**(12): p. 3231-40.
34. Smart, S.L., et al., *Deletion of the K<sub>v</sub>1.1 potassium channel causes epilepsy in mice*. Neuron, 1998. **20**(4): p. 809-19.
35. Yang, S.B., et al., *K<sub>v</sub>1.1-dependent control of hippocampal neuron number as revealed by mosaic analysis with double markers*. J Physiol, 2012. **590**(11): p. 2645-58.
36. Espinosa, J.S., J.S. Tea, and L. Luo, *Mosaic analysis with double markers (MADM) in mice*. Cold Spring Harb Protoc, 2014. **2014**(2): p. 182-9.
37. Muzumdar, M.D., L. Luo, and H. Zong, *Modeling sporadic loss of heterozygosity in mice by using mosaic analysis with double markers (MADM)*. Proc Natl Acad Sci U S A, 2007. **104**(11): p. 4495-500.
38. Zong, H., et al., *Mosaic analysis with double markers in mice*. Cell, 2005. **121**(3): p. 479-92.
39. Berg, D.A., et al., *Radial glial cells in the adult dentate gyrus: what are they and where do they come from?* F1000Res, 2018. **7**: p. 277.
40. Kerloch, T., et al., *Dentate Granule Neurons Generated During Perinatal Life Display Distinct Morphological Features Compared With Later-Born Neurons in the Mouse Hippocampus*. Cereb Cortex, 2019. **29**(8): p. 3527-3539.
41. Urban, N. and F. Guillemot, *Neurogenesis in the embryonic and adult brain: same regulators, different roles*. Front Cell Neurosci, 2014. **8**: p. 396.

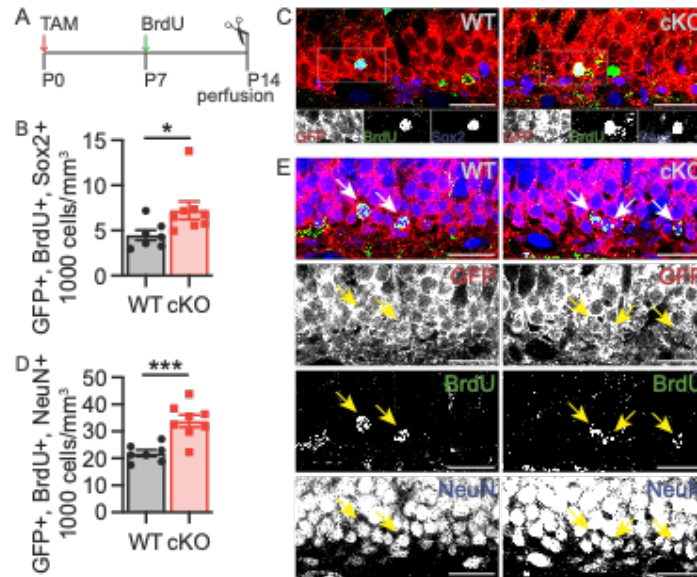
42. Almgren, M., M. Schalling, and C. Lavebratt, *Idiopathic megalencephaly-possible cause and treatment opportunities: from patient to lab*. Eur J Paediatr Neurol, 2008. **12**(6): p. 438-45.
43. Holth, J.K., et al., *Tau loss attenuates neuronal network hyperexcitability in mouse and Drosophila genetic models of epilepsy*. J Neurosci, 2013. **33**(4): p. 1651-9.
44. Danielson, N.B., et al., *Distinct Contribution of Adult-Born Hippocampal Granule Cells to Context Encoding*. Neuron, 2016. **90**(1): p. 101-12.
45. Dranovsky, A., et al., *Experience dictates stem cell fate in the adult hippocampus*. Neuron, 2011. **70**(5): p. 908-23.
46. Sahay, A., et al., *Increasing adult hippocampal neurogenesis is sufficient to improve pattern separation*. Nature, 2011. **472**(7344): p. 466-70.
47. Trosclair, K., et al., *Neuron-specific Kv1.1 deficiency is sufficient to cause epilepsy, premature death, and cardiorespiratory dysregulation*. Neurobiol Dis, 2020. **137**: p. 104759.
48. Gee, J.M., et al., *Imaging activity in neurons and glia with a Polr2a-based and cre-dependent GCaMP5G-IRES-tdTomato reporter mouse*. Neuron, 2014. **83**(5): p. 1058-72.
49. Gould, E., et al., *Learning enhances adult neurogenesis in the hippocampal formation*. Nat Neurosci, 1999. **2**(3): p. 260-5.
50. Kempermann, G., H.G. Kuhn, and F.H. Gage, *More hippocampal neurons in adult mice living in an enriched environment*. Nature, 1997. **386**(6624): p. 493-5.
51. Kuhn, H.G. and C.M. Cooper-Kuhn, *Bromodeoxyuridine and the detection of neurogenesis*. Curr Pharm Biotechnol, 2007. **8**(3): p. 127-31.

52. Wojtowicz, J.M. and N. Kee, *BrdU assay for neurogenesis in rodents*. Nat Protoc, 2006. **1**(3): p. 1399-405.
53. Bonaguidi, M.A., et al., *In vivo clonal analysis reveals self-renewing and multipotent adult neural stem cell characteristics*. Cell, 2011. **145**(7): p. 1142-55.
54. Brown, J.P., et al., *Transient expression of doublecortin during adult neurogenesis*. J Comp Neurol, 2003. **467**(1): p. 1-10.
55. Couillard-Despres, S., et al., *Doublecortin expression levels in adult brain reflect neurogenesis*. Eur J Neurosci, 2005. **21**(1): p. 1-14.
56. Plumpe, T., et al., *Variability of doublecortin-associated dendrite maturation in adult hippocampal neurogenesis is independent of the regulation of precursor cell proliferation*. BMC Neurosci, 2006. **7**: p. 77.
57. Kempermann, G., et al., *Early determination and long-term persistence of adult-generated new neurons in the hippocampus of mice*. Development, 2003. **130**(2): p. 391-9.
58. Duan, X., et al., *Disrupted-In-Schizophrenia 1 regulates integration of newly generated neurons in the adult brain*. Cell, 2007. **130**(6): p. 1146-58.
59. Ibrahim, S., et al., *Traumatic Brain Injury Causes Aberrant Migration of Adult-Born Neurons in the Hippocampus*. Sci Rep, 2016. **6**: p. 21793.
60. Cahill, S.P., et al., *Early survival and delayed death of developmentally-born dentate gyrus neurons*. Hippocampus, 2017. **27**(11): p. 1155-1167.
61. Ciric, T., S.P. Cahill, and J.S. Snyder, *Dentate gyrus neurons that are born at the peak of development, but not before or after, die in adulthood*. Brain Behav, 2019. **9**(10): p. e01435.

62. Dayer, A.G., et al., *Short-term and long-term survival of new neurons in the rat dentate gyrus*. J Comp Neurol, 2003. **460**(4): p. 563-72.
63. Denny, C.A., et al., *4- to 6-week-old adult-born hippocampal neurons influence novelty-evoked exploration and contextual fear conditioning*. Hippocampus, 2012. **22**(5): p. 1188-201.
64. Denny, C.A., et al., *Hippocampal memory traces are differentially modulated by experience, time, and adult neurogenesis*. Neuron, 2014. **83**(1): p. 189-201.
65. Kitamura, T., et al., *Adult neurogenesis modulates the hippocampus-dependent period of associative fear memory*. Cell, 2009. **139**(4): p. 814-27.
66. Saxe, M.D., et al., *Ablation of hippocampal neurogenesis impairs contextual fear conditioning and synaptic plasticity in the dentate gyrus*. Proc Natl Acad Sci U S A, 2006. **103**(46): p. 17501-6.
67. Nakashiba, T., et al., *Young dentate granule cells mediate pattern separation, whereas old granule cells facilitate pattern completion*. Cell, 2012. **149**(1): p. 188-201.
68. Tronel, S., et al., *Adult-born neurons are necessary for extended contextual discrimination*. Hippocampus, 2012. **22**(2): p. 292-8.
69. Ben Abdallah, N.M., et al., *Early age-related changes in adult hippocampal neurogenesis in C57 mice*. Neurobiol Aging, 2010. **31**(1): p. 151-61.
70. Urban, N., I.M. Blomfield, and F. Guillemot, *Quiescence of Adult Mammalian Neural Stem Cells: A Highly Regulated Rest*. Neuron, 2019. **104**(5): p. 834-848.
71. Bottes, S., et al., *Long-term self-renewing stem cells in the adult mouse hippocampus identified by intravital imaging*. Nat Neurosci, 2021. **24**(2): p. 225-233.

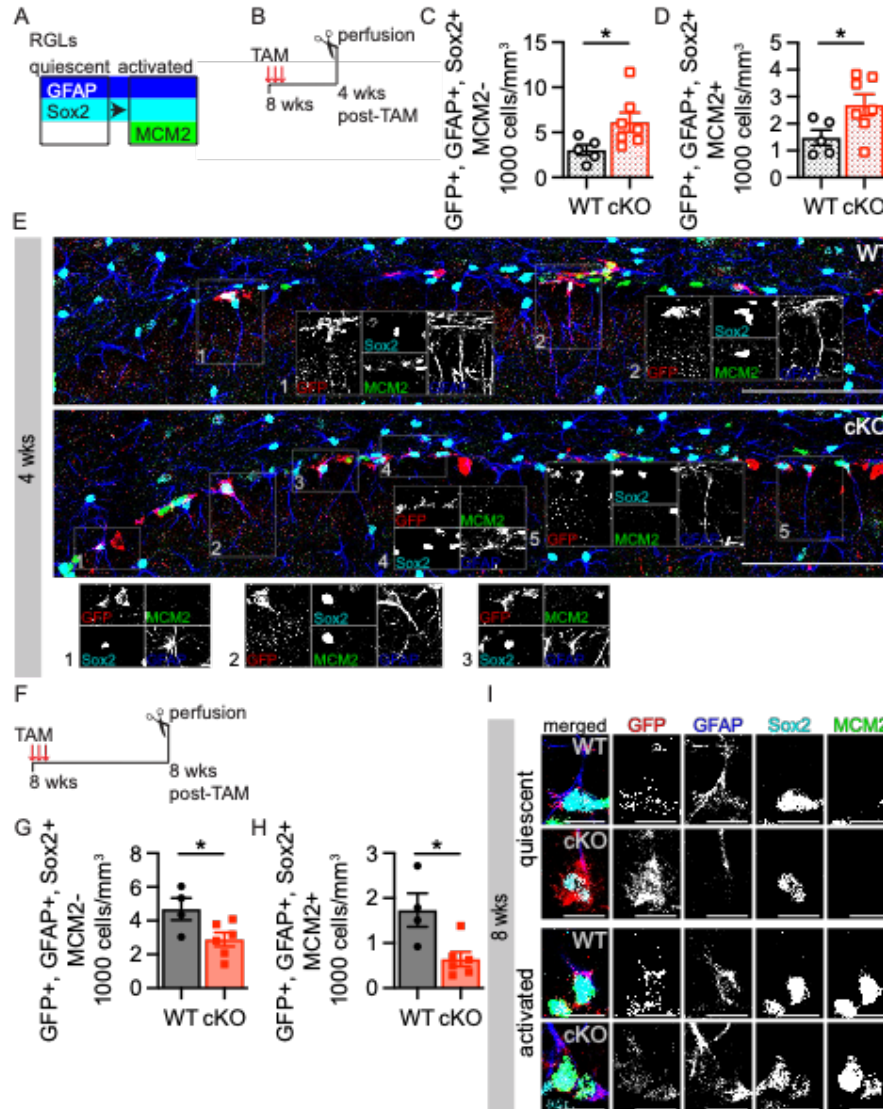
72. Pilz, G.A., et al., *Live imaging of neurogenesis in the adult mouse hippocampus*. Science, 2018. **359**(6376): p. 658-662.
73. Tronche, F., et al., *Disruption of the glucocorticoid receptor gene in the nervous system results in reduced anxiety*. Nat Genet, 1999. **23**(1): p. 99-103.
74. Tasic, B., et al., *Extensions of MADM (mosaic analysis with double markers) in mice*. PLoS One, 2012. **7**(3): p. e33332.
75. Livak, K.J. and T.D. Schmittgen, *Analysis of relative gene expression data using real-time quantitative PCR and the  $2^{-\Delta\Delta CT}$  Method*. Methods, 2001. **25**(4): p. 402-8.
76. Robertson, B., et al., *Novel effects of dendrotoxin homologues on subtypes of mammalian  $K_v1$  potassium channels expressed in *Xenopus* oocytes*. FEBS Lett, 1996. **383**(1-2): p. 26-30.
77. Verheugen, J.A., et al., *Voltage-gated and  $Ca^{2+}$ -activated  $K^+$  channels in intact human T lymphocytes. Noninvasive measurements of membrane currents, membrane potential, and intracellular calcium*. J Gen Physiol, 1995. **105**(6): p. 765-94.
78. Verheugen, J.A., D. Fricker, and R. Miles, *Noninvasive measurements of the membrane potential and GABAergic action in hippocampal interneurons*. J Neurosci, 1999. **19**(7): p. 2546-55.
79. Jinno, S., *Topographic differences in adult neurogenesis in the mouse hippocampus: a stereology-based study using endogenous markers*. Hippocampus, 2011. **21**(5): p. 467-80.
80. Tracy, T.E., et al., *Acetylated Tau Obstructs KIBRA-Mediated Signaling in Synaptic Plasticity and Promotes Tauopathy-Related Memory Loss*. Neuron, 2016. **90**(2): p. 245-60.

### 3.7 Main Figures



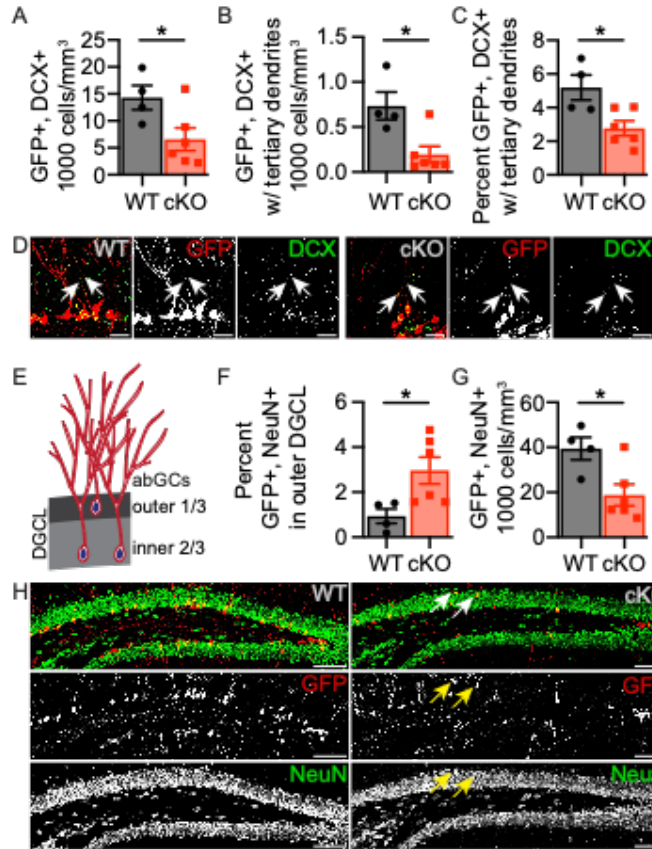
**Figure 3.1: Neonatal deletion of  $K_v1.1$  increases hippocampal neurogenesis.** (A) Neonatal lineage tracing protocol. Tamoxifen (TAM) was injected at postnatal day 0 (P0) to delete  $K_v1.1$  in neural stem cells (NSCs), and BrdU was injected at postnatal day 7 (P7) for lineage tracing. Brains were harvested at postnatal day 14 (P14). (B) Quantification (cells per  $\text{mm}^3$ ) at P14 of GFP+ NSCs and neural progenitor cells (NPCs) (GFP+, BrdU+, and Sox2+) produced from P7 dividing cells. An increase of GFP+, BrdU+, and Sox2+ cells was observed in  $K_v1.1$  cKO mice compared to  $K_v1.1$  WT mice ( $P = 0.0360$ ). (C) Representative image showing expression of GFP (red), BrdU (green), and Sox2 (blue) in the  $K_v1.1$  WT (left) and  $K_v1.1$  cKO (right) dentate gyrus. GFP, BrdU, and Sox2 staining within the boxed area are individually shown (below). Scale bar, 25  $\mu\text{m}$ . (D) Quantification (cells per  $\text{mm}^3$ ) at P14 of neurons (GFP+, BrdU+, and NeuN+) produced from P7 dividing cells.  $K_v1.1$  cKO mice displayed more neurogenesis compared to  $K_v1.1$  WT mice ( $P = 0.0007$ ). (E) Representative image displaying expression of GFP (red), BrdU (green), and NeuN (blue) in the  $K_v1.1$  WT (left) and  $K_v1.1$  cKO (right) dentate gyrus. GFP, BrdU, and NeuN signals are individually shown (below). GFP+, BrdU+, and NeuN+ cells are marked (arrows). Scale bar, 25  $\mu\text{m}$ . B and D:  $K_v1.1$  cKO ( $n = 8$ );  $K_v1.1$  WT ( $n = 7$ ). Unpaired two-tailed Student's t-test; \*  $P < 0.05$ , \*\*\*  $P < 0.001$ . Data are presented as mean  $\pm$  SEM.



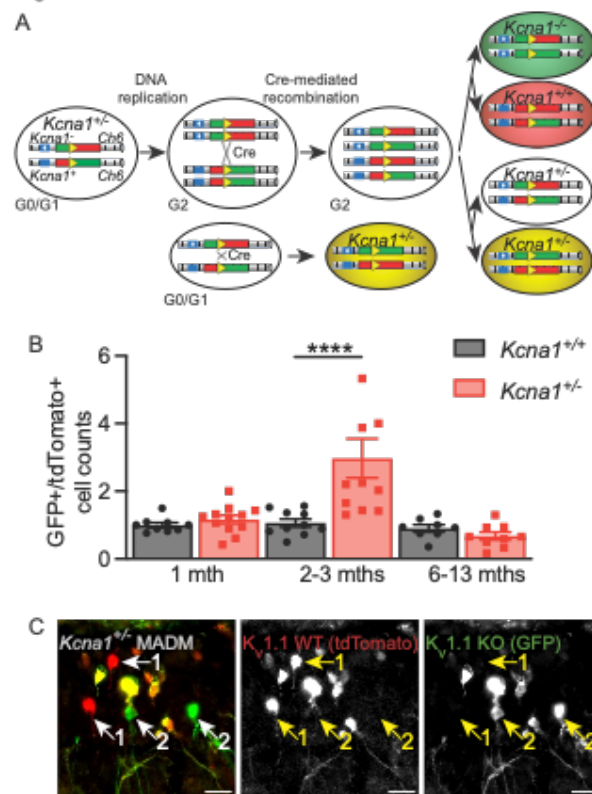


**Figure 3.2: Deletion of  $K_v1.1$  in adult neural stem cells (NSCs) results in an initial increase of radial glia-like NSCs (RGLs) before eventual depletion of the RGL pool.** (A) Diagram of cell marker expression during NSC and NPC development. Quiescent RGLs express GFAP and Sox2. As RGLs start proliferating, they express MCM2. (B) Protocol to assess short-term effects of  $K_v1.1$  cKO on adult hippocampal neurogenesis. At 8 weeks old,  $K_v1.1$  cKO mice and  $K_v1.1$  WT mice were injected with TAM for 3 consecutive days to induce Cre expression and *Kcna1* deletion. At 4 weeks post-TAM, we carried out immunostaining of GFP+ RGLs. (C and D) Quantification (cells per  $\text{mm}^3$ ) of adult RGLs at 4 weeks post-TAM. An increase in quiescent RGLs (GFP+, GFAP+, Sox2+, MCM2-) ( $P = 0.0481$ ) and activated RGLs (GFP+, GFAP+, Sox2+, MCM2+) ( $P = 0.0461$ ) in  $K_v1.1$  cKO mice ( $n = 7$ ) compared to  $K_v1.1$  WT mice ( $n = 5$ ) was revealed. (E) Representative image showing expression of GFP (red), GFAP (blue), Sox2 (cyan), and MCM2 (green) in the ventral blade of the dentate gyrus in  $K_v1.1$  WT (top) and  $K_v1.1$  cKO (bottom) mice. Within the  $K_v1.1$  WT overlay, quiescent (1) and activated (2) RGLs are boxed; and within the  $K_v1.1$  cKO overlay quiescent (1, 3, 4, and 5) and activated (2) RGLs are boxed. Each individual channel of the boxed areas is displayed. Scale bar, 100  $\mu\text{m}$ . (F) Protocol to assess long-

term effects of  $K_v1.1$  cKO on adult neurogenesis.  $K_v1.1$  cKO mice and  $K_v1.1$  WT mice were injected at 8 weeks of age with TAM for 3 consecutive days to induce Cre expression and *Kcna1* deletion. At 8 weeks post-TAM, we carried out immunostaining of GFP<sup>+</sup> RGLs. (G and H) Quantification (cells per  $\text{mm}^3$ ) of adult RGLs at 8 weeks post-TAM. Quiescent RGLs (GFP<sup>+</sup>, GFAP<sup>+</sup>, Sox2<sup>+</sup>, MCM2<sup>-</sup>) ( $P = 0.0391$ ) and activated RGL (GFP<sup>+</sup>, GFAP<sup>+</sup>, Sox2<sup>+</sup>, MCM2<sup>+</sup>) ( $P = 0.0158$ ) were decreased in  $K_v1.1$  cKO mice ( $n = 6$ ) compared to  $K_v1.1$  WT mice ( $n = 4$ ). (I) Representative images of RGLs in  $K_v1.1$  WT and  $K_v1.1$  cKO mice at 8 weeks post-TAM with merged and individual channels of GFP (red), GFAP (blue), Sox2 (cyan), and MCM2 (green) are shown. Scale bar, 10  $\mu\text{m}$ . C, D, G, H: Unpaired two-tailed Student's t-test; \*  $P < 0.05$ . Data are presented as mean  $\pm$  SEM.



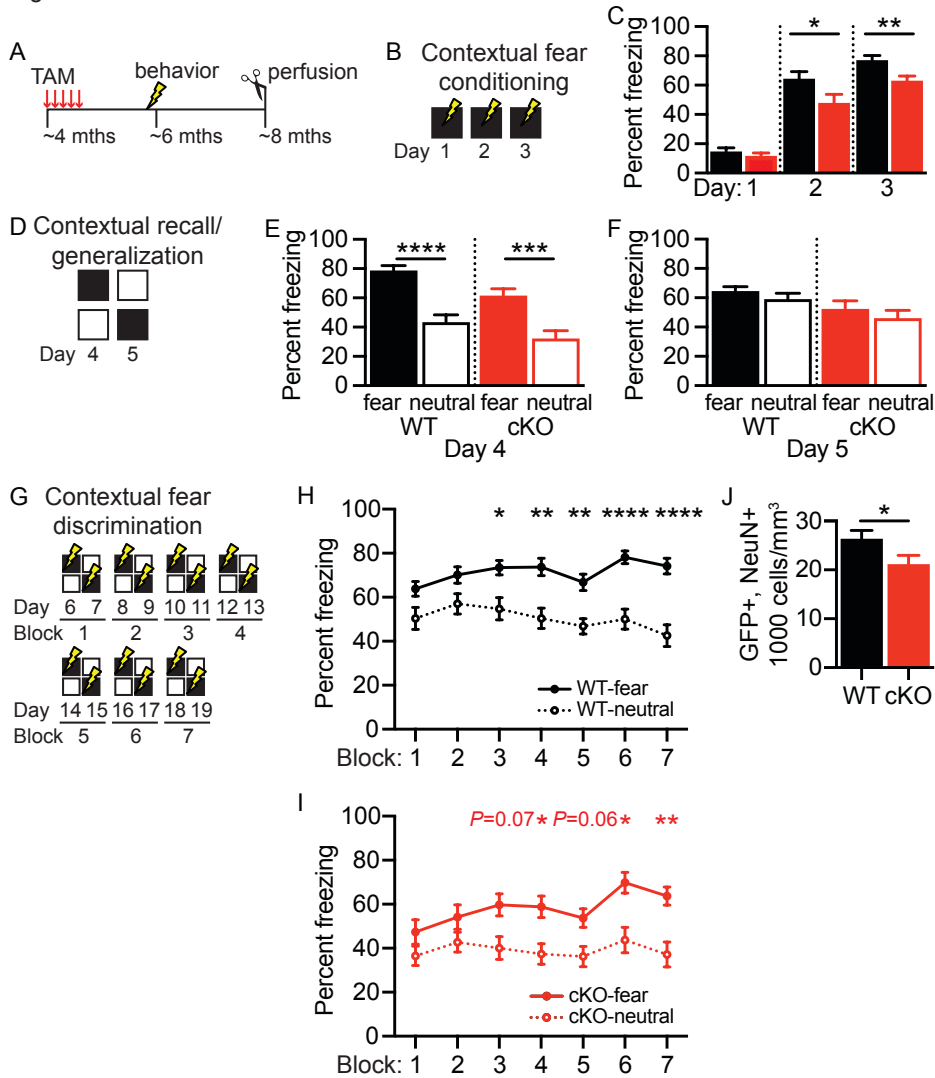
**Figure 3.3: Loss of *Kv1.1* impairs adult hippocampal neurogenesis by altering doublecortin-expressing (DCX+) cell maturation and adult-born granule cell (abGC) positioning.** (A) Quantification (cells per mm<sup>3</sup>) of GFP+, DCX+ cells. Fewer GFP+, DCX+ cells were found in *Kv1.1* cKO mice compared to *Kv1.1* WT mice ( $P = 0.0413$ ). (B) Quantification (cells per mm<sup>3</sup>) of more mature GFP+, DCX+ cells with tertiary dendrites. A decrease in GFP+, DCX+ cells with tertiary dendrites in *Kv1.1* cKO mice compared to *Kv1.1* WT mice was revealed ( $P = 0.0117$ ). (C) Percentage of GFP+, DCX+ cells that display more mature tertiary dendrite morphology is reduced in *Kv1.1* cKO mice compared to *Kv1.1* WT mice ( $P = 0.0165$ ). (D) Representative image of merged and individual signals of GFP (red) and DCX (green) in the dentate gyrus of *Kv1.1* WT mice (left) and *Kv1.1* cKO (right) mice. Branching of DCX+ cells with tertiary dendrites are marked (arrows). Scale bar, 25  $\mu\text{m}$ . (E) Cartoon of abGC development. AbGCs migrate away from the subgranular zone towards the molecular layer and usually position themselves within the inner two thirds of the dentate granule cell layer (DGCL). (F) Percentage of GFP+, NeuN+ cells in outer layer of the DGCL is diminished in *Kv1.1* cKO mice compared to *Kv1.1* WT mice ( $P = 0.0330$ ). (G) Quantification (cells per mm<sup>3</sup>) of GFP+, NeuN+ cells. GFP+, NeuN+ cells were decreased in *Kv1.1* cKO mice compared to *Kv1.1* WT mice ( $P = 0.0204$ ). (H) Representative image of overlaid and individual GFP (red) and NeuN (green) signals of the dentate gyrus from *Kv1.1* WT mice (left) and *Kv1.1* cKO (right) mice are shown. GFP+, NeuN+ cells in the outer third of the DGCL are marked (arrows). Scale bar, 100  $\mu\text{m}$ . A–C, G–H: *Kv1.1* cKO ( $n = 6$ ); *Kv1.1* WT ( $n = 4$ ). Unpaired two-tailed Student's *t*-test; \*  $P < 0.05$ . Data are presented as mean  $\pm$  SEM.



**Figure 3.4: MADM analysis reveals a transient increase in K<sub>v</sub>1.1-null progeny cells in the dentate gyrus of 2 to 3-month-old mice.** (A) Schematic of MADM method [36-38] for generating K<sub>v</sub>1.1-null (GFP+) and K<sub>v</sub>1.1-wildtype (tdTomato+) progeny. MADM-6 marker mice were bred to *Kcna1*<sup>-/-</sup> mice and Nestin-Cre mice. At G2 phase, Cre recombinase induces infrequent interchromosomal recombination and restores functional GFP and tdTomato genes. During chromosome segregation, equal numbers of either *Kcna1*<sup>-/-</sup> (GFP+) and *Kcna1*<sup>+/+</sup> (tdTomato+) progenies, or colorless *Kcna1*<sup>-/-</sup> and dual color *Kcna1*<sup>+/-</sup> (yellow) progenies are generated. Dual color *Kcna1*<sup>+/-</sup> (yellow) progenies can also be generated by interchromosomal recombination at G0/G1 phase (below). (B) Ratio of GFP+ to tdTomato+ cells in Nestin-Cre; *Kcna1*<sup>-/-</sup>; MADM-6 and Nestin-Cre; *Kcna1*<sup>+/+</sup>; MADM-6 control mice at 1-month-old, 2 to 3-month-old, and 6 to 13-month-old. The ratio of K<sub>v</sub>1.1-null (GFP+) to K<sub>v</sub>1.1-wildtype (tdTomato+) progeny cells is increased in 2 to 3-month-old Nestin-Cre; *Kcna1*<sup>-/-</sup>; MADM-6 mice compared to Nestin-Cre; *Kcna1*<sup>+/+</sup>; MADM-6 control mice ( $P < 0.0001$ ). There is no difference in the ratio of K<sub>v</sub>1.1-null (GFP+) to K<sub>v</sub>1.1-wildtype (tdTomato+) progeny cells between the two genotypes at 1-month-old and 6 to 13-month-old. Two-way ANOVA followed by Sidak's multiple comparisons test; genotype effect ( $F_{1,53} = 6.989$ ,  $P = 0.0108$ ), age effect ( $F_{2,53} = 10.23$ ,  $P = 0.0002$ ), and genotype x age interaction ( $F_{2,53} = 8.159$ ,  $P = 0.0008$ ); multiple comparisons: 1-month-old ( $P = 0.9648$ ), 2 to 3-month-old ( $P < 0.0001$ ), and 6 to 13-month-old ( $P = 0.9331$ ). (C) Representative image with overlay and individual signals displaying K<sub>v</sub>1.1-null progenies (GFP+, green), K<sub>v</sub>1.1-wildtype progenies (tdTomato+, red), and K<sub>v</sub>1.1-heterozygous (GFP+ and tdTomato+, yellow) from the dentate gyrus of 8-month-old Nestin-Cre; *Kcna1*<sup>+/-</sup>; MADM-6 mice. K<sub>v</sub>1.1-wildtype (1) and K<sub>v</sub>1.1-null (2) cells are marked (arrows). Scale bar, 25  $\mu$ m. Nestin-Cre; MADM-6 1-month-old ( $n = 9$ ); 2 to 3-month-old ( $n = 10$ ); 6 to 13-month-old ( $n = 8$ ). Nestin-Cre; *Kcna1*<sup>+/-</sup>; MADM-6: 1-month-

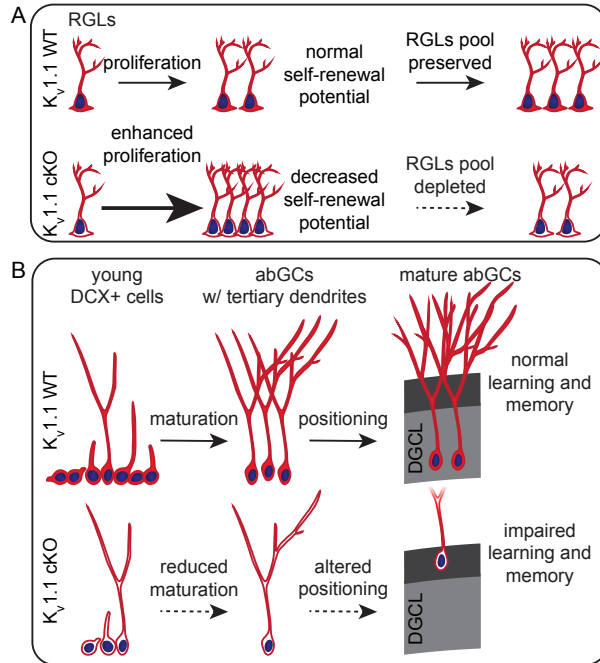
old (n = 12); 2 to 3-month-old (n = 11); 6 to 13-month-old (n = 9). \*\*\*\*P < 0.0001. Data are presented as mean  $\pm$  SEM. Data from 1-month-old and 2 to 3-month-old cohorts originally published in Figure 1 of Chou et al., 2021.

Fig. 5



**Figure 3.5:  $K_v1.1$  cKO mice display deficits in hippocampal-dependent learning and memory.** (A) Behavior paradigm for assessing learning and memory in  $K_v1.1$  cKO mice and  $K_v1.1$  WT mice. TAM was injected for 5 consecutive days in ~4-month-old mice. Contextual fear conditioning and discrimination test started at ~6.5 weeks post-TAM injection. The mice were perfused at ~8 months of age. (B) Protocol for contextual fear conditioning. On Days 1-3, the mice were shocked in the fear context. (C) Quantification of fear acquisition, revealing that  $K_v1.1$  cKO mice ( $n = 16$ ) froze less than  $K_v1.1$  WT mice ( $n = 19$ ) on both Day 2 and Day 3 (Day 1 ( $P = 0.3719$ ), Day 2 ( $P = 0.0339$ ), Day 3 ( $P = 0.0035$ )). (D) Protocol for contextual recall/generalization. On Day 4, these mice were exposed to the fear context without shock in the morning and introduced to a new shock-free neutral context in the afternoon. On Day 5, the order of the two contexts were switched. (E and F) Quantification of freezing during Recall and Generalization. On Day 4, both genotypes froze more in the fear context than the neutral context ( $K_v1.1$  WT ( $P < 0.0001$ ),  $K_v1.1$  cKO ( $P = 0.0003$ )). On Day 5, both genotypes froze similarly in the fear context and neutral context ( $K_v1.1$  WT ( $P = 0.2849$ ),  $K_v1.1$  cKO ( $P = 0.4097$ )). (G) Protocol for contextual

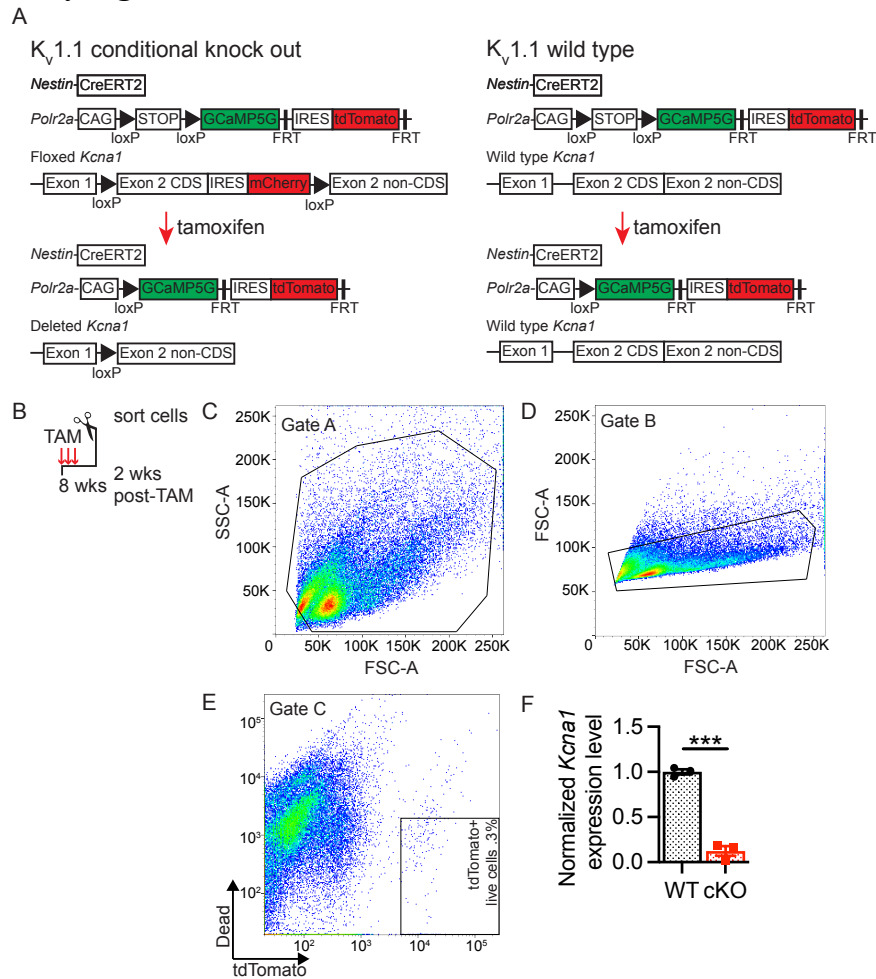
discrimination with shock administered only in the fear context. Data from two days were averaged to form a block. (H-I) Chart of percent freezing in the two contexts within each genotype over time.  $K_v1.1$  WT mice began discriminating between the two contexts by Block 3, while  $K_v1.1$  cKO mice did not consistently discriminate between the two contexts until Block 6. Mixed effects analysis with the Geisser-Greenhouse correction followed by Sidak's multiple comparisons test between fear and neutral context for both genotypes;  $K_v1.1$  WT: context effect ( $F_{1,36} = 17.34$ ,  $P = 0.0002$ ), block effect ( $F_{3,706,133.4} = 4.774$ ,  $P = 0.0017$ ), context x block interaction ( $F_{6,216} = 5.225$ ,  $P < 0.0001$ ); multiple comparisons: Block 1 ( $P = 0.2049$ ), Block 2 ( $P = 0.2112$ ), Block 3 ( $P = 0.0283$ ), Block 4 ( $P = 0.0036$ ), Block 5 ( $P = 0.0028$ ), Block 6 ( $P < 0.0001$ ), and Block 7 ( $P < 0.0001$ );  $K_v1.1$  cKO: context effect ( $F_{1,30} = 8.839$ ,  $P = 0.0058$ ), block effect ( $F_{3,454,103.6} = 9.590$ ,  $P < 0.0001$ ), context x block interaction ( $F_{6,180} = 4.441$ ,  $P = 0.0003$ ); multiple comparisons: Block 1 ( $P = 0.6384$ ), Block 2 ( $P = 0.5937$ ), Block 3 ( $P = 0.0696$ ), Block 4 ( $P = 0.0232$ ), Block 5 ( $P = 0.0614$ ), Block 6 ( $P = 0.0106$ ), and Block 7 ( $P = 0.0055$ ). (J) Quantification (cells per  $\text{mm}^3$ ) of GFP+, NeuN+ cells to assess the amount of abGCs in the dentate gyrus of  $K_v1.1$  cKO and  $K_v1.1$  WT behavioral cohorts. Neurogenesis was decreased in  $K_v1.1$  cKO mice compared to the  $K_v1.1$  WT mice ( $P = 0.0431$ ). C, E, F, and I: Unpaired two-tailed Student's t-test with Welch's correction;  $P < 0.10$  indicated, \*  $P < 0.05$ , \*\*  $P < 0.01$ , \*\*\*  $P < 0.001$ , \*\*\*\*  $P < 0.0001$ ; Data are presented as mean  $\pm$  SEM.



**Figure 3.6: Model of impaired adult neurogenesis in  $K_v1.1$  cKO mice with deletion of  $K_v1.1$  from adult neural stem cells (NSCs) induced by tamoxifen (TAM) injection.** (A) During early stages of neurogenesis,  $K_v1.1$  deletion in hippocampal NSCs enhances radial glial-like NSC (RGL) proliferation, leading to an initial increase of RGLs at 4 weeks post-TAM (center). Over-proliferation diminishes the RGLs' self-renewal potential and depletes RGLs in  $K_v1.1$  cKO mice, resulting in decreased RGLs by 8 weeks post-TAM (right). (B) In later stages of neurogenesis,  $K_v1.1$  cKO mice have fewer doublecortin-expressing (DCX+) cells (left), and these DCX+ cells have deficits in development with a reduction in the percentage and amount of abGCs (abGCs) with tertiary dendrites (center). Fewer mature abGCs (abGCs) are produced in  $K_v1.1$  cKO mice and these abGCs are more likely to be mispositioned in the outer third of the dentate granule cell layer (DGCL) (right). Thus,  $K_v1.1$  plays an important role in proper abGC maturation and integration into the DGCL and for preserving hippocampal-dependent learning and memory.

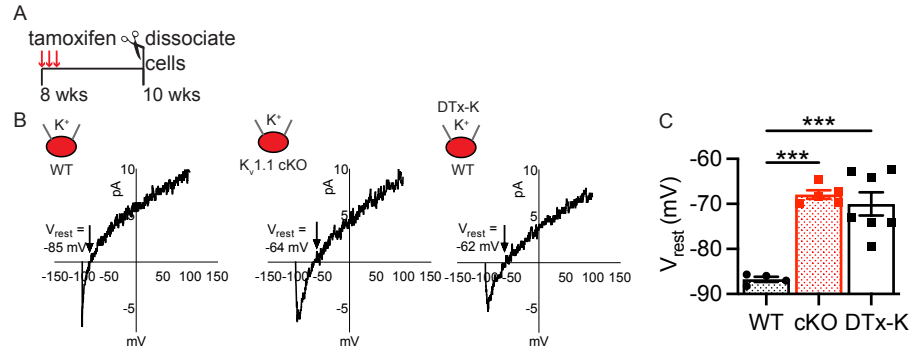


### 3.8 Supplementary Figures

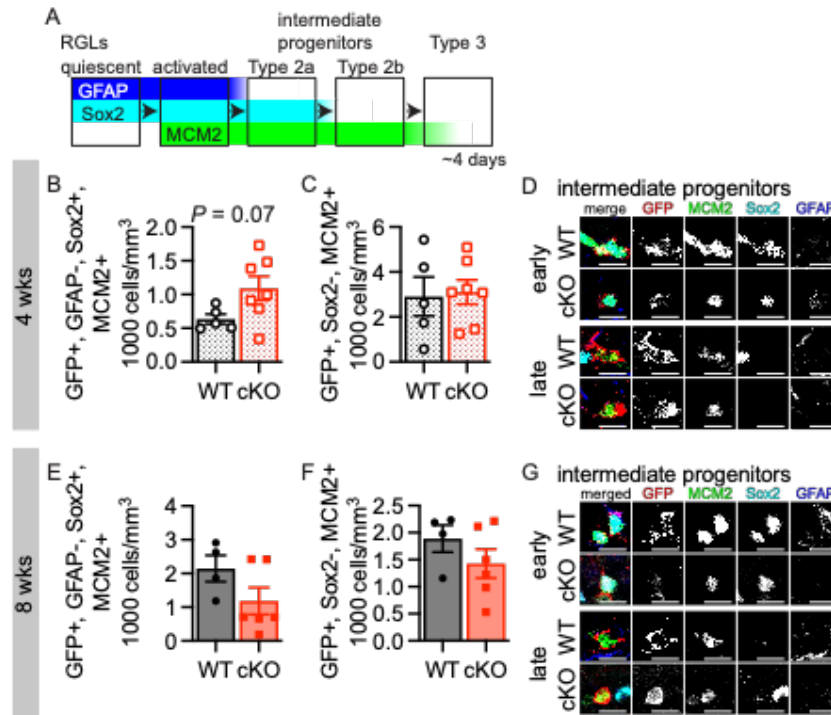


**Supplementary figure 3.1: Generation of K<sub>v</sub>1.1 cKO mice and validation of *Kcna1* gene deletion by qPCR.** (A) Strategy for cell-type specific K<sub>v</sub>1.1 knockout with temporal control via tamoxifen (TAM) administration. We bred *Nestin-CreERT<sup>2</sup>* mice, which expressed a TAM-inducible Cre recombinase in neural stem cells (NSCs), with *Kcna1<sup>fl/fl</sup>* mice and PC::G5-tdT reporter mice to create K<sub>v</sub>1.1 conditional knock out mice. In *Kcna1<sup>fl/fl</sup>* allele, the *Kcna1* exon 2 coding sequence (CDS) is flanked by loxP sites and removed by TAM-activated Cre recombinase. However, mCherry fluorescence in *Kcna1<sup>fl/fl</sup>* mice was not visible even with antibody amplification. Because Cre recombinase also allows for both tdTomato and GCaMP5G expression in the PC::G5-tdT transgene, we quantified the expression of these markers as a proxy for Cre expression. To establish a K<sub>v</sub>1.1 wildtype control line, we bred *Nestin-CreERT<sup>2</sup>* mice and PC::G5-tdT mice with *Kcna1* wildtype mice, thereby accounting for TAM exposure as well as Cre recombinase and reporter expression. (B) Protocol for validation of K<sub>v</sub>1.1 cKO by qPCR. We injected 8-week-old mice with TAM for 3 consecutive days to induce Cre expression and *Kcna1* deletion. After 2 weeks, we dissected out the dentate gyrus, suspended the cells, and sorted out tdTomato+ cells for qPCR to determine if *Kcna1* has been deleted. (C–E) Representative image demonstrating FACS gating strategy for isolation of tdTomato+ lineage. (C) Cells were first gated based on forward scatter area (FSC-A) and side scatter area (SSC-A) properties to eliminate debris (Gate A). (D) Second, cell doublets were excluded based on the area and width of the forward

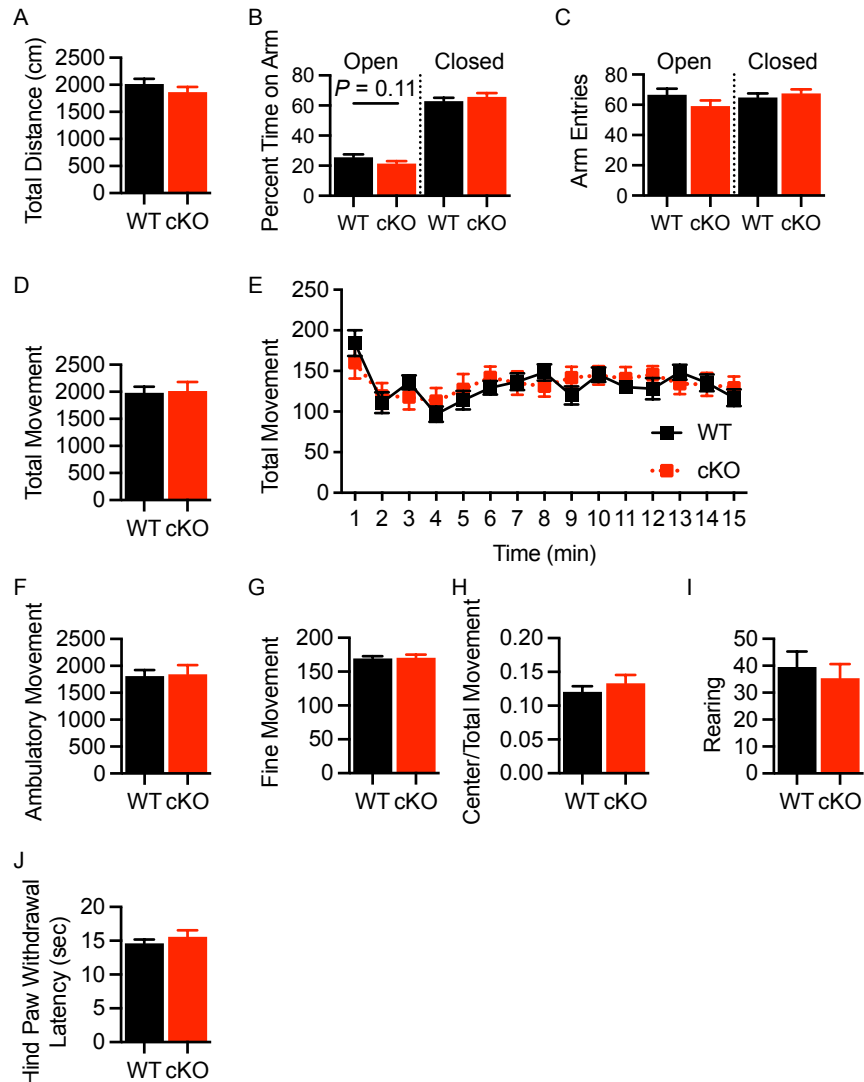
scatter area (Gate B). (E) Third, the cell population was selected based on the intensity of the tdTomato fluorescence and LIVE/DEAD<sup>TM</sup> stain 633 nm (Gate C). In total, 0.3% of the sorted cells were collected. (F) QPCR analysis of sorted tdTomato+ live cells. Cells were pooled, and qPCR analysis show that *Kcna1* mRNA expression was decreased in the cKO mice (n = 3) compared to Kv1.1 WT mice (n = 3) ( $P = 0.0001$ ). Unpaired two-tailed Student's t-test; \*\*\*  $P < 0.001$ . Data are presented as mean  $\pm$  SEM.



**Supplementary figure 3.2: Loss of  $K_v1.1$  function in  $K_v1.1$  cKO cells. (A) Protocol for validation of  $K_v1.1$  cKO by cell-attached patch recording.** We injected 8-week-old mice with TAM for 3 consecutive days to induce Cre expression and *Kcnal* deletion. After 2 weeks, we dissected out the dentate gyrus, suspended the cells, and carried out cell-attached patch recordings from tdTomato+ cells. (B) Representative I-V curves of  $K_v1.1$  WT cell (left),  $K_v1.1$  cKO cell (center), and  $K_v1.1$  WT cells treated with Dendrotoxin-K (DTx-K, 10 nM) (right). Resting membrane potentials for each cell type are indicated. (C) Summary of resting membrane (resting membrane potential) measurements. TdTomato+  $K_v1.1$  cKO cells ( $n = 5$ ) and  $K_v1.1$  WT cells treated with DTx-K ( $n = 7$ ) displayed depolarized resting membrane potential compared with  $K_v1.1$  WT cells ( $n = 4$ ). One-way ANOVA with Holm-Sidak correction for multiple comparisons; ( $F_{2,13} = 20.51$ ,  $P < 0.0001$ ), multiple comparisons: WT vs. cKO ( $P = 0.0002$ ), WT vs. DTx-K ( $P = 0.0002$ ), and cKO vs. DTx-K ( $P = 0.4730$ ). \*\*\* $P < 0.001$ . Data are presented as mean  $\pm$  SEM.



**Supplementary figure 3.3: Deletion of  $K_v1.1$  in adult neural stem cells (NSCs) results in a trend towards increased early glial-like intermediate progenitor cells (Type 2a) at 4 weeks post-tamoxifen (TAM).** (A) Cell-marker expression during adult hippocampal neurogenesis. Quiescent RGLs are GFAP<sup>+</sup> and Sox2<sup>+</sup> and start expressing MCM2 when they become activated. As RGLs develop into Type 2a cells they lose their GFAP expression but remain Sox2<sup>+</sup> and MCM2<sup>+</sup>. Sox2 expression is lost as Type2a cells become more neuronal-like intermediate progenitors (Type 2b). They continue to express MCM2 until they become post-mitotic neuroblasts (Type 3). (B and C) Quantification (cells per mm<sup>3</sup>) of Type2a cells (GFP<sup>+</sup>, GFAP<sup>-</sup>, Sox2<sup>+</sup>, MCM2<sup>+</sup>) and Type 2b/3 cells (GFP<sup>+</sup>, GFAP<sup>-</sup>, Sox2<sup>-</sup>, MCM2<sup>+</sup>) at 4 weeks post-TAM. A trend towards statistical significance ( $P = 0.0680$ ) was observed for increased Type 2a cells in  $K_v1.1$  cKO mice ( $n = 7$ ) compared to  $K_v1.1$  WT mice ( $n = 5$ ) at 4 weeks post-TAM. No difference was noted in the amount of Type 2b cells between the two genotypes ( $P = 0.8418$ ). (D) Representative images of Type 2a and Type 2b/3 cells of  $K_v1.1$  cKO mice and  $K_v1.1$  WT mice at 4 weeks post-TAM are shown with merged and individual expression of GFP (red), GFAP (blue), Sox2 (cyan), and MCM2 (green). Scale bar, 10  $\mu$ m. (E and F) Quantification (cells per mm<sup>3</sup>) of Type 2a (GFP<sup>+</sup>, GFAP<sup>-</sup>, Sox2<sup>+</sup>, MCM2<sup>+</sup>) and Type 2b/3 cells (GFP<sup>+</sup>, GFAP<sup>-</sup>, Sox2<sup>-</sup>, MCM2<sup>+</sup>) at 8 weeks post-TAM. At 8 weeks post-TAM, similar amounts of Type 2a ( $P = 0.1391$ ) and Type 2b/3 cells ( $P = 0.2686$ ) were found in  $K_v1.1$  cKO mice ( $n = 6$ ) and  $K_v1.1$  WT mice ( $n = 4$ ). (G) Representative image of Type 2a and Type 2b/3 cells in  $K_v1.1$  cKO mice and  $K_v1.1$  WT mice at 8 weeks post-TAM are shown with merged and individual expression of GFP (red), GFAP (blue), Sox2 (cyan), and MCM2 (green). Scale bar, 10  $\mu$ m. B, C, E, F: Unpaired two-tailed Student's t-test;  $P < 0.10$  indicated; Data are presented as mean  $\pm$  SEM.




**Supplementary figure 3.4:  $K_v1.1$  cKO mice showed no abnormality in elevated plus maze, open field, and hot plate test.** (A–C) Quantification of elevated plus maze behavioral parameters in  $K_v1.1$  cKO ( $n = 16$ ) and  $K_v1.1$  WT mice ( $n = 19$ ). No significant differences were found in locomotor activity (total distance traveled ( $P = 0.2652$ )), exploration of the open arms (percent time on open arm ( $P = 0.1079$ ), percent time on closed arm ( $P = 0.3838$ ), open arm entries ( $P = 0.1826$ ), or closed arm entries ( $P = 0.4879$ )). (D–I) Quantification of open field test behavioral parameters in  $K_v1.1$  cKO and  $K_v1.1$  WT mice. No significant differences were seen in locomotor activity (total movement ( $P = 0.8644$ ), total movement over time between genotype ( $P = 0.8606$ ), ambulatory movement ( $P = 0.8704$ ), fine movement ( $P = 0.8435$ )), baseline anxiety (center/total movement ( $P = 0.3979$ )), or exploratory activity (rearing ( $P = 0.7873$ )). (J) Quantification of pain sensitivity via hotplate test in  $K_v1.1$  cKO and  $K_v1.1$  WT mice. Similar pain sensitivity, as measured by hind paw withdrawal latency ( $P = 0.3763$ ) was observed. A, D, F, G, and J: Unpaired two-tailed Student’s *t*-test with Welch’s correction; B and C: Unpaired two-tailed Student’s *t*-test with Welch’s correction comparing genotypes for both open and closed arms E: Two-way repeated measures ANOVA with the Geisser-Greenhouse correction; I: Unpaired two-tailed Mann Whitney U-test; Data are presented as mean  $\pm$  SEM.

## Publishing Agreement

It is the policy of the University to encourage open access and broad distribution of all theses, dissertations, and manuscripts. The Graduate Division will facilitate the distribution of UCSF theses, dissertations, and manuscripts to the UCSF Library for open access and distribution. UCSF will make such theses, dissertations, and manuscripts accessible to the public and will take reasonable steps to preserve these works in perpetuity.

I hereby grant the non-exclusive, perpetual right to The Regents of the University of California to reproduce, publicly display, distribute, preserve, and publish copies of my thesis, dissertation, or manuscript in any form or media, now existing or later derived, including access online for teaching, research, and public service purposes.

DocuSigned by:



3BBE71EAC789480...

Author Signature

12/1/2021

Date